DOKUZ EYLÜL UNIVERSITY
GRADUATE SCHOOL OF NATURAL AND APPLIED SCIENCES

IN-LINE CUTTING OPERATION CONTROL IN FINISHING BY MEASURING SURFACE ROUGHNESS

by
Özer TAGA

November, 2015
İZMİR

IN-LINE CUTTING OPERATION CONTROL IN FINISHING BY MEASURING SURFACE ROUGHNESS

A Thesis Submitted to the
Graduate School of Natural and Applied Sciences of Dokuz Eylül University
In Partial Fulfillment of the Requirements for the Degree of Doctor of Philosophy in Mechatronic Engineering, Mechatronic Engineering Program

by
Özer TAGA

November, 2015
İZMİR

Ph.D. THESIS EXAMINATION RESULT FORM

We have read the thesis entitled **"IN-LINE CUTTING OPERATION CONTROL IN FINISHING BY MEASURING SURFACE ROUGHNESS"** completed by **ÖZER TAGA** under supervision of **PROF.DR. ZEKİ KIRAL** and we certify that in our opinion it is fully adequate, in scope and in quality, as a thesis for the degree of Doctor of Philosophy.

Prof. Dr. Zeki KIRAL

Supervisor

Prof. Dr. Haldun KARACA

Thesis Committee Member

Assist. Prof. Dr.Levent ÇETİN

Thesis Committee Member

Assoc. Prof. Dr. Cevdet GÖLOĞLU

Examining Committee Member

Assoc. Prof. Dr. Kutlay SEVER

Examining Committee Member

Prof.Dr. Ayşe OKUR
Director
Graduate School of Natural and Applied Sciences

ACKNOWLEDGMENTS

This work has been carried out at TÜBİTAK-SAGE, Defence Industries Research and Development Institute, Structural and Mechanical Design Division, Mechanical System Dept. in Ankara, Turkey and supported by Dokuz Eylül Üniversity.

My sincere thanks goes to my advisors Prof. Dr. Zeki Kıral and Prof. Dr. Erol Uyar for the supervision of this work and their flexibility, Prof. Dr. Haldun Karaca, Asist. Prof. Dr. Levent Çetin for their support and advice during our thesis meetings. Moreover, I would like to express my gratitude to Zuhal Temiz for making life easier with student affairs formalities.

I would like to thank Dr. Kemal Yaman, Dr. Bülent Özkan, and Burak Durak for their constructive suggestions during the many discussions we had and for their support. Morever thanks to Dr. Harun Gökçe and Engin Metin Kaplan for their help in measurement data allocation. Not to forget, thanks to Cemil Bülbül, Murat Avcı, Harun Kahya and Suat Ege Yıldızoğlu for their valuable contributions throughout this study.

Above all, I can't thank my beloved family enough for standing by my side under all circumstances throughout my entire life. My deepest gratitude goes to them, my father Mustafa Taga, mother Urfiye Taga, my wife Merve Taga, my brothers Özcan Taga and Özkan Taga.

Özer TAGA

IN-LINE CUTTING OPERATION CONTROL IN FINISHING BY MEASURING SURFACE ROUGHNESS

ABSTRACT

In this thesis, a milling system based on real-time surface roughness measurement during machining process is developed using Artificial Neural Network technique. In the developed system, desired surface roughness is provided with determining the optimum feed rate and cutting speed. Surface roughness control has an important role to achieve high surface quality for the metal cutting.

Dynamic behavior of the system is investigated in the study. Natural frequency modal analysis and experimental studies of the system are mentioned. Then, hardware and software studies of the Surface Roughness Control System (SRCS) are elucidated. An algorithm determining the operating principle of the system is developed. According to this algorithm, the optimum cutting parameters are predicted for end milling (finishing) operation by measuring semi finish machining surface roughness via an optic sensor and then end milling operation is performed with the cutting parameters determined by the system.

In the last part of the study, surface qualities are observed for the milling process before and after the intervention of the system and the results are compared. The experimental results show that the developed milling system can be integrated with modern machining systems in order to obtain the desired surface quality levels.

Keywords: Cutting parameters, in-line control, surface roughness, artificial neural network, optical sensor

YÜZEY PÜRÜZLÜLÜĞÜ ÖLÇÜMÜYLE BİTİRME OPERASYONUNDA KESME PARAMETRELERİNİN HATTA KONTROLÜ

ÖZ

Bu tez kapsamında, yapay sinir ağları yöntemi kullanılarak frezeleme operasyonu sırasında hatta yüzey pürüzlülük kontrol sistemi geliştirilmiştir. Geliştirilen sistem vasıtasıyla, en iyi (optimum) ilerleme hızı ve kesme hızının belirlenmesi suretiyle istenilen yüzey pürüzlülüğü sağlanmıştır. Yüzey pürüzlülüğü kontrolü, talaşlı imalat için hassas yüzey kalitesi gerektiren işlerde büyük bir önem arz etmektedir.

Çalışmada sistemin dinamik davranışı incelenmiştir. Sistemin doğal frekans modal analiz ve deneysel çalışmalarından bahsedilmiştir. Ardından Yüzey Pürüzlülük Kontrol Sistemi (YPKS) donanım ve yazılım çalışmaları anlatılmıştır. Çalışma prensibini belirlemek için bir algoritma geliştirilmiştir. Bu algoritmaya göre yarı bitirme işleme yapılan yüzeyde optik sensör vasıtasıyla yüzey pürüzlülüğü ölçümü ile optimum işleme parametrelerinin önceden tayin edilmiştir ve sisteme dış bir müdahale gerektirmeden sistemin belirlenen optimum parametrelere göre bitirme (finiş) operasyonunu gerçekleştirmesi sağlanmıştır.

Çalışmanın son kısımda, sistemin müdahalesi öncesi ve sonrası yüzey kaliteleri incelenmiştir; sonuçlar kıyaslanmıştır. Deneysel sonuçlar geliştirilen işleme sisteminin modern işleme sistemlerine entegrasyonu ile istenilen yüzey kalitesinin elde edilebileceğini göstermiştir.

Anahtar kelimeler: Kesme parametreleri, hatta kontrol, yüzey pürüzlülüğü, yapay sinir ağı, optik sensör

CONTENTS

Page

LIST OF FIGURES

Page

LIST OF TABLES

Page

CHAPTER ONE
INTRODUCTION

1.1 Introduction

One of the most significant subjects in the area of material removal is surface finishing. Black (1979) defined metal cutting as the removal of metal chips from a workpiece in order to obtain a finished product with desired attributes of size, shape, and surface roughness. Surface finishing is a method used very commonly in fields such as molding, automotive, aerospace and defense industries. Controlled surface finishing has become much more important, particularly in sectors requiring precise surface quality, just as aerospace and defense industries.

Contemporarily, for many different purposes, machines are being developed by means of improving processing technology. Widespread mass-production in all areas, competitive environment and large production requirements have made tools, machining time and quality control costs much more important over time. Especially, the increase of CNC machines enabled the production of high precision parts in less time and with lower costs. However, machining vibrations, tool wear and wrong cutting parameters come into prominence as the preventive factors of the desired and efficient usage of this technology. Today, although very complex geometries can be machined much faster with a high dimensional accuracy by the current status of machining technologies, the intended maturity in the surface roughness issue has not been reached yet.

1.2 State of Art and Motivation

Researchers have paid great attention on the improvement of the surface roughness due to the industrial importance of the subject. In many studies, primarily conducted studies, the correlations between surface roughness and cutting parameters such as cutting speed, feed rate and depth of cut have been analyzed. By means of

the experimental works, the specifications of surface roughness based on the change in cutting parameters were determined by using different methods.

GEP (Gene Expression Programming) method was used for predicting surface roughness with cutting parameters in end milling. Cutting speed, feed rate and depth of cut data was collected for predicting surface roughness. In the last part of the study, a linear equation predicting the surface roughness was formulated (Çolak, Kurbanoğlu&Kayacan, 2007).

The experimental studies were realized for the characteristic of the surface quality in end milling operation. In the study, the effects of spindle speed, cutting velocity and depth of cut on surface roughness were defined and a multi regression model was found out. Here, according to end milling parameters, the problem was to understand the control of final form of the machined surface. Surface roughness value was estimated with 12% error in accordance with the model including the effect of spindle speed, cutting velocity and depth of cut (Hayajneh, Tahat & Bluhm, 2007).

Taguchi design application was studied on to optimize the surface quality in the face milling operation. With the scope of the study, feed rate, cutting speed and depth of cut were selected as the control factors; different tool cutters were selected as the noise factors for simulating temperature and various cutting conditions. The most important factor was found out with ANOVA analysis and the optimal cutting combinations were defined for the best surface roughness value. At the end, Taguchi design was verified with the verification tests (Zhang, Chen & Kirby, 2007).

Göloğlu and Sakarya (2008) investigated the optimum cutting parameters for machining DIN 1.2738 mold steel with high speed steel end mills using Taguchi parameter design. Also, they studied the effects of cutter path strategies on surface roughness with the same method. According to their studies, the most influential factors are feed rate for one direction and spiral cutter path strategies and depth of cut for back and forth cutter strategy on surface roughness.

Agarwal (2012) mentioned the importance of defining appropriate machining parameters before the cutting process in order to get the desired surface quality. Multi regression model was developed in accordance with independent variables as cutting speed, feed rate and depth of cut and dependent variable as surface roughness, R_a. Prediction performance of the model was tested. As a result of theoretical and experimental studies, R_a value was carried out with 5% error.

The possibility of applying multiple regression methods to surface roughness was mentioned on machining process. An approximation of surface roughness was proposed by measuring the cutting forces that occur during machining, apart from cutting parameters. Proposed methods were experimentally verified according to the different cutting conditions (Rosales, Vizan, Diez& Alanis, 2011).

A method was developed by modeling the cutting forces, which arise during machining process and related them to tool wear, instead of surface roughness. Normalized tangential and radial force model coefficients were reduced to a single parameter for observing wear. With this method, tool wear was investigated by performing experiments on different workpiece materials. Also, the in-line tool wear traceability and wear rate availability in failure zone were investigated with this method (Nouri, Fussell, Ziniti & Linder, 2014).

Ali and Dhar (2010) developed an ANN (Artificial Neural Network) model using tool wear and cutting parameters to determine surface roughness. 25 hidden neurons and feed forward back propagation neural network model was chosen to create an optimum network. As a result, with the minimum amount of lubricant under environmental conditions, the model turned out at advantage for the response of tool wear and surface roughness.

Chi and Chen (2010) introduced a methodology based on genetic wavelet network to predict surface roughness with an error less than 3%. ANN was developed for prediction. Learning mechanism was realized based upon in-line prediction of

nonlinear mapping, vibration acceleration and cutting parameters in Elman algorithm.

An in-process surface roughness recognition system was developed to predict surface roughness based on vibration and rotation data. In the study, an accelerometer was used as an in-process sensor. Surface roughness was predicted with a back propagation ANN model trained with four input neurons as cutting speed, feed rate, depth of cut and vibration. As a result of experimental studies, surface roughness was predicted with approximately 96% accuracy by ANN recognition system in various cutting conditions (Tsai, Chen & Lou, 1999).

The effect of feed rate on surface roughness for 6061 Aluminum was investigated to reduce automotive component manufacture cycle time in machining. According to observation, surface roughness generally increased with an increase of feed rate (Kuttolamadom, Hamzehlouia & Mears, 2010).

The influence of cutting parameters was emphasized such as cutting speed, feed rate and depth of cut on the surface roughness of material St-52 in face milling. In their study, Bayesian neural network model was employed to predict the surface roughness with an error of 6.3%. Also, as a result of experiments the most influential factor was determined as the feed rate (Bajic, Lela & Zivkovic, 2008).

A surface roughness model was proposed for face milling operations based on profile, axial and radial runout errors of cutting inserts. (Baek, Ko & Kim, 2001).

Ehmann and Hong (1994) developed a new method called Surface-Shaping System to represent the surface generation process. The system consisted of two parts: tool kinematics modeling and tool geometry modeling. For this purpose, computer simulation software was developed for graphical representation and evaluation of the generated surface.

The cutting parameter optimization of end milling process was studied to improve the surface quality as well as high material removal rate using PCA-based Taguchi method (Moshat, Datta, Bandyopadhyay & Pal, 2010).

Chen and Savage (2001) studied on the prediction of surface roughness under different cutting conditions such as workpiece material and tool size. For this purpose, a fuzzy-nets approach was developed for the multilevel in-process surface roughness recognition system called FN-M-ISRR. Surface roughness was predicted by extrapolation from collected vibration signals and cutting condition data. It was reported that the proposed fuzzy system predicted the surface roughness with 90% accuracy during milling operation.

A method was developed for simulating the machined surface by using the acceleration data. The algorithm was developed in terms of cutting conditions, cutting tool, workpiece and runout parameters. Then, the surface roughness was predicted by using the measured acceleration and geometric model of end milling process (Lee, Kang, Jeong, Lee & Kim, 2001).

The surface roughness of thin-walled CK45 material parts was investigated during the milling operation. They studied the effects of geometric parameters on the surface roughness using analytical approximation techniques by utilizing the mathematical model of the system (Michalik, Zajac, Hatala, Mital & Fecova, 2004).

Routara, Bandyopadhyay and Sahoo (2009) claimed that surface roughness is a statement denoting the surface topography. Surface roughness also has considerable effects on the measures such as fatigue strength, corrosion resistance and creep life.

For the prediction of surface roughness or optimization and modeling of cutting parameters, there are also other measurement practices. Contact-type surface roughness measurement systems are the classical methods when the surface roughness measurement is considered. Generally in machining, contact-type stylus profilometers are used to determine the surface roughness. Tomkiewicz (2010) used

image processing method for the determination of roughness levels. In his study, he captured the images of the surface during machining and approximated the surface roughness with the ANNs method by converting the images into digital signals.

Optical and laser systems seem important in the researches made on non-contact surface roughness measuring systems. Bradley (2000) performed some tests by adapting the optical surface roughness sensor to the coordinate-measuring machine.

In this study, a machining system, which is able to manufacture components with desired surface quality without an external intervention, is developed. The developed system is able to machine by using optimum cutting parameters determined by the ANN method in accordance with surface roughness requirement. The surface roughness value is measured with an integrated optical surface roughness sensor. Experimental works are conducted by using a 3-axis CNC machine produced as a part of this study. The contribution of the developed system to the desired surface quality of the manufactured parts has been evaluated.

1.3 Outline of the Thesis

In the following, an outline is given to guide the reader through the thesis chapters. Subject of the chapter and the main points covered are given briefly:

Chapter 1:

This chapter has focused on the current situation and the motivation behind this work has been briefly discussed. Moreover the main objectives have been defined with the boundary conditions involved.

Chapter 2:

In this chapter, theoretical background of the thesis is briefly described. Cutting theory, artificial neural network and surface roughness are mentioned as a heading in this chapter.

Chapter 3:

In this chapter, dynamic characteristic of Surface Roughness Control System (SRCS) is given in detail. Firstly, finite element analysis was performed in order to determine the mode shapes of the system. Then experimental setup was built for verifying analysis results and collecting vibration data. In the experimental studies, firstly hammer test was performed to find out natural frequencies of the system. Then, experimental studies were performed for idle condition and during machining.

Chapter 4:

In this chapter, the hardware and software of SRCS are given in detail. Firstly, the components of SRCS and the specification of the optical surface roughness sensor are defined. Then, ANN structure of SRCS is determined. At the end, the software of SRCS is given with the control structure of SRCS.

Chapter 5:

In this chapter, experimental studies and results for SRCS are given in detail. Firstly, experimental studies are performed collecting input data for training ANN model of SRCS. Then, experimental studies for verification of SRCS are performed for different conditions. At the end, verification of the system is proved by means of the experimental results.

Chapter 6:

Finally, in the chapter six, the summaries of whole studies are explained shortly. Also, the significant results obtained from experimental study are given.

CHAPTER TWO
THEORITICAL BACKGROUND

2.1 Introduction

In this chapter, theoretical background of the thesis is briefly described. As a beginning, the cutting theory is described in general to understand a metal removal operation. Also, machine dynamics are mentioned to understand effects of vibration in milling prosess in the same part of the chapter. In the second part of the chapter, an Artifical Neural Network (ANN) is expressed; types of neural network and learning algorithm are explained in detail. In the last part of the chapter, Surface Roughness is defined in machining prosess. Then, the factors affecting surface roughness are listed in machining.

2.2 Cutting Theory

Final shaping of many mechanical parts is carried out by machining operations. Metal removal processes are applied in bulk deformation processes such as forging-rolling and casting processes to get desired surface quality, shapes and dimensions. Cutting operations are known as metal removal from blank in general. The subsequent grinding operations provide exact surface quality and exact dimensions to the part. The most common cutting operations are turning, milling, and drilling. Although, mechanical principles of all metal cutting operations are same, geometry and kinematics of these operations may differ from each other.

2.2.1 Orthogonal Cutting Theory

Two dimensional orthogonal cutting theory is used for explaining mechanics of metal removal process although the most common cutting operations are three dimensional and geometrically complex. Metal removal is obtained under perpendicular angle between material and tool cutting edge in orthogonal cutting. More complex three dimensional oblique cutting operations are evaluated with

geometrical and kinematic transformations applied to orthogonal cutting operation in general. Orthogonal and oblique cutting processes are shown in Figure 2.1.

In orthogonal cutting, tool is used with the cutting edge perpendicular to the direction of cutting velocity. A metal chip with width of cut and depth of cut are sheared away from workpiece. Cutting process is assumed to be uniform along the cutting edge in orthogonal cutting. In this way, two dimensional plane strain deformation becomes a reality without side spreading of the materials, so cutting forces are composed of tangential (direction of velocity) and feed forces (direction of normal).

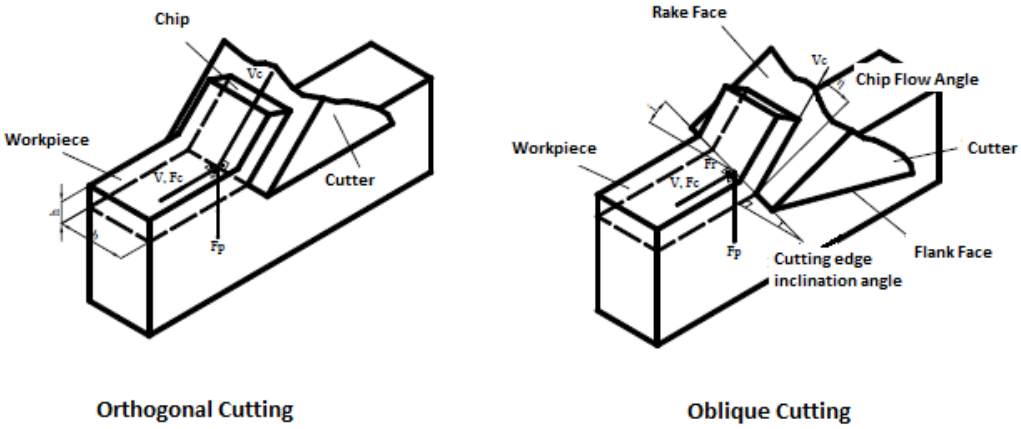

Figure 2.1 Geometries of orthogonal and oblique cutting processes (Altıntaş, 2012)

There are three deformation zones in orthogonal cutting as shown in the cross-sectional view in Figure 2.2. When the tool edge penetrates into the workpiece to form a chip, primary shear zone is formed. Secondary deformation zone is formed from moving along the chip face of tool. The friction area of tool flank is called the tertiary zone.

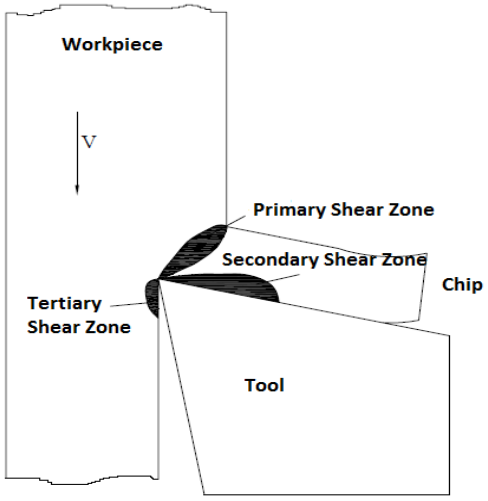

Figure 2.2 Deformation zones in orthogonal cutting (Taylan, 2006)

The chip initially sticks to the rake face of tool and sticking region is formed in this region. The friction stress in the sticking zone is approximately equal to yield stress of the material. After the chip stops sticking, the chip starts sliding over the rake face with a constant sliding friction coefficient. The chip is removed from the tool face, and loses contact with the rake face of tool. The length of contact zone depends on the cutting speed, tool geometry and material properties. There are basically two types of assumptions in the analysis of primary shear zone. Merchant (1944), developed an orthogonal cutting model to predict the shear zone for thin plane. Lee and Shaffer (1951), Palmer and Oxley (1959) developed their analysis for predicting shear angle on thick shear deformation zone in accordance with the laws of plasticity. In their study, the primary shear deformation zone is predicted for thin zone.

Deformation geometry and cutting forces are shown on the cross sectional view of the orthogonal cutting in Figure 2.3. It is assumed that the cutting edge is sharp without a chamfer or radius, and it is mentioned the deformation at thin shear zone. The shear angle (Φ) is defined as the between the direction of cutting speed (V_c) and the shear plane. It is assumed that the shear stress (τ_s) and the normal stress (σ_s) are constant on the shear plane. The resultant force (F_R) on the chip is applied on the shear zone, and calculated in accordance with average constant friction at chip-tool

contact zone. Here, the resultant force (F_R) is formed from the cutting force (F_C) and tool force (F_P).

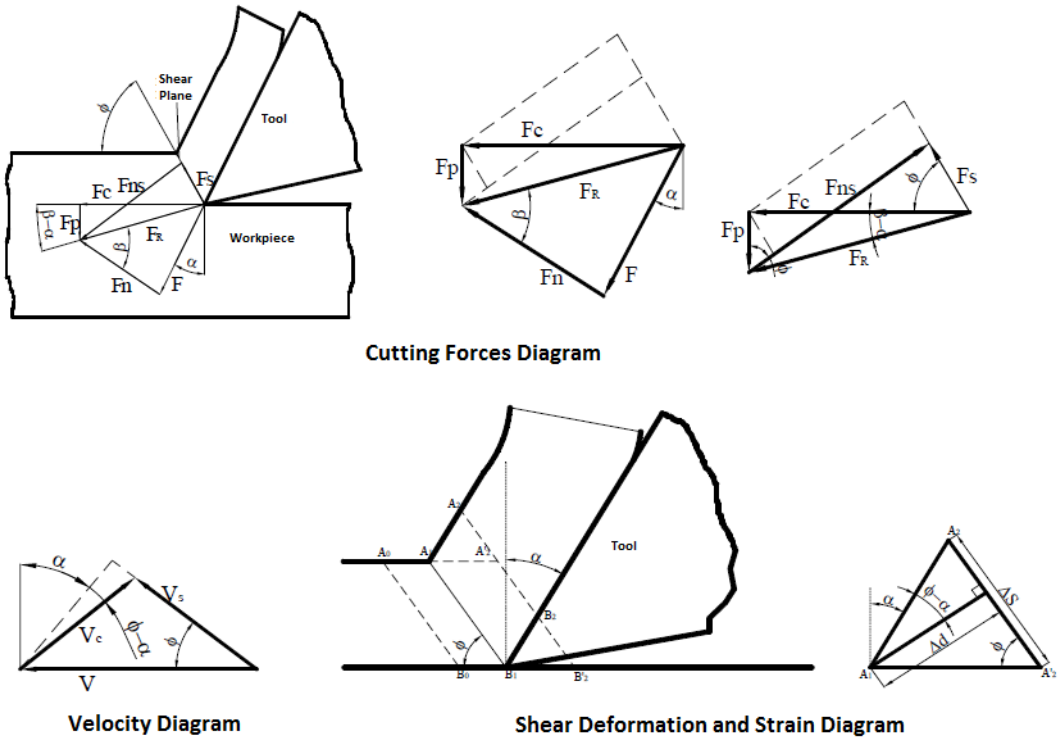

Figure 2.3 Mechanics of orthogonal cutting (Altıntaş, 2012)

$$F_R = \sqrt{F_C^2 + F_P^2} \tag{2.1}$$

Tool force or thrust force is in the direction of uncut chip thickness, and cutting force or power force is in the direction of cutting velocity.

The prediction of temperature distribution at the tool–chip interface is very important in determining the maximum speed and feed rate that give the most optimal material removal rate without excessive tool wear. The binding materials within the cutting tools may be weakened or diffused to the moving chip material at their critical diffusion or melting temperature limits. The fundamental machinability study requires the identification of a maximum cutting speed and uncut chip values that correspond to the critical temperature limit where the tool wears rapidly. By using the approximate solutions summarized above, one can select a cutting speed

and feed rate that would correspond to a tool–chip interface temperature (T_{int}) that lies just below the diffusion and melting limits of materials present in a specific cutting tool. The detailed and fundamental scientific and experimental treatment of the cutting process is covered in Oxley (1989).

2.2.2 Oblique Cutting Theory

The geometry of oblique cutting is shown in Figure 2.4. Cutting velocity (V) is perpendicular to the cutting edge in orthogonal cutting, but there is an acute angle between the cutting edge and normal plane in an oblique cutting.

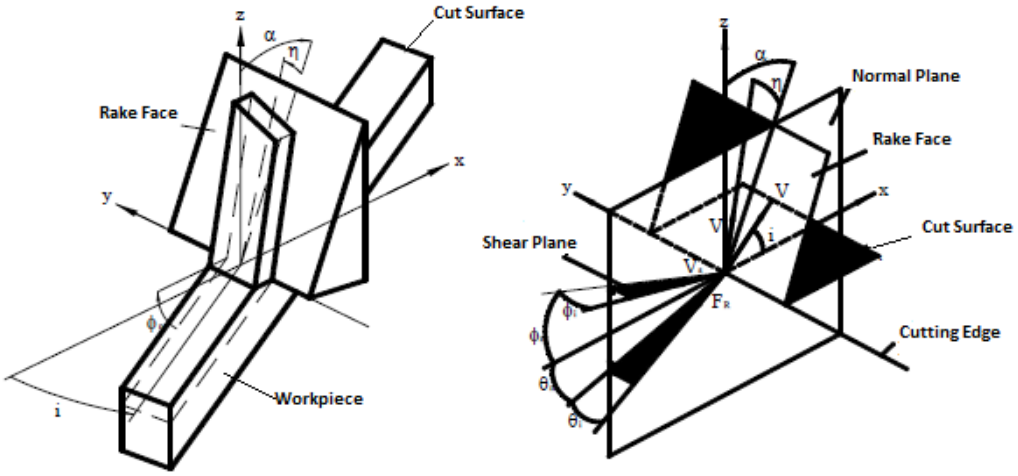

Figure 2.4 The geometry of the oblique cutting process (Altıntaş, 2012)

The difference between the orthogonal cutting mechanism and the oblique cutting mechanism may be better explained by revisiting to Figure 2.1. A plane to normal of the cutting edge and parallel plane to cutting velocity is defined as normal plane or P_n. Shearing and chip motion are identical on all the normal planes parallel to the cutting velocity (V) and perpendicular to the cutting edge. Resultant force and all the forces on the chip-rake face contact zone are on the same plane P_n in orthogonal cutting. There is no cutting force in the third direction perpendicular to normal plane. Cutting velocity has an oblique angle in the oblique cutting, and so the directions of shear, friction, chip flow and resultant force vectors have components in all three cartesian coordinates (x, y, z). In Figure 2.4, x axis is perpendicular to the cutting

edge lies on the cut surface, y is aligned with the cutting edge, and z is perpendicular to the xy plane. The forces exist in all three directions in the oblique cutting. The important planes are the cut surface, the rake face, the cut surface xy, the normal plane xz or P_n, and the velocity plane P_v in the oblique cutting. The mechanics of oblique cutting in the normal plane are equivalent to the orthogonal cutting, thus all the velocity and force vectors are projected on the normal plane. In Figure 2.5, the angle between the shear and xy plane is called the normal shear angle Φ_n. The shear velocity makes the oblique shear angle Φi with the normal vector of cutting edge on the normal plane. The sheared chip moves over the rake face plane with the chip flow angle η. The chip is the same direction with friction force (between the chip and rake face) and the chip flow. Between z axis and normal vector on the rake face is defined as the normal rake angle α. Resultant force F_R is composed of Friction force on the rake face, F, normal force, F_n and friction angle β.

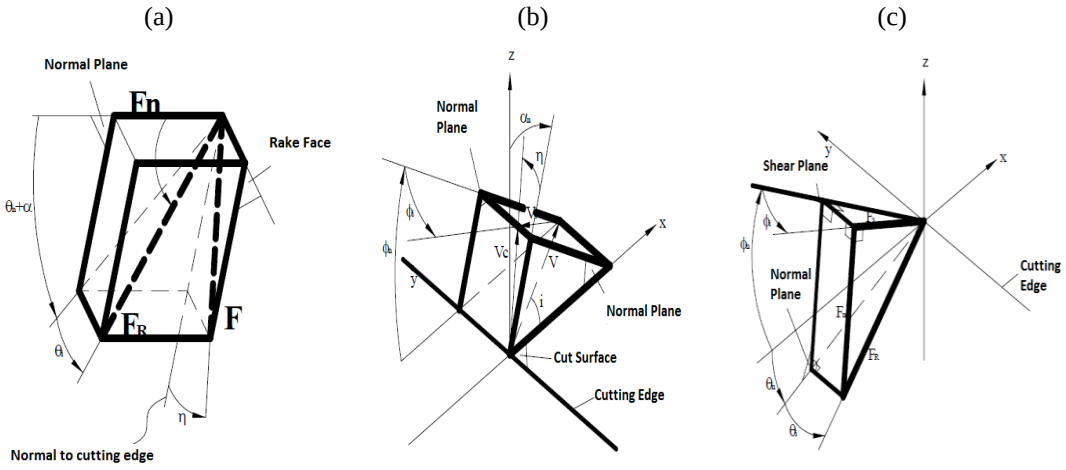

Figure 2.5 a) Force, b) Velocity and c) Shear diagrams in the oblique cutting

2.2.3 Material Removal in Milling Process

The milling operation is an intermittent cutting process using cutter's one or more teeth. Also, the milling operation is a process where the milling cutter moves rotational or transitional motion on the workpiece. In material removal process, either the workpiece is fixed and the cutter is moving or the workpiece is moving, and the cutter is fixed. The process where material or workpiece is moving, and

cutter is fixed is called as the turning process. The process where the cutter rotates while it moves and material is fixed is called as the milling process.

In the milling operation, a milling cutter is held in a rotating spindle, while the workpiece clamped on the table is linearly moved toward the cutter. Material removal process is formed from a relative motion between cutter and workpiece. These are the cutting motion, feed motion and assistant motions. According to teeth number of the cutter, the milling operation is more productive than the other material removal operations.

Both up and down milling operations can be observed at end milling operations. The geometry of chip formation in milling is shown in Figure 2.6.

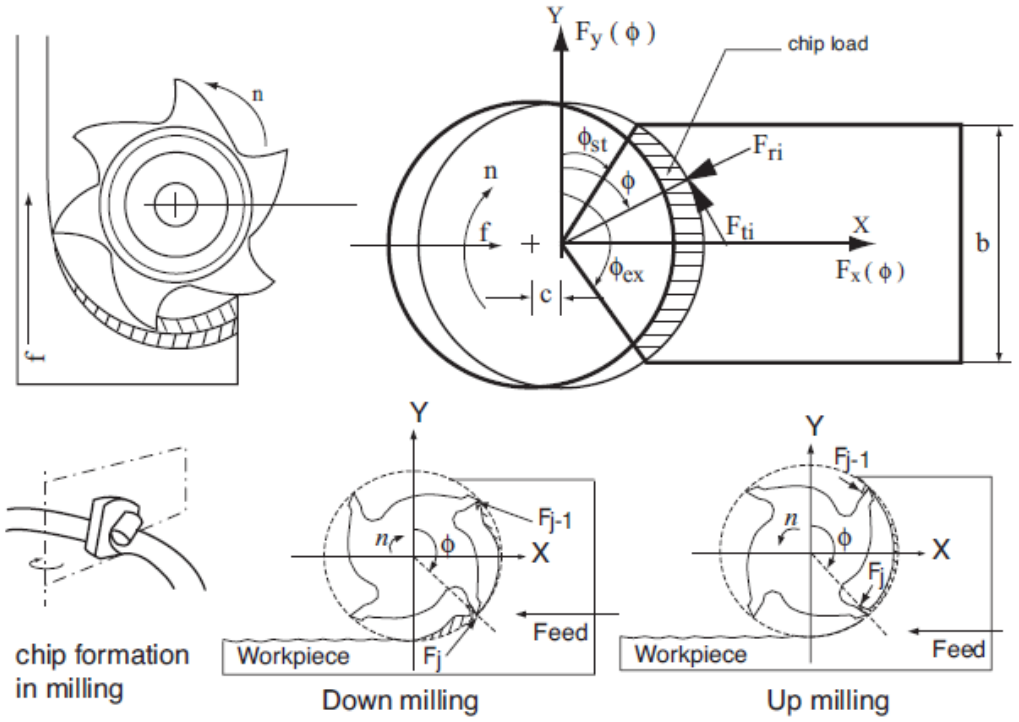

Figure 2.6 Geometry of milling process (Altıntaş, 2012)

2.2.4 Modelling Machine Dynamics in Milling Process

Machine tool vibrations play an important role in hindering productivity during machining. Excessive vibrations accelerate tool wear and chipping, cause poor

surface finish, and may damage the spindle bearings. A brief review of basic vibration theory is provided first. As experimental modal analysis techniques are most readily used in modern machining facilities, a practical review of modal analysis theory and its practice in machining is then presented. The basics of vibration engineering should enable the reader to understand machine tool vibrations and their avoidance in practice.

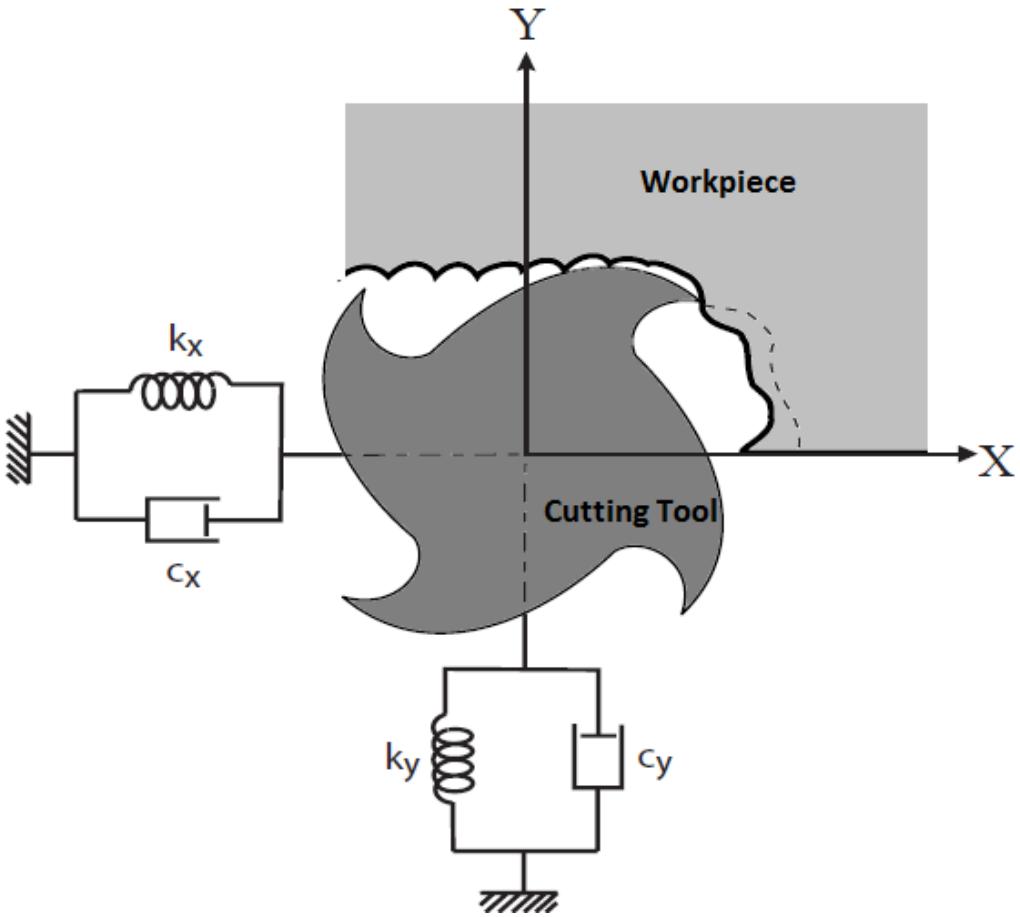

Figure 2.7 Two degrees of freedom diagram in the milling operation

In the milling operation, the free vibration model of x and y directions is given in Figure 2.7. Dynamic model of the cutting tool contains all the structure of the machine system and dynamics of the cutting tool. Workpiece and the cutting tool vibrate together during the cutting process. The governing equations of motion of the structure at x and y directions are represented by the following differential equations

$$\ddot{x}(t) + 2\xi\omega_{nx}\dot{x}(t) + \omega_{nx}^2 x(t) = \frac{\omega_{nx}^2}{k_x} F_x(t) \quad (2.2)$$

$$\ddot{y}(t) + 2\xi\omega_{ny}\dot{y}(t) + \omega_{ny}^2 y(t) = \frac{\omega_{ny}^2}{k_y} F_y(t) \quad (2.3)$$

Where ω_{nx}, ω_{ny} denote the natural frequencies, ξ_x and ξ_y denote the structural damping ratios, k_x and k_y denote the spring constant at feed direction x and normal direction y. The dynamic cutting forces, which occur during machining are denoted by $F_x(t)$ and $F_y(t)$.

2.3 Artificial Neural Network

Artificial Neural Network (ANN) is a mathematical model that tries to simulate the structure and functionalities of biological neural networks. Although computers can analyze very complex numeric processes, they are inadequate on understanding and handling to be gained experiences. Human brain is a highly complex, nonlinear, and parallel information processing system. However, human brain needs most of times to process an operation, for understanding processes are needed very short time to perform.

In general, an artificial neural network is the computer program which is developed to be inspired by the human brain. An ANN system has learning characteristics as well as it has memories and capabilities on the relations with all data. Nowadays, subdivisions of the artificial intelligence such as ANN, fuzzy logic and genetic algorithm can be found wide investigation and application areas.

ANN models some functions of the human nervous system, and catch some abilities of this system. Artificial neural network is parallel data processing system of the simple neurons, models the certain functions of the human neural system. Neural connections, simple elements are networks for connecting parallel densely. A classical ANN model is shown in Figure 2.8.

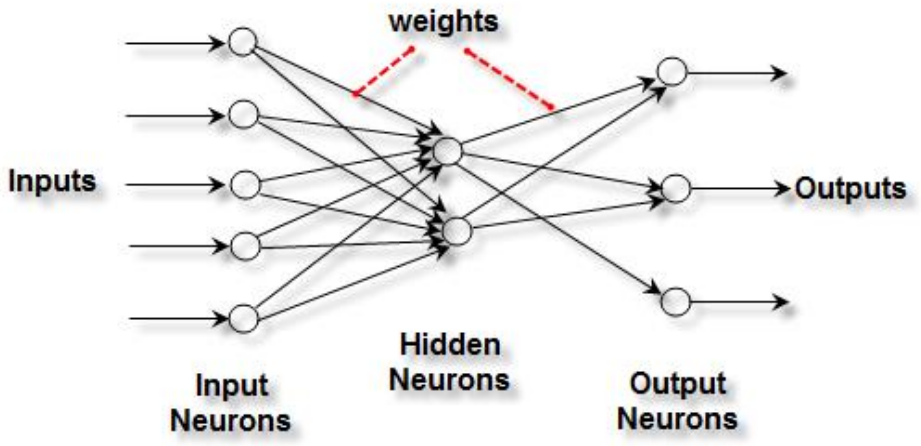

Figure 2.8 A simple ANN model

As seen in Figure 2.8, in the basic ANN model, the input cluster is $x_1, x_2, \ldots, x_m$ expressed as X in the vector form. Each input signal is multiplied by the weight ratios $w_{k1}, w_{k2}, \ldots, w_{km}$ and w_{kb}. The sum of the dual multiplications shown in the vector form W_k, is calculated as below.

$$net(X, W_k) = W_k^T X \tag{2.4}$$

At this point;

$$W_k = [w_{k1} w_{k2} \ldots w_{km} w_{kb}]^T \tag{2.5}$$

$$X = [x_1 x_2 \ldots x_m b_k]^T \tag{2.6}$$

After the calculation of the sum of the weighted value, the output of neuron is produced by applying an activation function

$$y_k = f(W_k^T X) \tag{2.7}$$

or

$$y_k = f(\sum_{i=1}^{m} w_{kj} x_i) \tag{2.8}$$

Sigmoid function is used as an activation function in the study. Sigmoid function, as opposed to classical artificial neural network functions, can simulate the behavior of nonlinear systems. This function is defined as follows:

$$f(net) = \frac{2}{1+e^{-a.net}} - 1 \tag{2.9}$$

where a denotes the slope of sigmoid function.

2.3.1 Types of Neural Networks

Many network models have been developed for 50 years. These models took advantages of biologic nervous system and well known theories in engineering. In general, artificial neural network is parted to feed forward network and recurrent network. Feed forward networks are successful on an image processing; recurrent networks are successful on solutions of optimization problems.

2.3.1.1 Reccurrent Neural Network (RNN)

The most prominent feature of recurrent neural network is that the signal obtained from the output layer is applied to input layer. An example of this structure is shown in Figure 2.9. Thus there is no feedback loop structure. Self-feedback of each neuron's output is reapplied to its input. In addition, this structure is feedback of a single-layer neural network. Feedback should also be applied in multi-layer network. The feedback loop creates a huge impact on the learning ability and performance of the artificial neural network. They are characterized in that they exhibit nonlinear dynamic behavior.

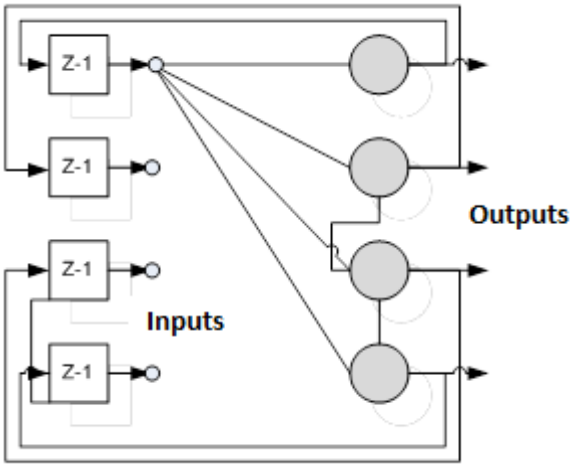

Figure 2.9 Recurrent neural network (RNN)

2.3.1.2 Feed Forward Neural Network (FNN)

Feed forward networks are the one way networks where the information moves in only one way from input to output shown in Figure 2.10. The outputs of the previous layer may be taken as inputs. Feed forward networks are divided into single –layer and multi-layer.

In single-layer feed forward network, only one node is used for input-output functionality of the networks. Mostly, the desired input-output functionality cannot be accomplished with a single layer. Therefore, this layer has the same properties except the connection weight formed by combining the layers. In the simplest form, it can be considered as input signals are applied to the input layer of a layered neural network. Signals in the input layer are connected to the output layer with weights, is called the single layer neural network. In this structure, the information is processed from input to output. Input layer is not considered as a layer because there is no process in the input layer.

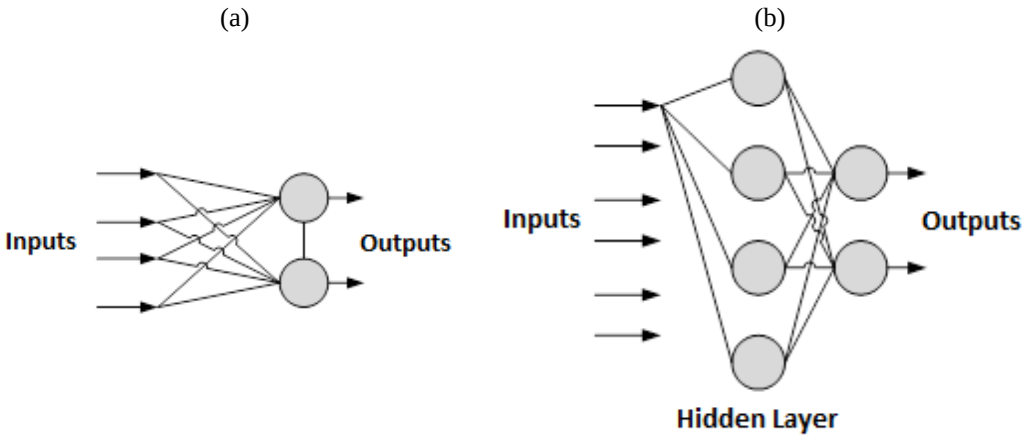

Figure 2.10 a) Single layered feed forward network b) Multilayer feed forward network

Multilayer feed forward networks can be distinguished by carrying one or more hidden layers (Figure 2.8). Hidden layer creates the relationship between the input layer and output layer. When the size of the input layer is increased, the capacity to carry of the hidden layer will be more important. Network structure is fully connected to feed forward network. Some of the network in each neuron can be connected with each other. The fragmented structure of such network is called multilayer feed forward networks.

2.3.2 Learning Algorithm

Learning process in neural network, according to a certain weight of the bond which provides the connection between nerve cells is achieved by charging the rules of procedure. Learning rule, in response to the value provided by the input signals and transfer function equation is known as an amending all or some of the weight on the local memory. Depending on the nature of the learning rule input signals allows the change over time of processing elements. In this way, the network can adapt itself to the desired answer and edit their inside knowledge, and so can be learned.

Artificial neural networks are trained by example instead of programming.

2.3.2.1 Backpropagation Algorithm

Backpropagation algorithm creates the structure adapted to almost every problem in artificial neural networks. Back propagation uses learning mechanism with feedback. Although the structure of the artificial neural network is feed forward, feedback has been concerned for a learning line and supervised learning is used in this neural network model (Lippmann, 1987).

Backpropagation learning uses continuous input type. There is a function that is taken into processing for activation. Backpropagation uses sigmoid function in general and delta rule is used for learning function (Fausett, 1993).

According to Equation 2.10, using a function that can be derived is very important for backpropagation type of artificial neural network because derivative is described as the variance on the curve. In other words, it means minimizing the error, the derivative of the error equals to 0. Backpropagation learns the derivative of the error on the weight, w_{ij} so errors approach zero at the end of the each iteration. For this reason, backpropagation has successful area of usage and the architecture shown in Figure 2.11.

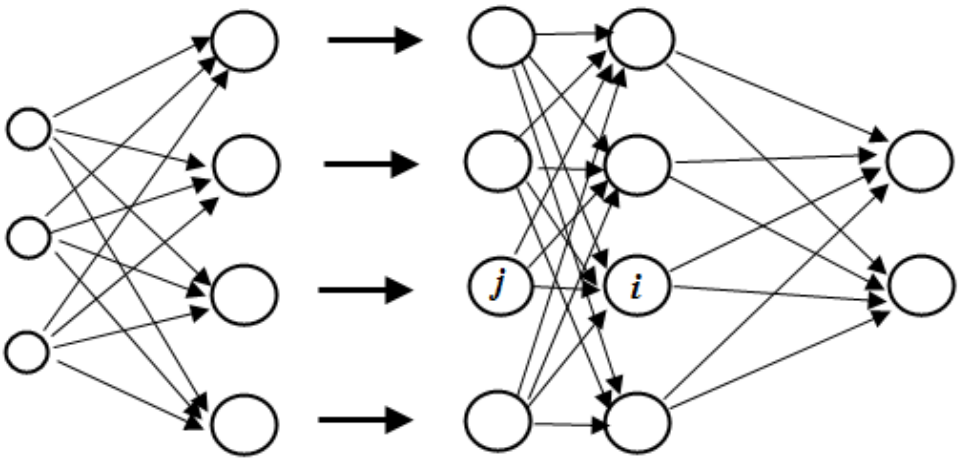

Figure 2.11 The architecture of the backpropagation algorithm

Sigmoid function used in backpropagation algorithm and the derivative of this function are given the expressions 2.10 and 2.11.

$$f_{sigmoid}(x) = \frac{2}{1+e^{-x}} - 1 \tag{2.10}$$

$$f'_{sigmoid}(x) = \frac{1}{2}\left|1 + f_{sigmoid}(x)\right|\left|1 - f_{sigmoid}(x)\right| \tag{2.11}$$

In this thesis, the multilayer feed forward network is used as ANN model. There are one input layer, two hidden layers and one output layer with each neuron fully connected with neurons of adjacent layer. Four input neurons and two output neurons are for the input and output variables. In modeling, the input elements are given as surface roughness, depth of cut, tool diameter and work-piece material. Output elements are composed of cutting speed and feed rate. Sigmoid function is used for multilayer feed forward network in this study. Backpropagation algorithm is selected as a training algorithm.

2.4 Surface Roughness

According to selected process, type of the tool and machining conditions; machining surface errors are formed from the effect of physical, chemical, temperature and mechanical movement between tool and workpiece on the machined surface during shaping by material removing. This state creates an irregular deviation above and below the nominal surface line, is called as *Surface Roughness*.

Same materials may be machined with different types of methods for the same surface roughness value. These are sometimes different behaviors on corrosion, friction, wear and fatigue resistance for the same materials. Machining direction on surface and distribution of what affect the performance of material as well as surface roughness.

In general, optimum surface quality is aimed to achieve in finishing based on cutting speed and feed rate by decreasing the effects of negative factors such as cutting tool error, vibration, material on the cutting tool during the machining process.

2.4.1 Factors Affecting Surface Roughness

More than one factor affect surface roughness. The most important of them are listed below.

- Deformation on machined material because of fixturing,
- Movement mechanism faults,
- Structural faults of machined material,
- Irregular chip flow during machining operation of brittle materials,
- Chip flow failure,
- Cutting speed,
- Feed rate,
- Depth of cut,
- Cooling and lubricating conditions of the cutting tool,
- Chemical composition and metallurgic structure of workpiece,
- Cutting tool design, geometry and capacity,
- Type of machine, rigidity of machine, and working condition,
- Fixtures and apparatus,
- Cutting strategies,
- Geometric failure in bearing and tool, etc.

2.4.2 Surface Roughness Parameters

Surface roughness most commonly refers to the variations in the height of the surface relative to a reference plane. It is measured either along a single line profile

or along a set of parallel line profiles (surface maps). It is usually characterized by one of the two statistical height descriptors advocated by the American National Standards Institute (ANSI) and the International Standardization Organization (ISO). These are (1) R_a, CLA (center-line average), or AA (arithmetic average) and (2) the standard deviation or variance (σ), R_q or root mean square (RMS). Two other statistical height descriptors are skewness (S_k) and kurtosis (K); these are rarely used. Another measure of surface roughness is an extreme-value height descriptor R_t (or R_y, R_{max}, or maximum peak-to-valley height or simply P–V distance). Four other extreme-value height descriptors in limited use, are: R_p (maximum peak height, maximum peak-to-mean height or simply P–M distance), R_v (maximum valley depth or mean-to-lowest valley height), R_z (average peak-to-valley height), and R_{pm} (average peak-to-mean height). A profile is considered, z(x), in which profile heights are measured from a reference line Figure 2.12.

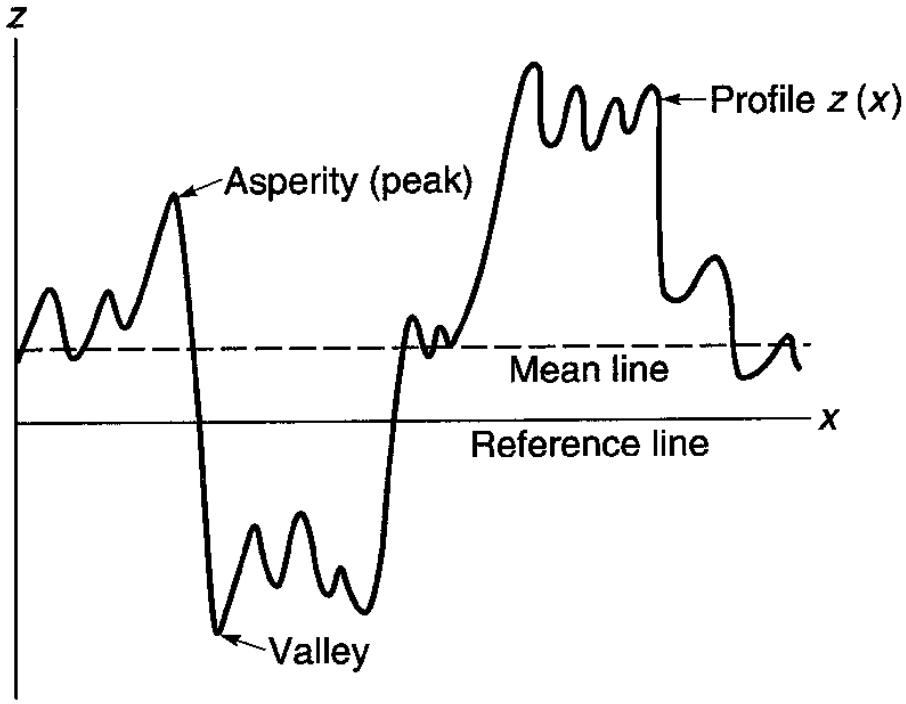

Figure 2.12 Schematic of a surface profile z(x) (Bhushan, 2001)

A center line or mean line are defined such that the area between the profile and the mean line above the line is equal to that below the mean line. R_a, CLA, or AA is the arithmetic mean of the absolute values of vertical deviation from the mean line

through the profile. The standard deviation σ is the square root of the arithmetic mean of the square of the vertical deviation from the mean line.

In mathematical form, written:

$$R_a = CLA = AA = \frac{1}{L}\int_0^1 |z - m|\, dx \tag{2.12}$$

and

$$m = \frac{1}{L}\int_0^1 z\, dx \tag{2.13}$$

where L is the sampling length of the profile (profile length).

The variance is given as

$$\sigma^2 = \frac{1}{L}\int_0^1 (z - m)^2\, dx = R_q^2 - m^2 \tag{2.14}$$

where, σ is the standard deviation and R_q is the square root of the arithmetic mean of the square of the vertical deviation from a reference line, or

$$R_q^2 = RMS^2 = \frac{1}{L}\int_0^1 (z^2)\, dx \tag{2.15}$$

For the special case where *m* is equal to zero,

$$R_q = \sigma \tag{2.16}$$

In many cases, the R_a and σ are interchangeable, and for Gaussian surfaces

$$\sigma \sim \sqrt{\frac{\pi}{2}} R_q \sim 1.25 R_a \tag{2.17}$$

The value of R_a is an official standard in most industrialized countries. Table 2.1 gives internationally adopted R_a values together with the alternative roughness grade number. The σ is most commonly used in statistical analyses.

Table 2.1 Center-line average and roughness grade

R_a Values up to a Value in μm	Roughness Grade Number
0.025	N1
0.05	N2
0.1	N3
0.2	N4
0.4	N5
0.8	N6
1.6	N7
3.2	N8
6.3	N9
12.5	N10
25.0	N11

The skewness and kurtosis in the normalized form are given as

$$S_k = \frac{1}{\sigma^3 L}\int_0^L (z-m)^3\,dx \tag{2.18}$$

and

$$K = \frac{1}{\sigma^4 L}\int_0^L (z-m)^4\,dx \tag{2.19}$$

More discussion of these two descriptors will be presented later.

Five extreme-value height descriptors are defined as follows: R_t is the distance between the highest asperity (peak or summit) and the lowest valley; R_p is defined as the distance between the highest asperity and the mean line; R_v is defined as the distance between the mean line and the lowest valley; R_z is defined as the distance

between the averages of five highest asperities and the five lowest valleys; and R_{pm} is defined as the distance between the averages of the five highest asperities and the mean line. The reason for taking an average value of asperities and valleys is to minimize the effect of unrepresentative asperities or valleys which occasionally occur and can give an erroneous value if taken singly. R_z and R_{pm} are more reproducible and are advocated by ISO. In many tribological applications, height of the highest asperities above the mean line is an important parameter because damage may be done to the interface by the few high asperities present on one of the two surfaces; on the other hand, valleys may affect lubrication retention and flow. Various surface profiles having the same R_a value are shown in Figure 2.13.

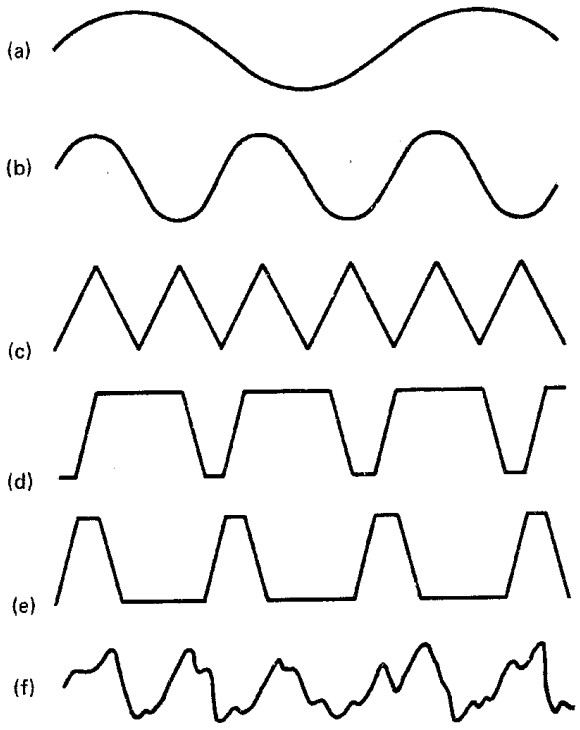

Figure 2.13 Various surface profiles having the same R_a value (Bhushan,2001)

The height parameters R_a (or σ in some cases) and R_t (or R_p in some cases) are most commonly specified for machine components. For the complete characterization of a profile or a surface, none of the parameters discussed earlier are sufficient. These parameters are seen to be primarily concerned with the relative departure of the profile in the vertical direction only; they do not provide any information about the slopes, shapes, and sizes of the asperities or about the

frequency and regularity of their occurrence. It is possible, for surfaces of widely differing profiles with different frequencies and different shapes, to give the same R_a or σ (R_q) values **(**Figure 2.13**)**. These single numerical parameters are useful mainly for classifying surfaces of the same type that are produced by the same method. Average roughness parameters for surface maps are calculated using the same mathematical approach as that for a profile presented here.

CHAPTER THREE
DYNAMIC CHARACTERISTICS OF THE SYSTEM

3.1 Introduction

Different methods can be used determine the dynamic characteristics of the system such as analytical, numerical and experimental methods. For instance, if a system is a fixed-free beam, the first natural frequency of the beam can be obtained analytically as given below,

$$f_{n1} = \frac{3.53}{2\pi} \times \sqrt{\frac{EI}{mL^3}} \quad \text{(Hz)} \tag{3.1}$$

where *E* stands for the Young's modulus of the beam material, *I* stands for the area moment of inertia of the beam, *m* stands for the mass of the beam and *L* stands for the length of the beam. Unfortunately, analytical expressions cannot be derived for the structures having complex geometries. Numerical methods may be useful to analyze the static and/or dynamic behaviors of such geometries. The most effective method for solid mechanics application is the Finite Element Method. Firstly, the structure is modeled by a modeling software or in a preprocessing program. If the problem is a beam, even a line can be modeled. Solid and shell structures can be modeled as well. Later, meshing process is done. For solid mechanics, it is always good to choose rectangular mesh for 2D problems and hexahedron mesh for 3D problems. After, boundary conditions, external forces and material properties are defined to the structure and rigorous matrix operations can be performed to find the nodal and/or elemental responses. A sample finite element model is given in Figure 3.1.

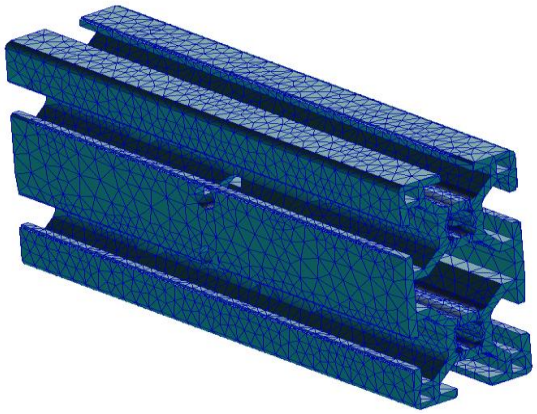

Figure 3.1 Sample finite element model

Another way to obtain dynamic characteristics of the systems is experimental methods. It is the most reliable method because it includes material defects and geometric errors.

There are different equipment to determine the modal behavior of a structure such as impact hammer and shaker. A transducer is a device that converts one type of energy to another. The conversion can be to/from electrical, electro-mechanical, electromagnetic, photonic, photovoltaic, or any other form of energy. While the term transducer commonly implies use as a sensor/detector, any device which converts energy can be considered as a transducer. Accelerometer, velocimeter or force transducer is used to convert mechanical data to electrical one.

By an impact hammer, natural frequencies can be calculated by the help of computer software. For example, an impact hammer can be applied to the different points of a fixed-free beam. Nodal points and the most deflected points can be found and then the free vibration characteristics of the system can be obtained.

An accelerometer is used to obtain acceleration data from any point of the considered structure. This data can be used to calculate velocity and displacement in time or in frequency domain.

Peak-picking means electing the frequencies of the peaks, either from the whole spectrum or from selected regions. These frequencies are generally reported on the

plot. Not all the peaks are evaluated. When they are so tall that they get out of the plot, they are filtered out. There is also a minimal threshold value: the weakest signals are ignored. It is fundamental to understand how this threshold is set.

The mode shapes can also be calculated from FRF data. The imaginary part of FRF is important in this manner. The peak amplitude of the imaginary part of the FRF defines mode shapes as it seen in Figure 3.2.

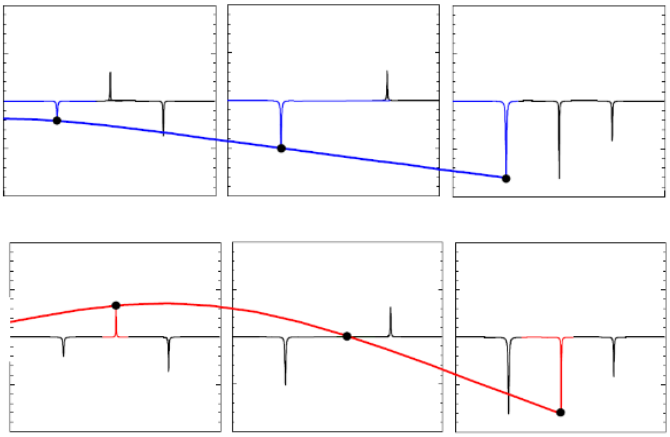

Figure 3.2 Mode shape calculations (Avitable, 2003)

The peak amplitude method is used to determine damping loss factors and damping ratios. The width of the frequency response magnitude curve is taken when the magnitude is 1/0.707 times the peak value. After frequencies ω_1 and ω_2 are taken, they are used to find the damping properties as given below.

$$\text{Structural Loss factor:} \quad \eta = \frac{\omega_2^2 - \omega_1^2}{2\omega_n^2} \tag{3.2}$$

$$\text{Damping Ratio (viscous damping models):} \quad \xi = \frac{\eta}{2} \tag{3.3}$$

3.2 Finite Element Analysis of the System

In this part of the study, the system is modeled for the finite element analysis by using MSC Patran Software. Then, the finite element analysis is performed with

MSC Nastran Solver in order to calculate the modal response of the CNC milling machine.

3.2.1 Finite Element Models of the System

Analysis model is divided in two sub models such as main body and spindle assembly for finite element analysis studies.

Firstly, the finite element model of the main body of the CNC is shown in Figure 3.3. Here, sigma profiles used in the system are represented by 1D bar elements. Bridge of the CNC was modeled with quad4 type 2D surface mesh. A remote node was created for spindle assembly; inertia and mass values of the spindle assembly were defined to this node. Here, bar elements were connected to the bridge and each other with RB2 multi point constraints (MPCs). Also, point mass is connected to the body with RB3 MPCs.

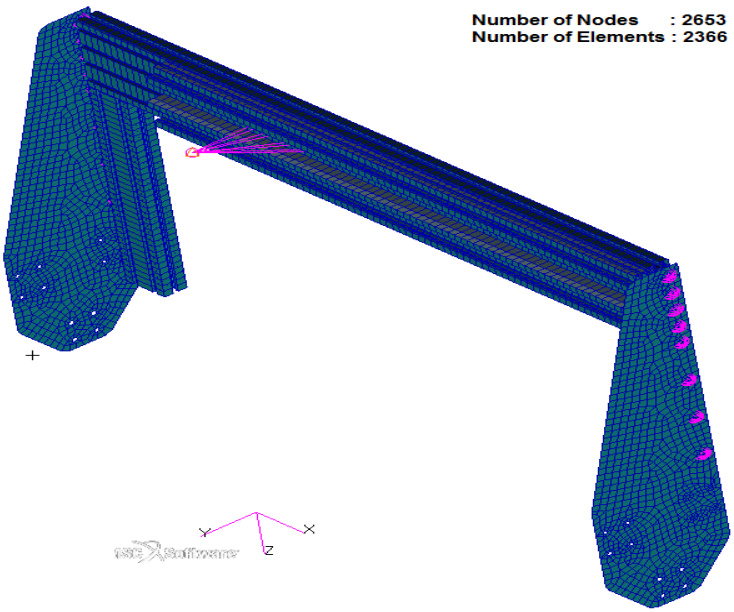

Figure 3.3 Finite element model of main body of the system

Analysis model of the spindle assembly is shown in detail in Figure 3.4. All parts were modeled with Tet10 type 3D solid elements. RB2 MPCs were used for all bolt connections.

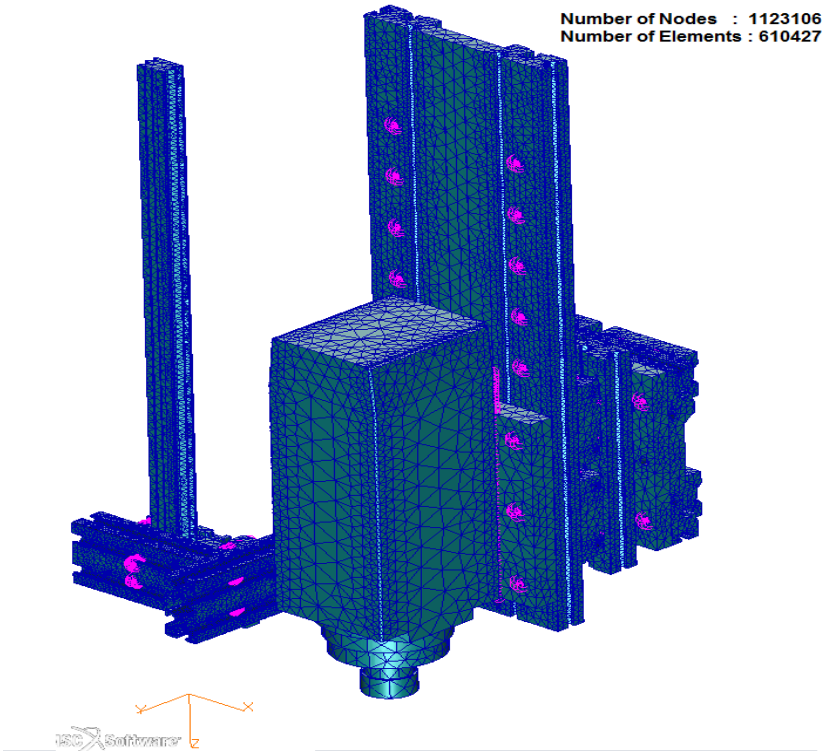

Figure 3.4 Finite element model of spindle assembly of the system

3.2.2 Natural Frequency Analysis of the System

Mode shape is the shape of the free vibration of a mechanical system at the corresponding natural frequency. Several mode shapes will be associated with different natural frequencies. The experimental technique of modal analysis discovers these mode shapes and the frequencies. There are different ways to determine mode shapes. Analytically, for a continuous system, mode shapes of simple geometries can be calculated. Moreover, finite element method is powerful technique to obtain natural frequencies and mode shapes for complex geometries. Another way to determine dynamic characteristics of the systems is experimental methods. Vibration data can be integrated or differentiated to obtain another type of data. For instance, once acceleration is found, velocity and displacements can be calculated by integration. Furthermore, time domain data can be converted to frequency domain by fast Fourier transform (FFT).

The first three mode shapes of the spindle assembly were computed as 13.77 Hz, 26.55 Hz and 66.92 Hz as shown in Figure 3.5.

(a)

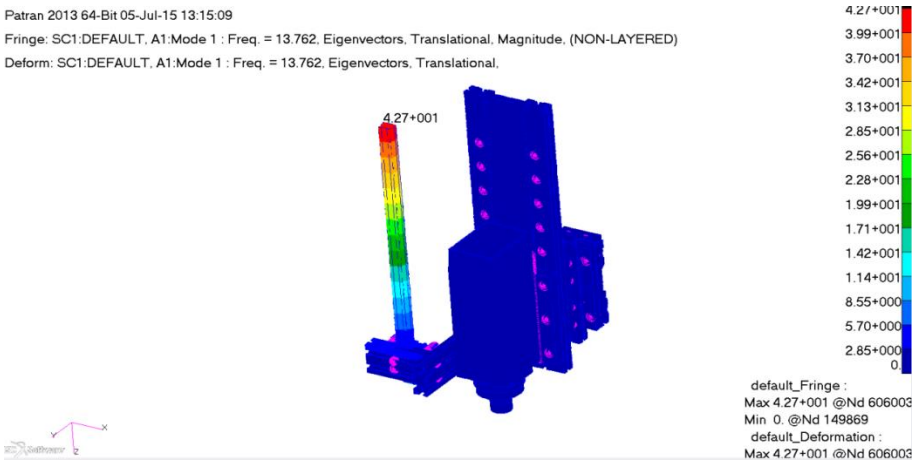

(b)

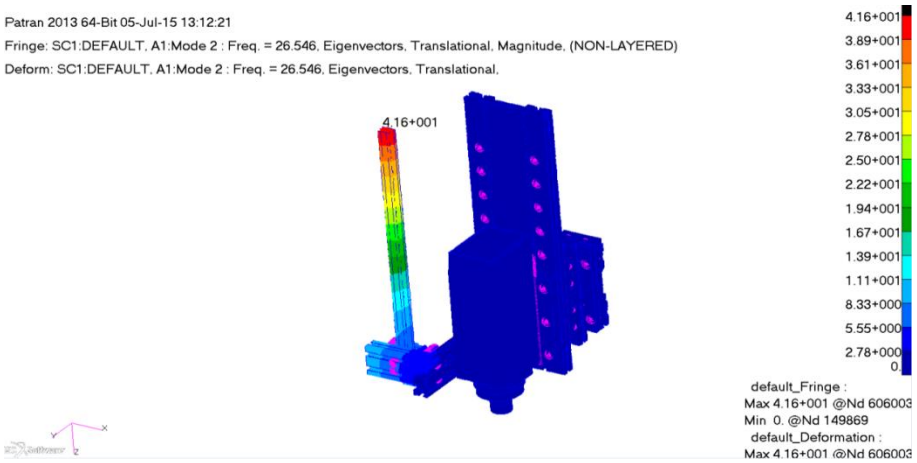

(c)

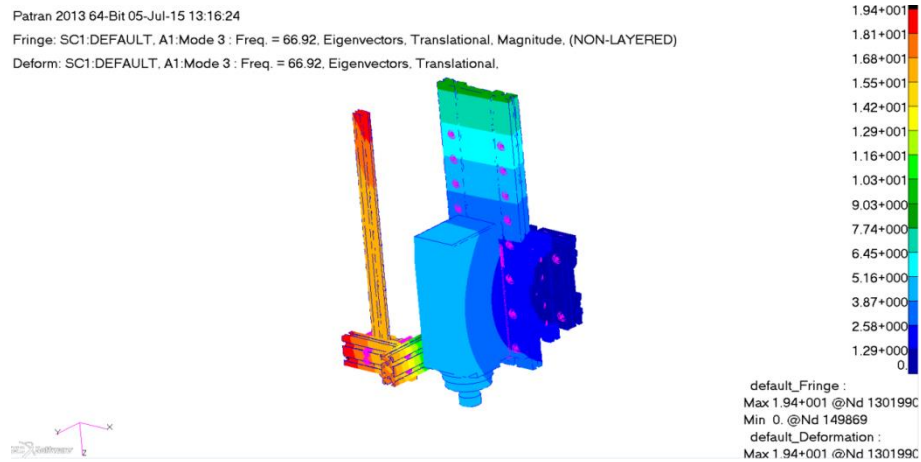

Figure 3.5 Natural frequency analysis results for the first three mode shapes of the spindle assembly (a) Mode 1 (b) Mode 2 (c) Mode 3

The first three mode shapes of main body are computed at 49.31 Hz, 62.47 Hz and 68.61 Hz shown in Figure 3.6.

(a)

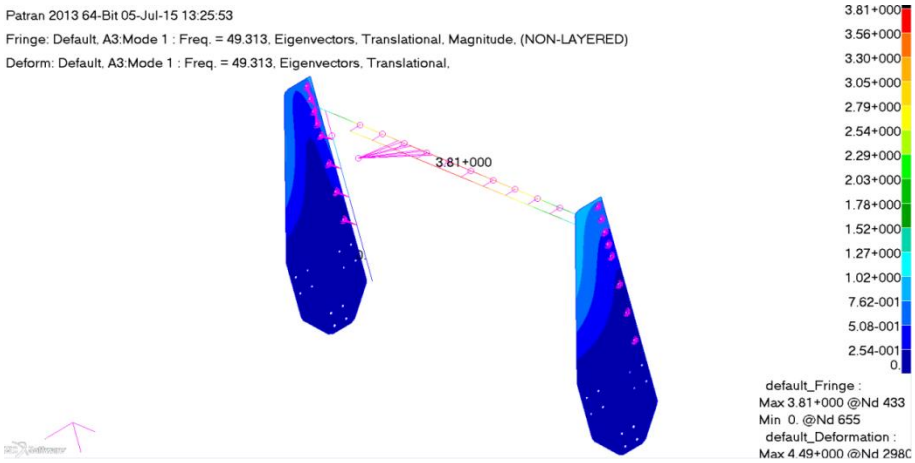

(b)

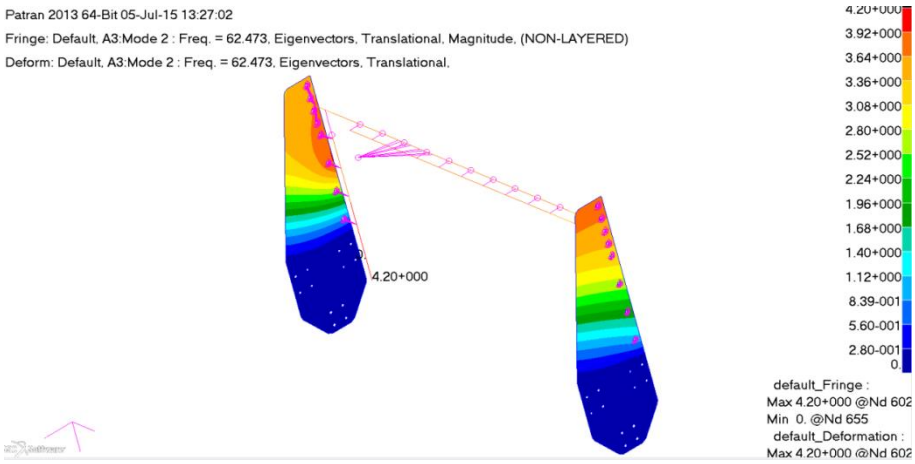

(c)

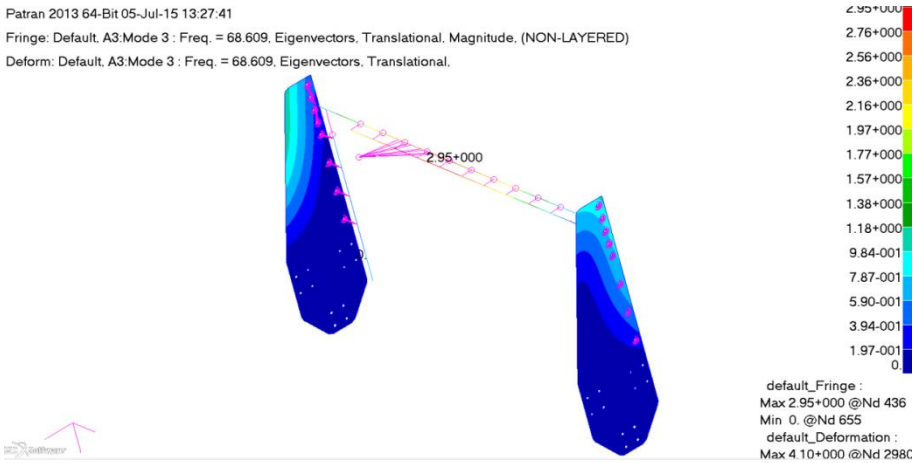

Figure 3.6 Natural frequency analysis results for the first three mode shapes of the main body (a) Mode 1 (b) Mode 2 (c) Mode 3

3.3 Experimental Studies for Vibration Measurement

Obtaining dynamic characteristics of a system by experimental method is the most reliable methods because it includes material defects and geometric errors. For this reason, an experimental setup is developed in accordance to line diagram shown in Figure 3.7. Experimental setup is composed of Surface Roughness Control System (SRCS), control computer of SRCS, vibration measurement equipment and data acquisition system.

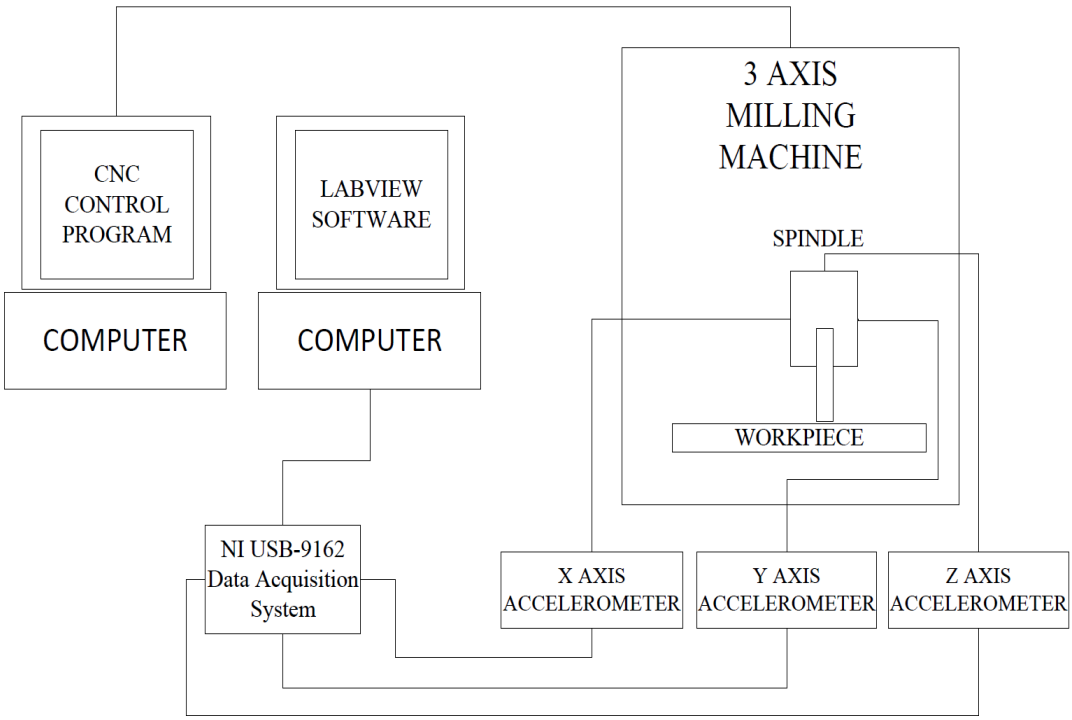

Figure 3.7 Line diagram of the vibration measurement system

In this study, natural frequencies of the CNC machine were investigated by performing impact test. An impact hammer of Brüel & Kjaer 8208, seen in Figure 3.8, was used for performing impact test.

Figure 3.8 Impact hammer for natural frequency measurement used for experimental studies

It is small in size; light, cheap and used for diagnostic purposes for measurement of FRF properties. On the other hand, it has some disadvantages such as high crest factor, possibility of permanent damage to the structure and problem in coherence function. Technical specifications of impact hammer used in this study are given in Table 3.1.

Table 3.1 Technical specifications of Brüel&Kjaer 8208 impact hammer

Technology	CCLD/IEPE
Sensitivity	0.225 mV/N
Range Full Scale	22.2 kN
Maximum Force	44.4 kN
Maximum Compression	22.2 kN
Frequency Range	0.6kHz
Operating Temperature Range	-73 to 60° C

Accelerometers were used to measure vibration response of a system. For this reason, accelerometers were mounted on Spindle surface for collecting acceleration data from x, y and z axes and on x axis of the sensor surface. The accelerometer used in the vibration measurement is PCB 333B42 as shown in Figure 3.9. Technical specifications of the accelerometer are given in Table 3.2.

Figure 3.9 PCB 333B42 accelerometer

Table 3.2 Technical specifications of PCB 333B42 accelerometer

Measurement Range	±10 g pk
Sensitivity (±10 %)	500 mV/g
Resonant Frequency	≥ 20 kHz
Frequency Range	0.5 to 3000 Hz
Broadband Resolution (1 to 10000 Hz)	0.00005 g rms
Operating Temperature Range	-18 to 66 ˚C
Connection Type	USB 2.0 Hi-Speed

Data acquisition system was used for collecting data from accelerometers and transferring these data to the measurement system computer shown in Figure 3.10. Data acquisition system, National Instruments NI USB 9162l, has four input channels.

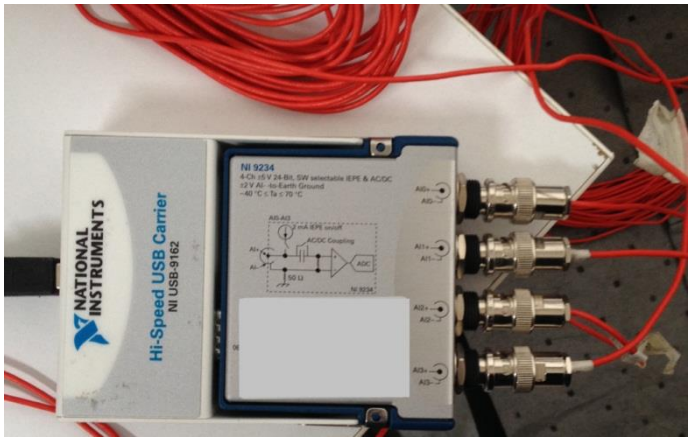

Figure 3.10 Data acquisition system used in vibration tests

LabView software was used for processing data gathered via data acquisition system. Raw acceleration data was recorded in ".txt" format in the LabView software.

Experimental setup for vibration measurement is shown in Figure 3.11.

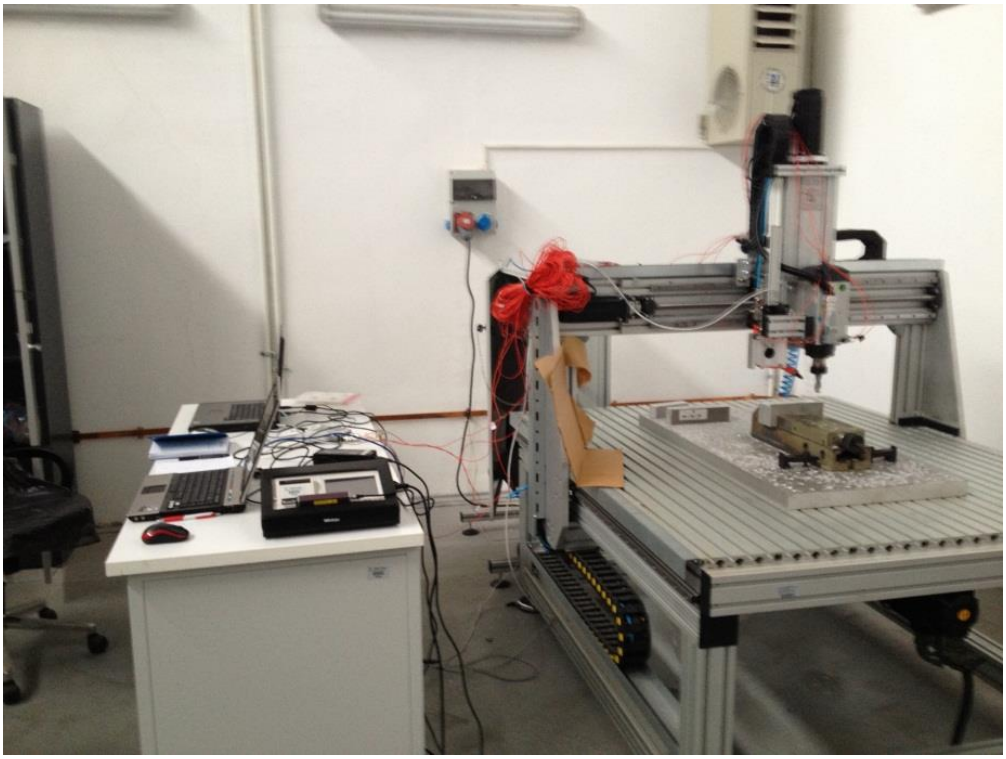

Figure 3.11 Developed experimental setup for vibration measurement

Also, mounted accelerometers on the experimental system are shown in Figure 3.12.

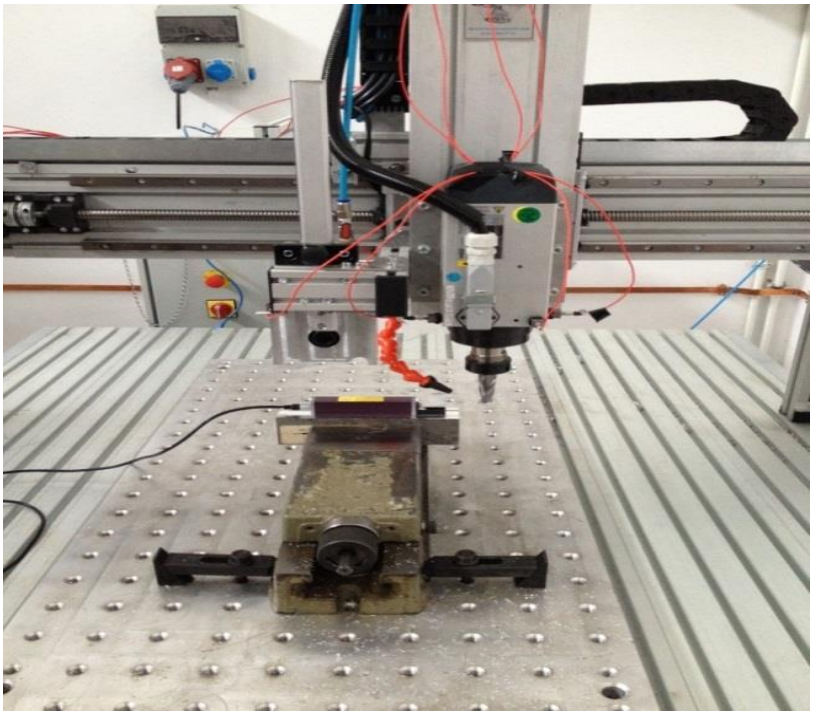

Figure 3.12 Mounted accelerometers on the system

Finally, acceleration data recorded with LabView software is converted to vibration data in frequency domain using MATLAB for interpreting the system's dynamic behavior.

3.4 Results of Natural Frequency Measurements

In this part, the results of the experimental studies are presented and compared with the results obtained from the finite element analysis. Here, impact tests were performed with impact hammer on the bridge of the CNC system and spindle body and then data was measured from accelerometers mounted on the spindle and optic roughness sensor.

Frequency spectra of the impact responses are analyzed in order to determine the natural frequencies of the structure. Logarithmic scale is used to see the peaks clearly. The average of five acceleration data is used in analyzes. It will be compared with the Power Spectral Density (PSD) data later.

In Figure 3.13,the fast fourier transform (FFT) response of the system is given. The impact test was performed in x axis direction and collected from three different points.

(a)

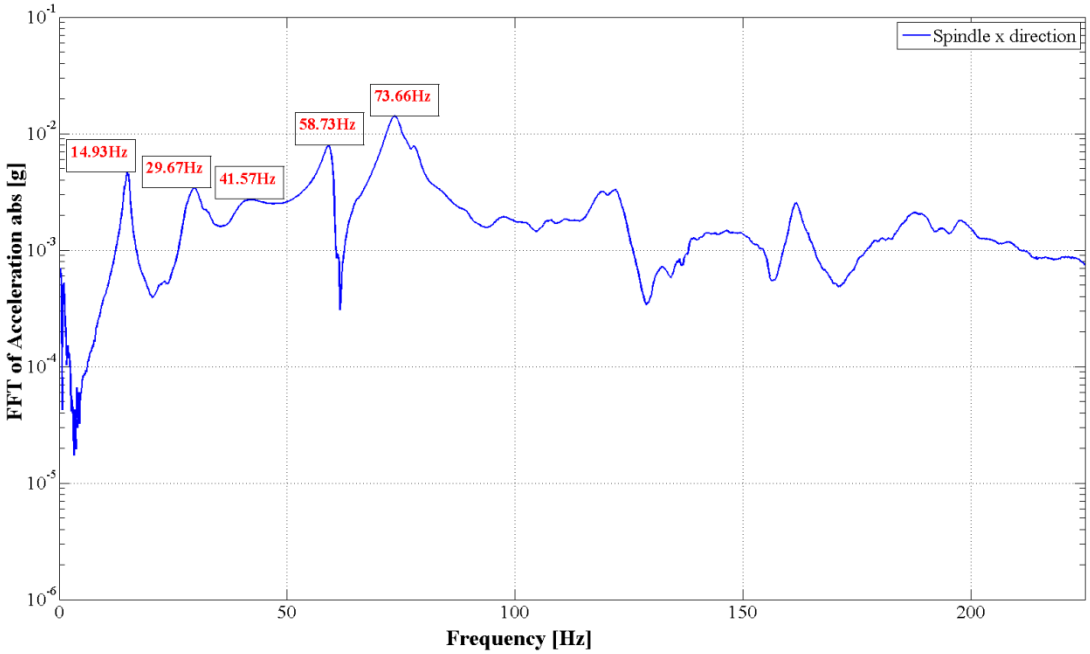

(b)

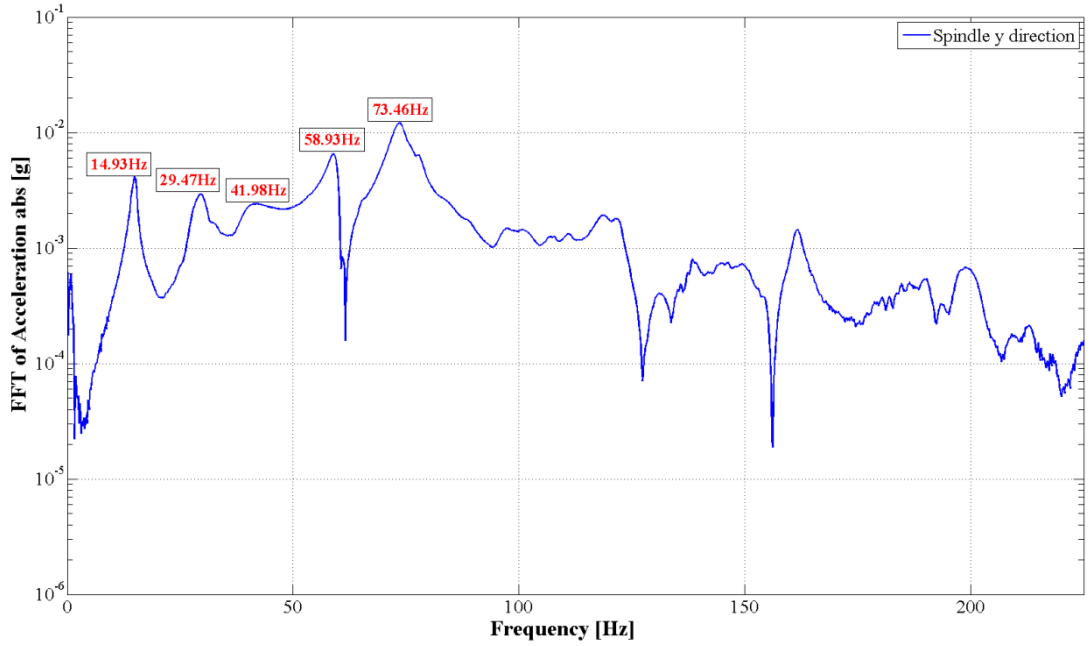

Figure 3.13 Hammer test for x axis direction (a) spindle x axis (b) spindle y axis (c) z axis measurement

(c)

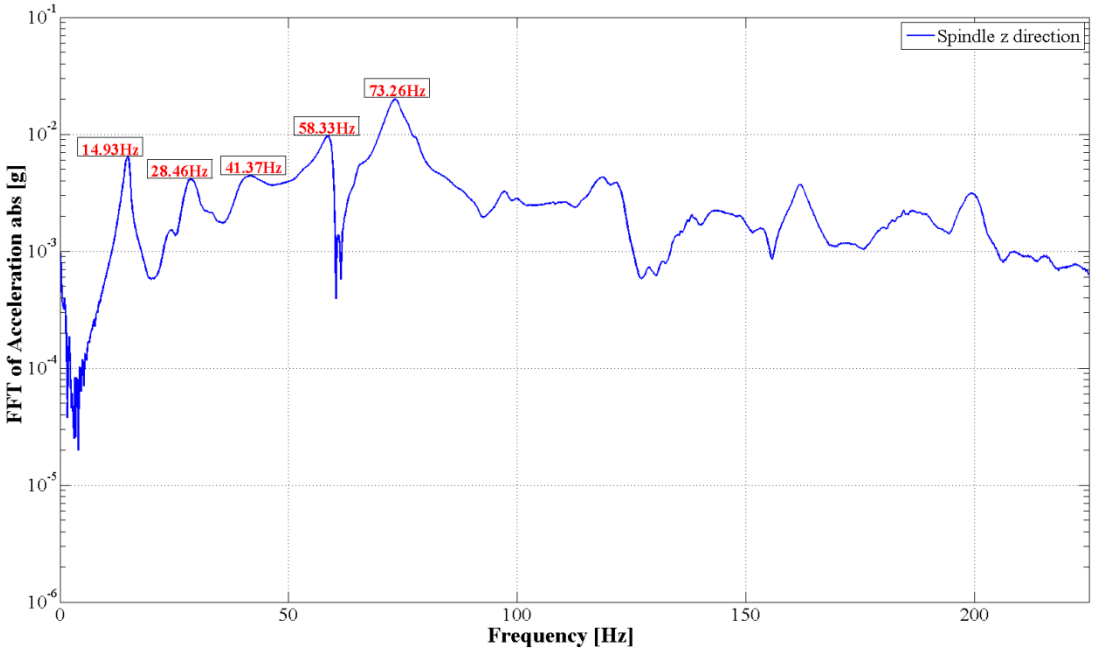

Figure 3.13 Hammer test for x axis direction (a) spindle x axis (b) spindle y axis (c) z axis measurement (Cont.)

In Figure 3.14, impact test was performed in y axis direction and impact responses were collected from three different locations.

(a)

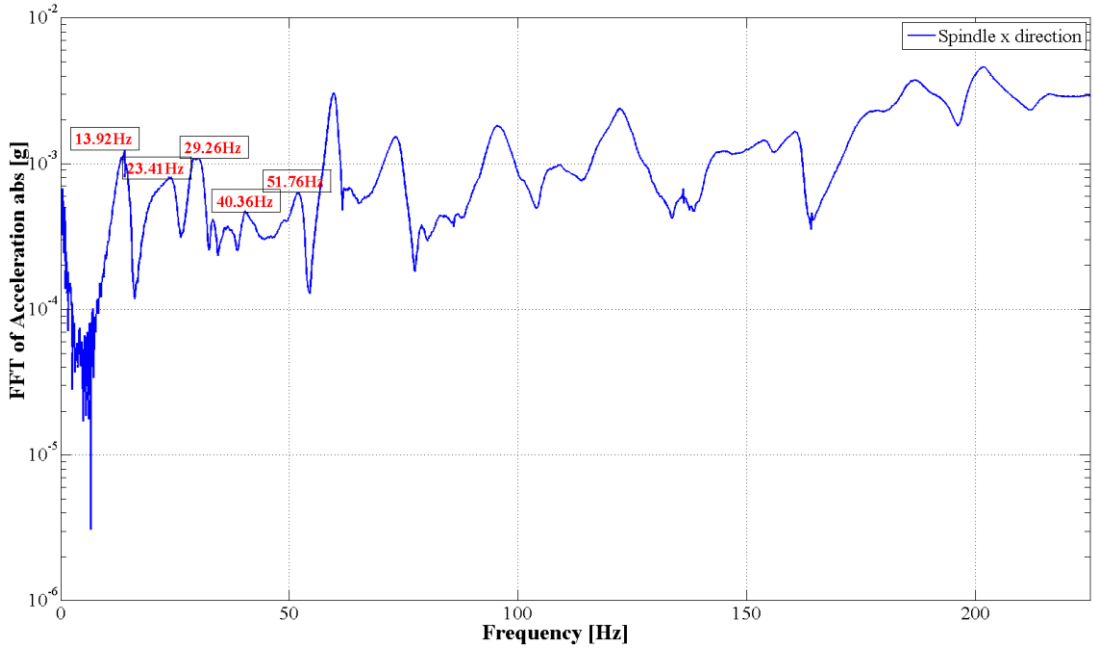

Figure 3.14 Hammer test for y axis direction (a) spindle x axis (b) spindle y axis (c) spindle z axis measurement

(b)

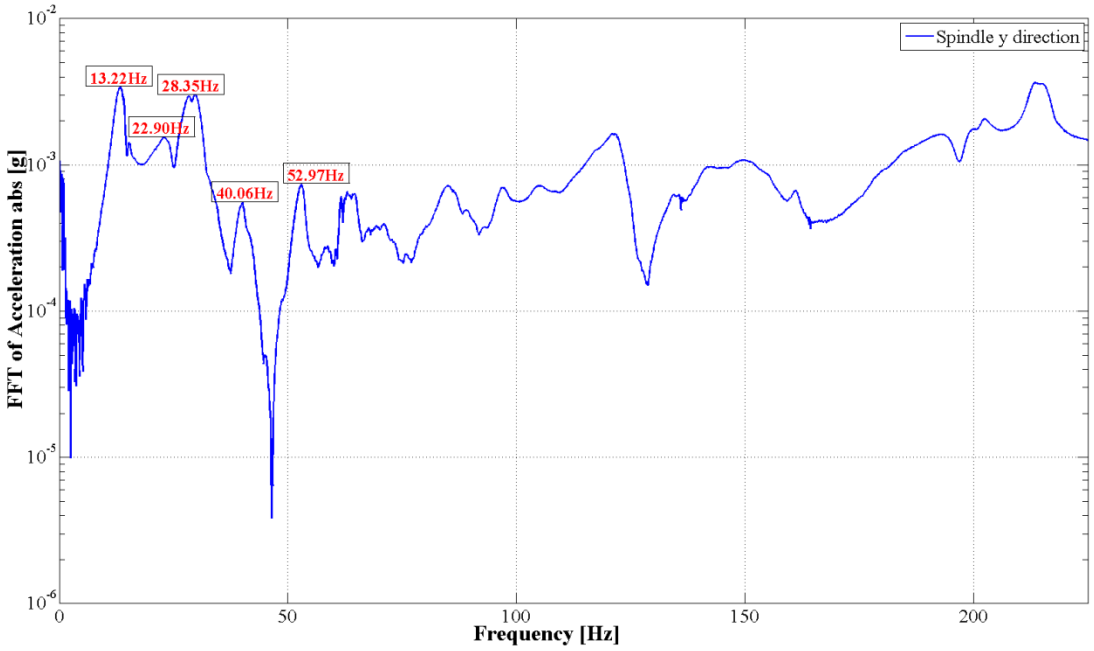

(c)

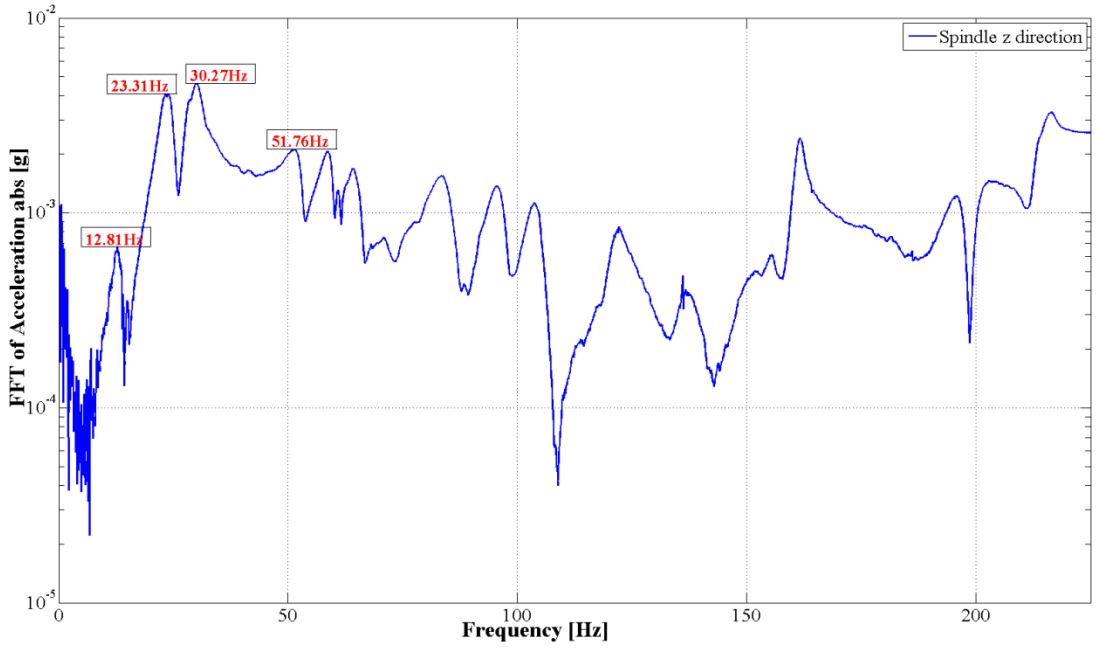

Figure 3.14 Hammer test for y axis direction (a) spindle x axis (b) spindle y axis (c) spindle z axis measurement (Cont.)

As it is seen in the Figure 3.13 and 3.14, first three natural frequencies of the structure are approximately fall within 13-15 Hz, 28-30 Hz and 59-61 Hz.

3.5 Vibration Measurements During Machining

In this part of the study, vibration measurements were performed while the system is idle state, which means that the depth of cut is zero and during machining. These studies were carried out with same experimental setup mentioned in section 3.3. 165 measurements were carried out with the values given in Table 3.3.

Table 3.3 The Experimental sets for vibration measurement for d=0 mm

Cutting Speed (m/min)	Feed Rate (mm/min)	Depth of Cut (mm)
	100	
	200	
0	300	
63	400	
126	500	
188	600	
251	700	
314	800	0
377	900	
440	1000	
503	1100	
565	1200	
628	1300	
	1400	
	1500	

The aim is to measure the accelerations on spindle and axis movements while the machining process is not in progress. In addition, the real vibration influence on the optical sensor is to be determined for each case. The results of the vibration measurements for idle state are given in Figure 3.15.

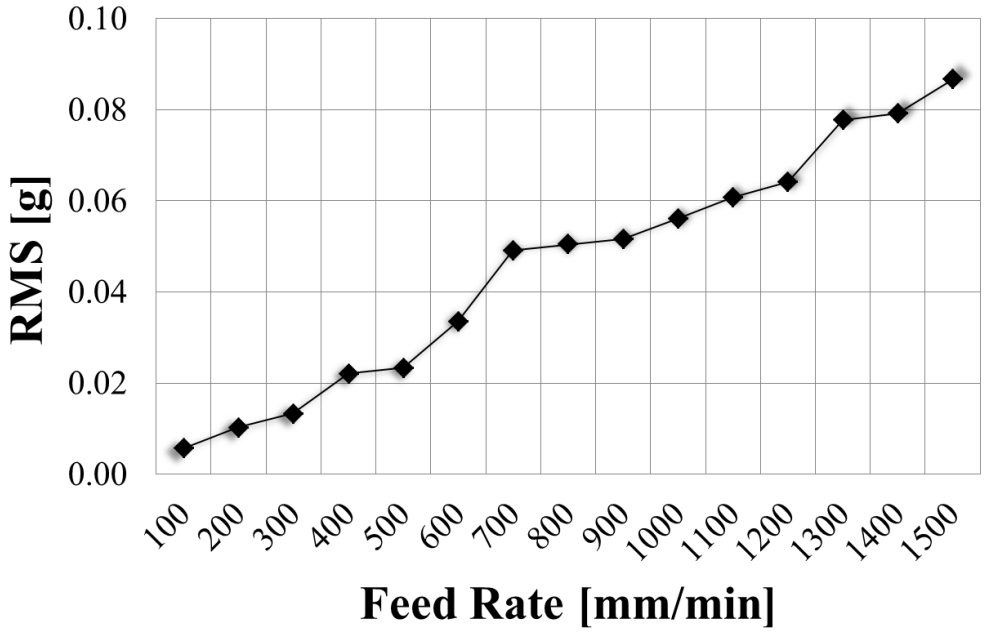

Figure 3.15 The variation between RMS of sensor z axis and feed rate is given for cutting speed, Vc=0 m/min and depth of cut, d=0 mm

96 experiments were performed using material AA5083 for two different depth of cut as 0.2 mm and 0.5 mm in accordance with the parameters given in Table 3.4. The coolant is not used in the experimental studies so dry machining is performed for the vibration measurement during the machining process.

Table 3.4 The Experimental Sets for vibation measurement during machining process

Cutting Speed (m/min)	Feed Rate (mm/min)	Depth of Cut (mm)	Workpiece Material
63 126 188 251 314 377 503 628	100 200 400 600 800 1000	0.2 0.5	AA5083

As a result of studies done in accordance with parameters given above, the effects of cutting speed, feed rate and depth of cut on the vibration of the system are discussed. Accelerations in x, y, z directions of spindle and x direction of optical sensor versus time is given for cutting speed Vc=628 m/min, feed rate f=1000 mm/min and depth of cut d=0.2 mm in Figure 3.16.

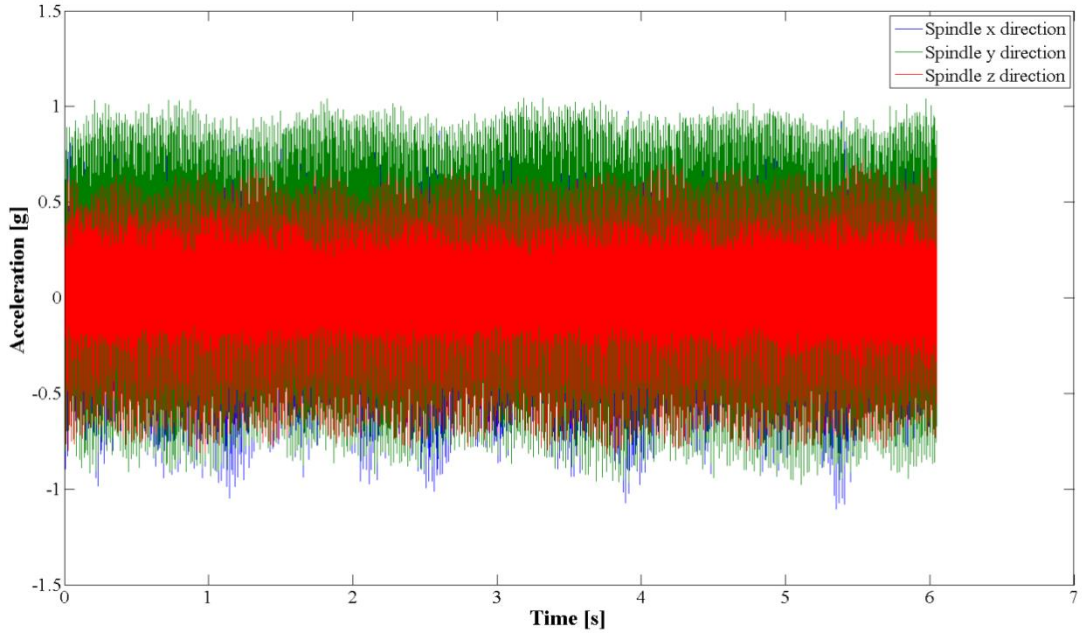

Figure 3.16 Spindle acceleration responses for cutting speed Vc=628 m/min, feed rate f=1000 mm/min and depth of cut d=0.2 mm

In Figure 3.17, Power Spectral Density (PSD) of accelerations for x, y, z directions of spindle are given for cutting speed, Vc=628 m/min, feed rate f=1000 mm/min and depth of cut d=0.2 mm.

(a)

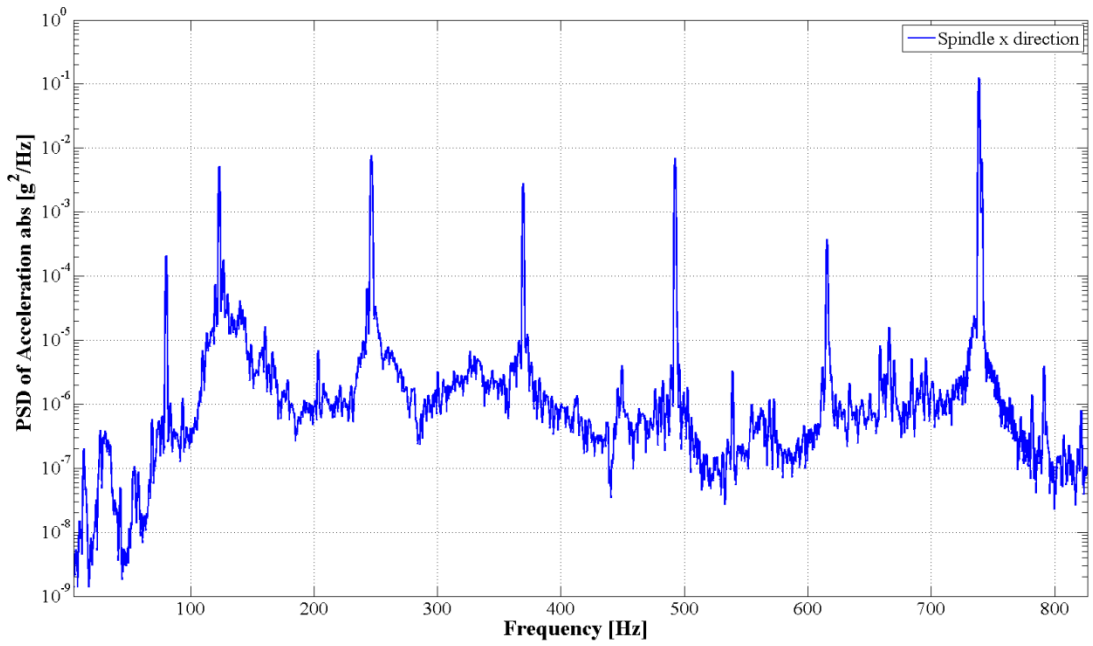

(b)

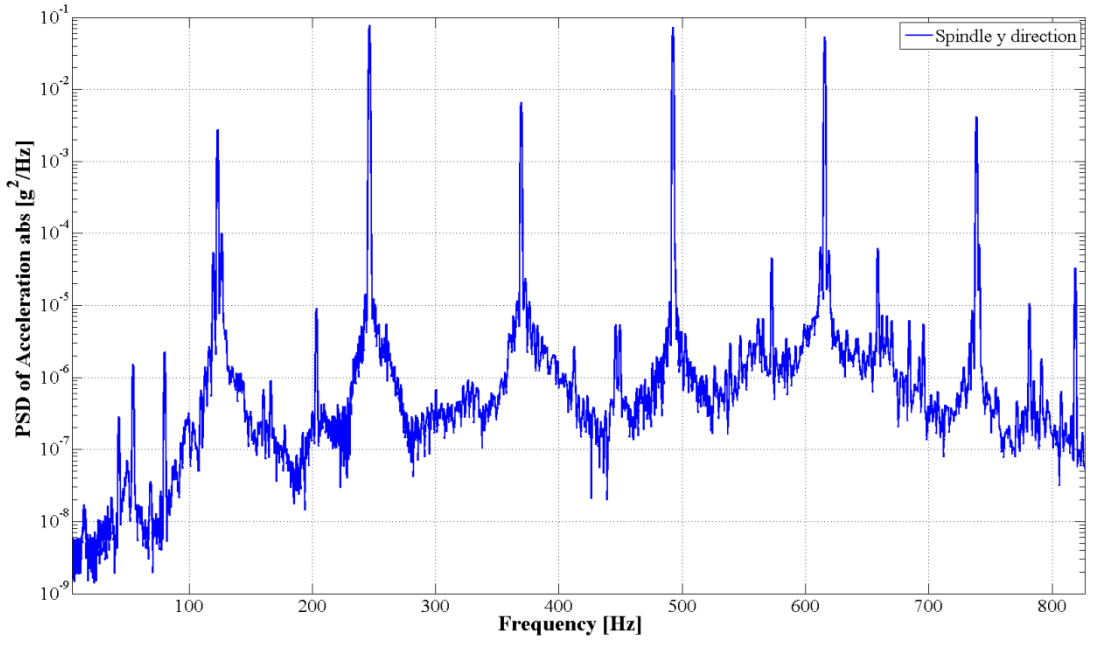

Figure 3.17 PSD Vc=628 m/min, f=1000 mm/min, d=0.2 mm depth of cut (a) x axis (b) y axis (c) z axis

(c)

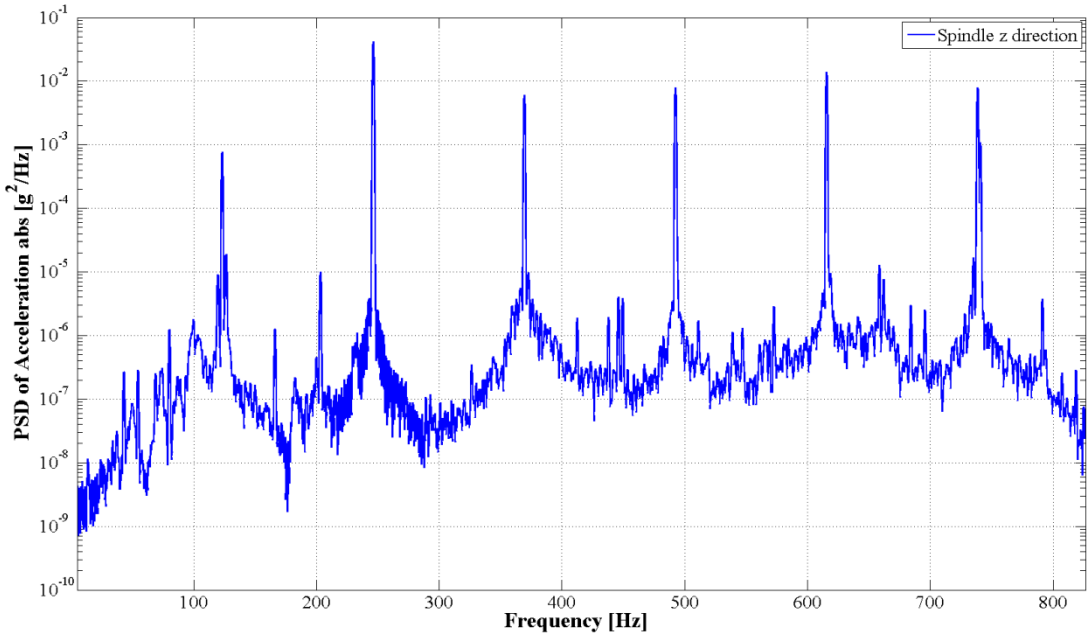

Figure 3.17 PSD Vc=628 m/min, f=1000 m/min, d=0.2 mm depth of cut (a) x axis (b) y axis (c) z axis (Cont.)

In Figure 3.18, acceleration responses are given for cutting speed, Vc=628 m/min, feed rate f=100 mm/min and depth of cut d=0.2mm.

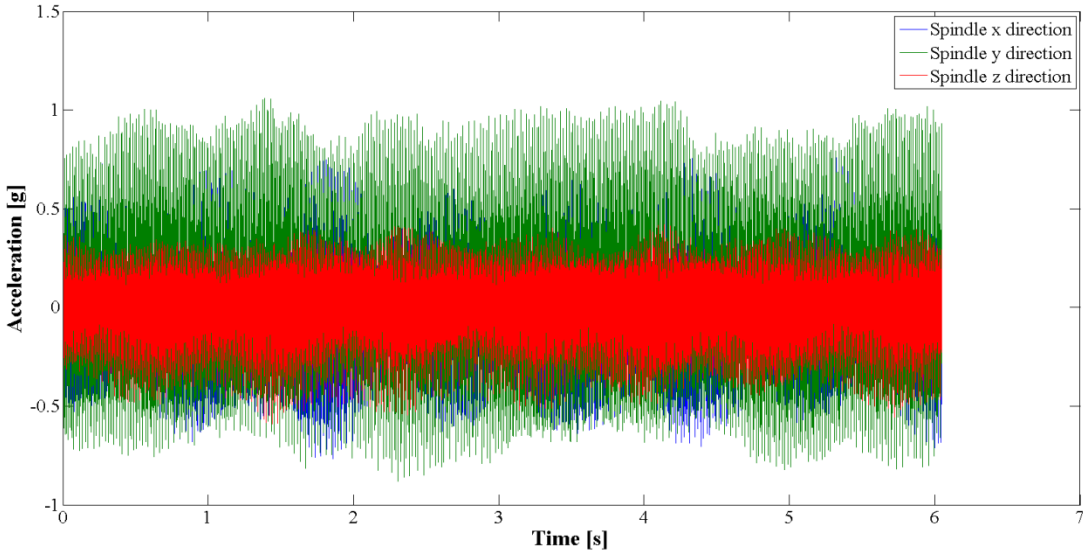

Figure 3.18 The acceleration responses for cutting speed Vc=628 m/min, feed rate f=100 mm/min and depth of cut d=0.2mm

In Figure 3.19, PSD of accelerations of spindle in x, y, z directions are given for cutting speed, Vc=628 m/min, feed rate f=100 mm/min and depth of cut d=0.2 mm.

(a)

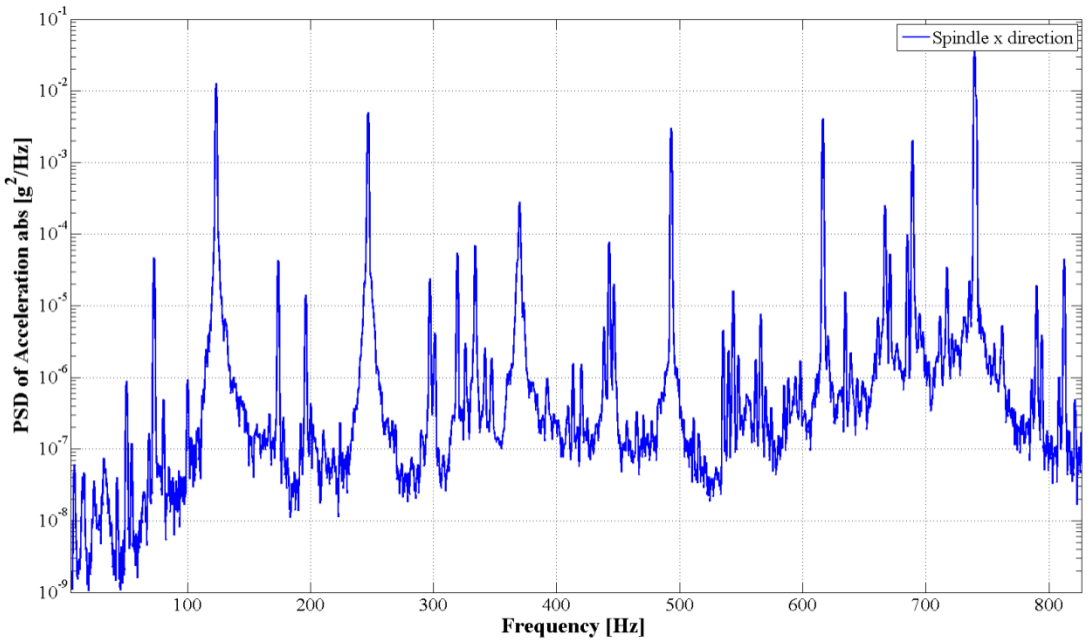

(b)

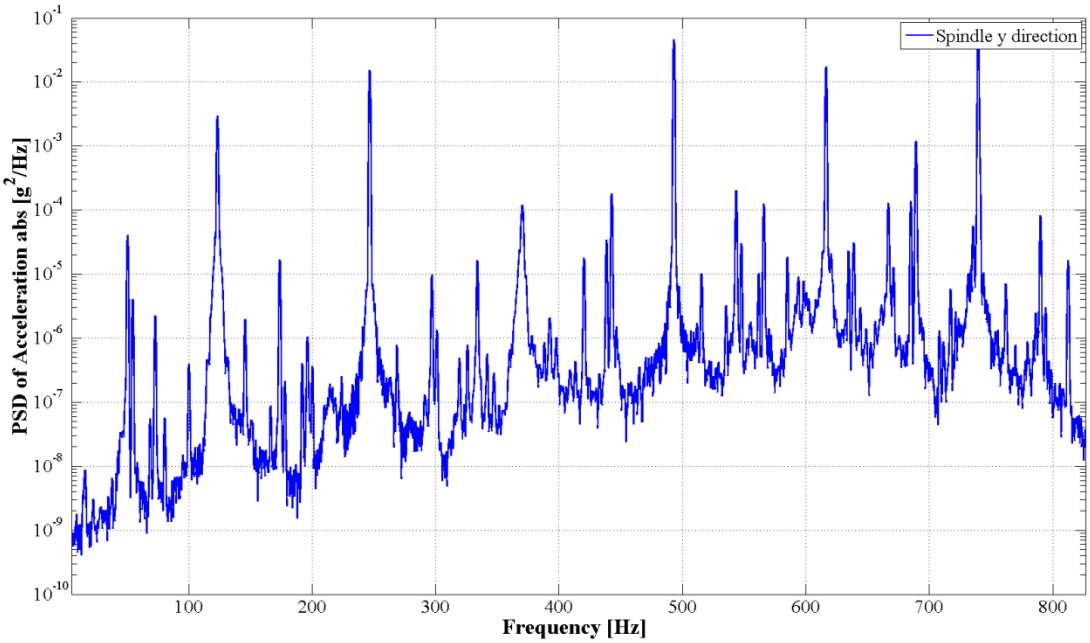

Figure 3.19 PSD Vc=628 m/min, f=100 mm/min and d=0.2 mm depth of cut (a) x axis (b) y axis (c) z axis

(c)

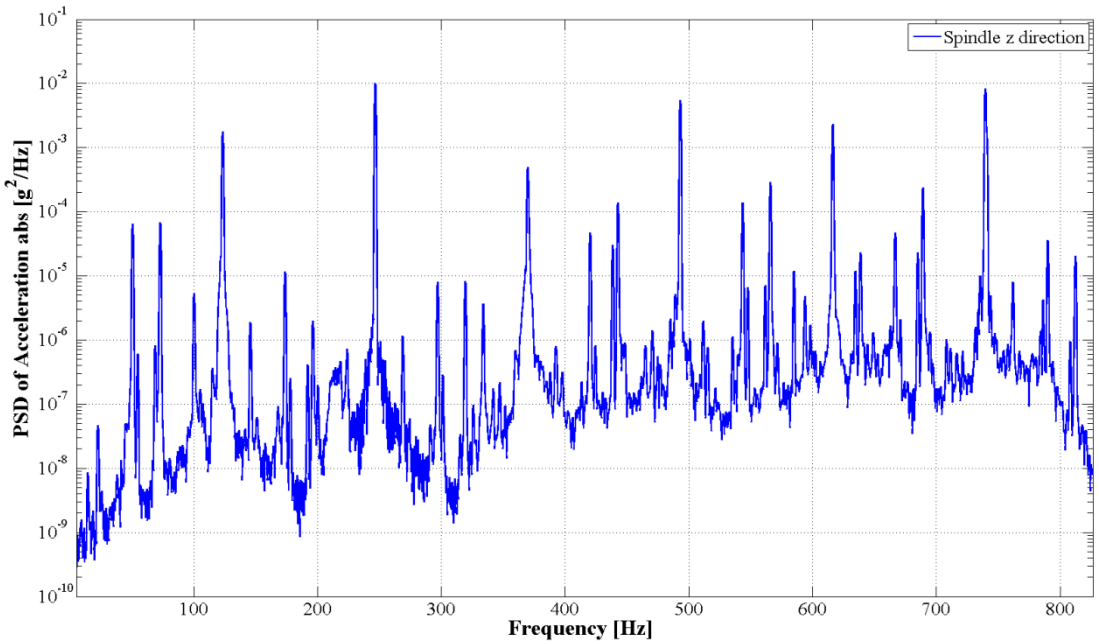

Figure 3.19 PSD Vc=628 m/min, f=100 mm/min and d=0.2 mm depth of cut (a) x axis (b) y axis (c) z axis (Cont.)

In Figure 3.20, acceleration responses of spindle in x, y, z directions are given for cutting speed, Vc=628 m/min, feed rate f=1000 mm/min and depth of cut d=0.5 mm.

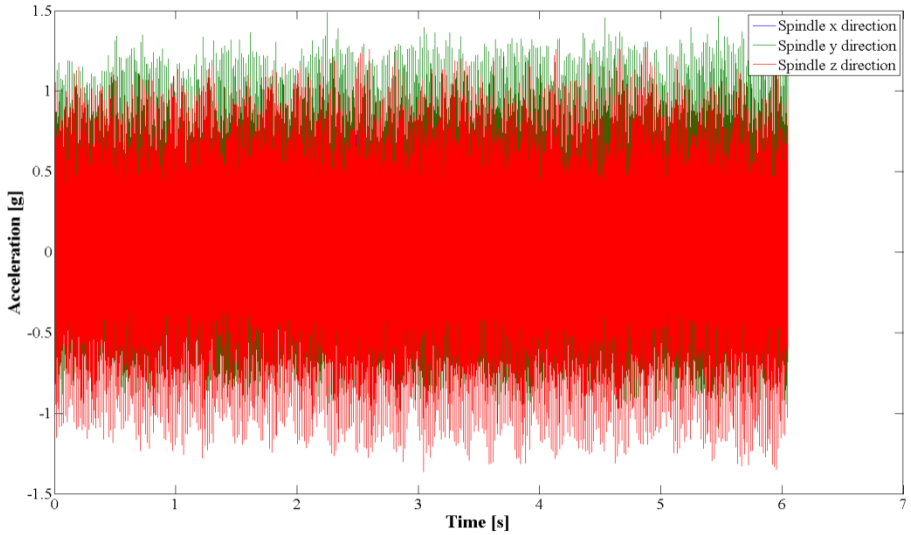

Figure 3.20 The accelerations for Vc=628 m/min, f=1000 mm/min and d=0.5 mm

In Figure 3.21, PSD of accelerations versus frequency for x, y, z directions of spindle are given for cutting speed, S=628 m/min; feed rate, f=1000 mm/min and depth of cut, d=0.5 mm.

(a)

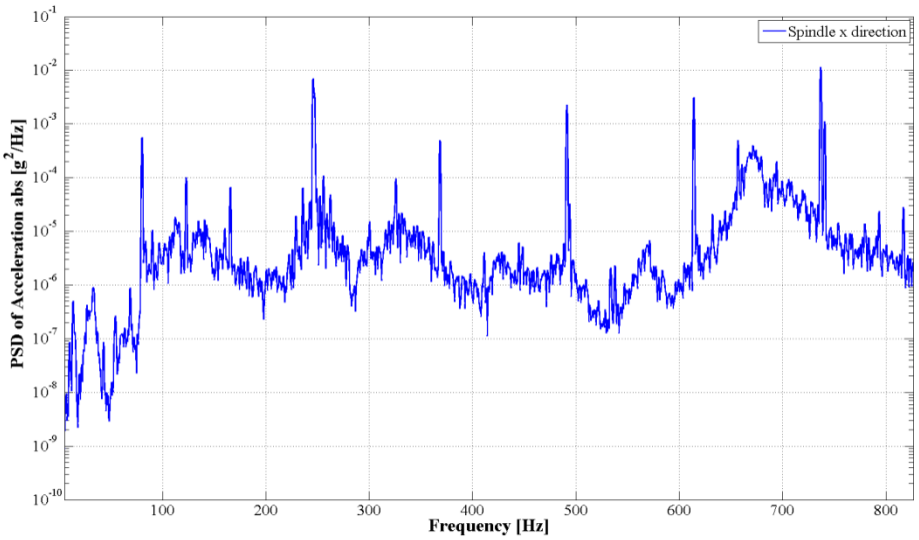

(b)

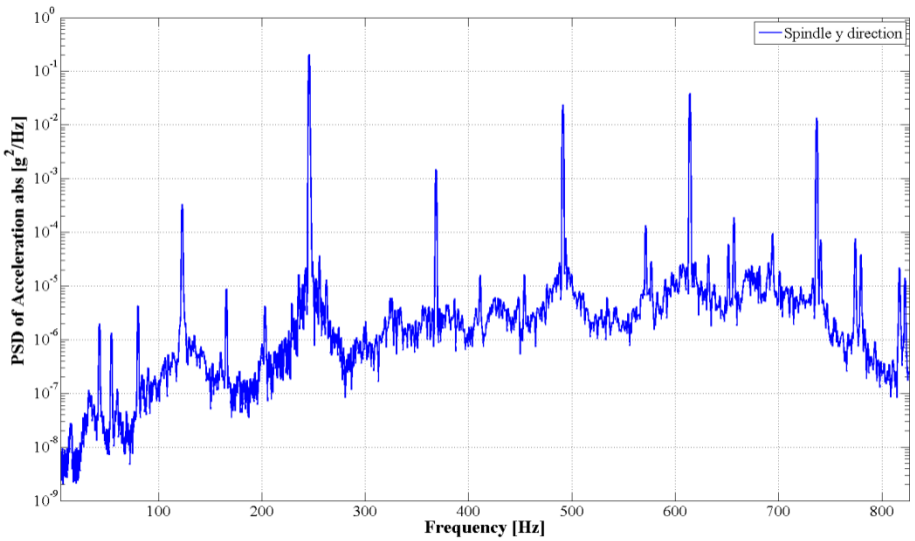

Figure 3.21 PSD for Vc=628 m/min, f=1000 mm/min and d=0.5 mm depth of cut (a) x axis (b) y axis (c) z axis

(c)

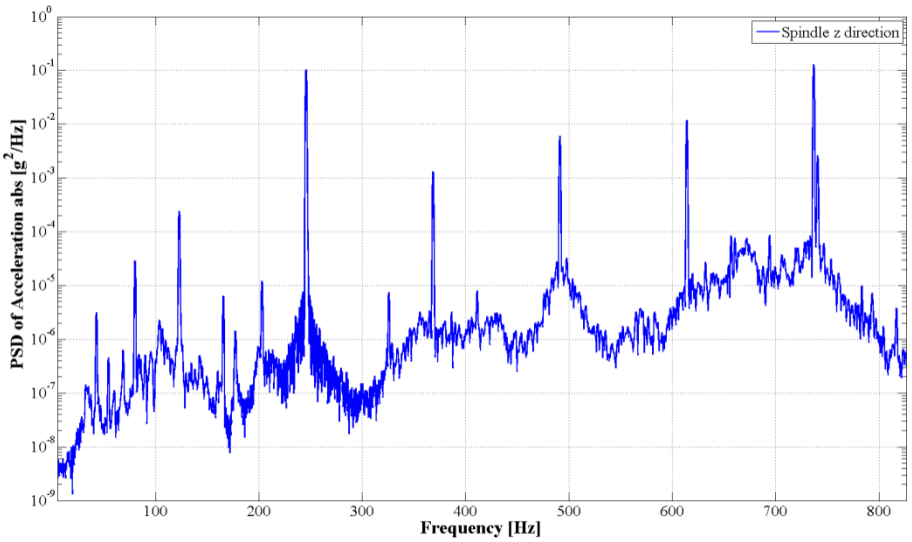

Figure 3.21 PSD Vc=628 m/min, f=1000 mm/min and d=0.5 mm depth of cut (a) x axis (b) y axis (c) z axis (Cont.)

In Figure 3.22, accelerations of spindle in x, y, z directions and x direction of optical sensor is given for cutting speed, Vc=63 m/min, feed rate f=1000 mm/min and depth of cut d=0.5 mm.

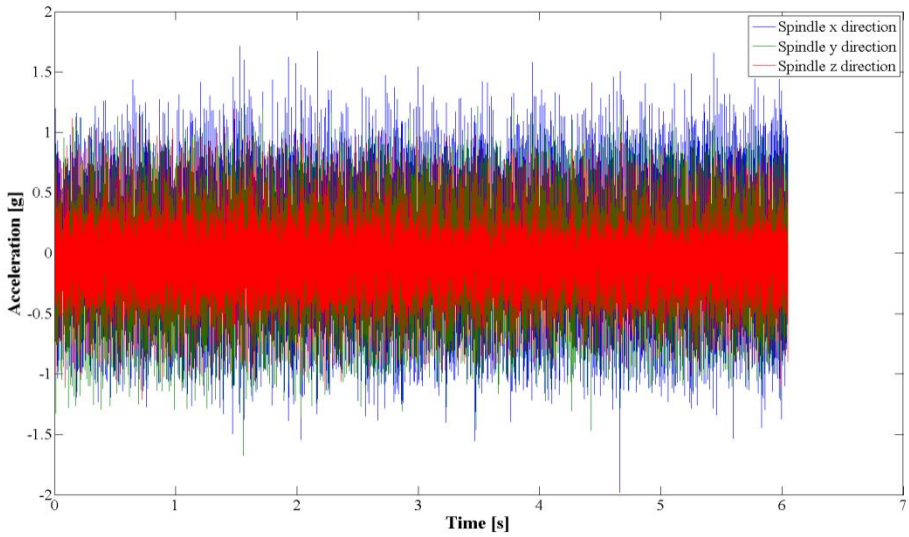

Figure 3.22 The acceleration responses for Vc=63 m/min, f=1000 mm/min and d=0.2 mm.

In Figure 3.23, PSD of accelerations versus frequency for x, y, z directions of spindle are given for cutting speed, Vc=63 m/min; feed rate, f=1000 mm/min and depth of cut, d=0.2 mm.

(a)

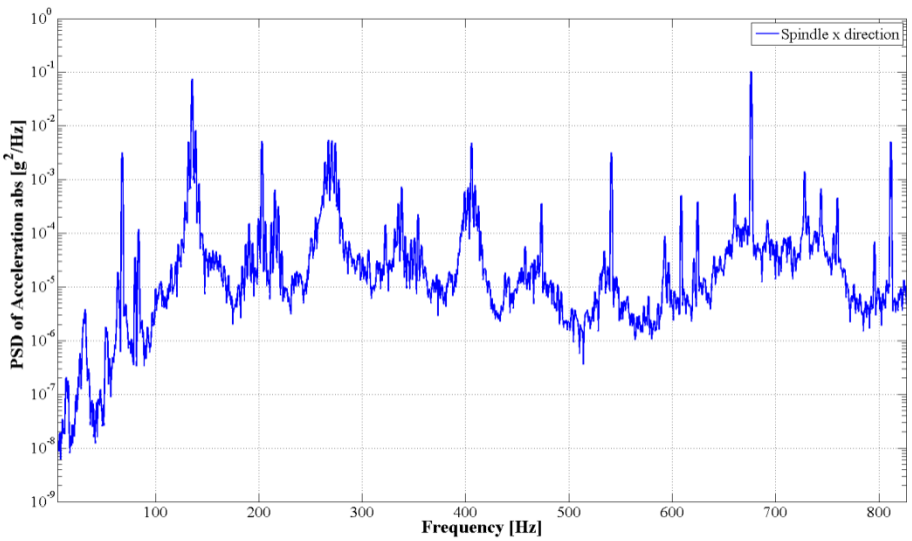

(b)

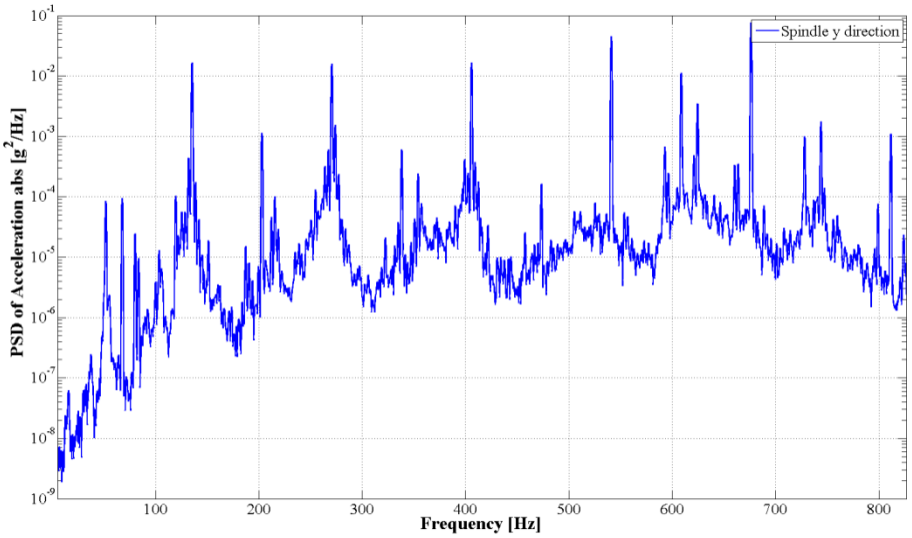

Figure 3.23 PSD Vc=63 m/min, f=1000 mm/min, d=0.2 mm depth of cut (a) x axis measurement (b) y axis direction (c) z axis direction

(c)

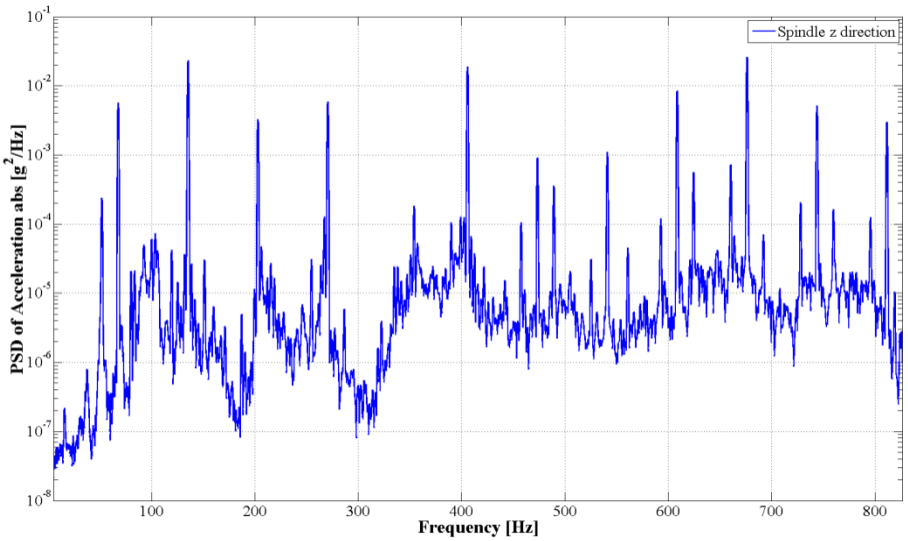

Figure 3.23 PSD Vc=63 m/min, f=1000 mm/min, d=0.2 mm depth of cut (a) x axis measurement (b) y axis direction (c) z axis direction (Cont.)

3.6 Comparison of the Results and Discussions

In idle and during machining processes, collected acceleration values, Fast Fourier Transform (FFT) and Power Spectral Density (PSD) response of these acceleration values on the system were given previously. It is observed that the acceleration values during machining process vary between -1.5g and +1.5g.

The RMS value is equal to the square-root of the area under the PSD-frequency curve given in Equation (3.4).

$$RMS(x) = \sqrt{\int_0^\infty G_x(f)df} \tag{3.4}$$

where $G_X(f)$ is the Power Spectral Density in g^2/Hz.

According to the results of the experiments, changes in the RMS value depending on feed rate, cutting speed, depth of cut and surface roughness are presented in Figures 3.24-3.39. Figure 3.24 shows the change in the RMS depending on the feed

rate under constant cutting speed at 63 m/min and a fixed depth of cut of 0.2 mm for AA5083 material.

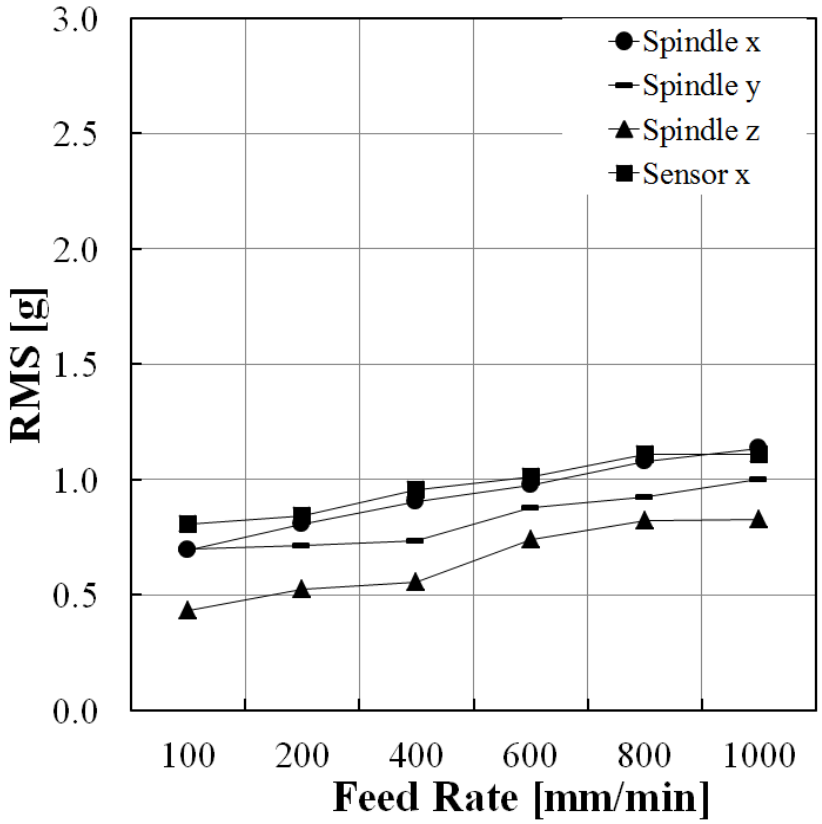

Figure 3.24 The change in RMS value depending on feed rate at 63 m/min cutting speed and 0.2 mm depth of cut for material AA5083

Figure 3.24 illustrates the relation between the feed rate and RMS value for independent axes.

Figure 3.25 shows the change in the RMS values depending on the feed rate under constant cutting speed at 628 m/min and a 0.2 mm depth of cut. It is observed that the RMS value increases with the increase in the feed rate in a similar way presented in Figure 3.24.

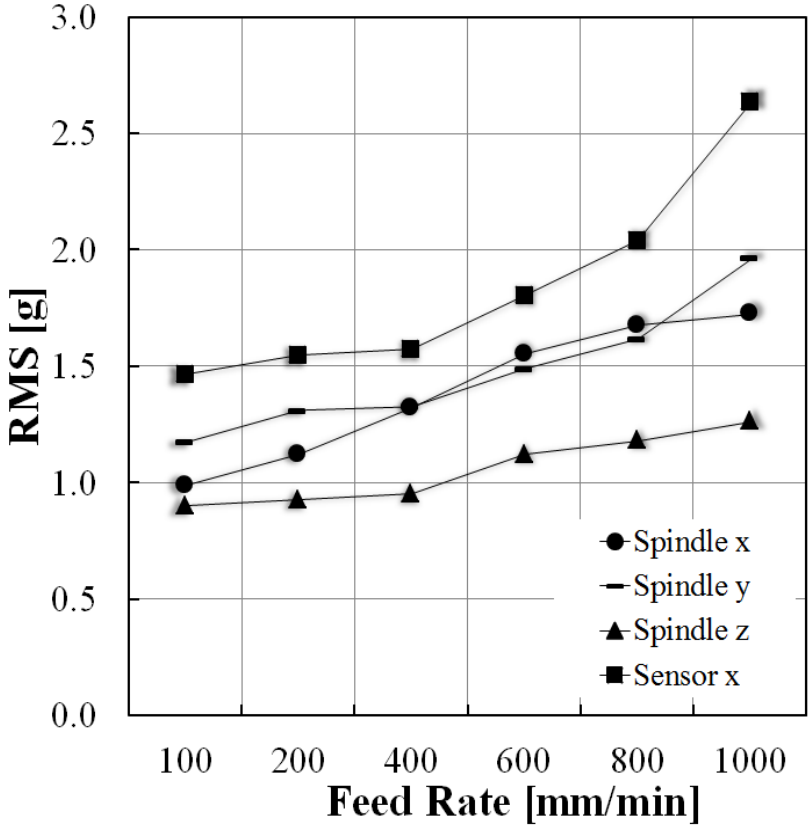

Figure 3.25 The change in RMS depending on feed rate at 628 m/min cutting speed and 0.2 mm depth of cut for material AA5083

Figure 3.26 shows the change in the RMS values depending on the cutting speed under constant feed rates at 100 mm/min and a 0.2 mm depth of cut.

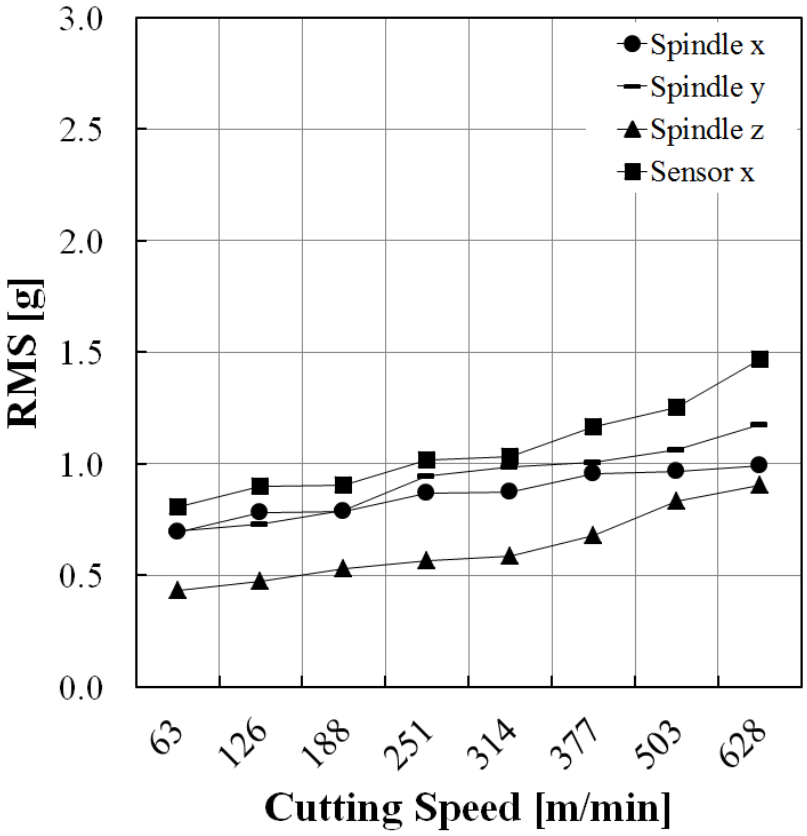

Figure 3.26 The change in RMS depending on cutting speed at 100 mm/min feed rate and 0.2 mm depth of cut for material AA5083

It is observed that the RMS value increases with the increase in the cutting speed in Figure 3.26.

Figure 3.27 shows the change in the RMS values depending on the cutting speed under constant feed rates at 1000 mm/min and a 0.2 mm depth of cut.

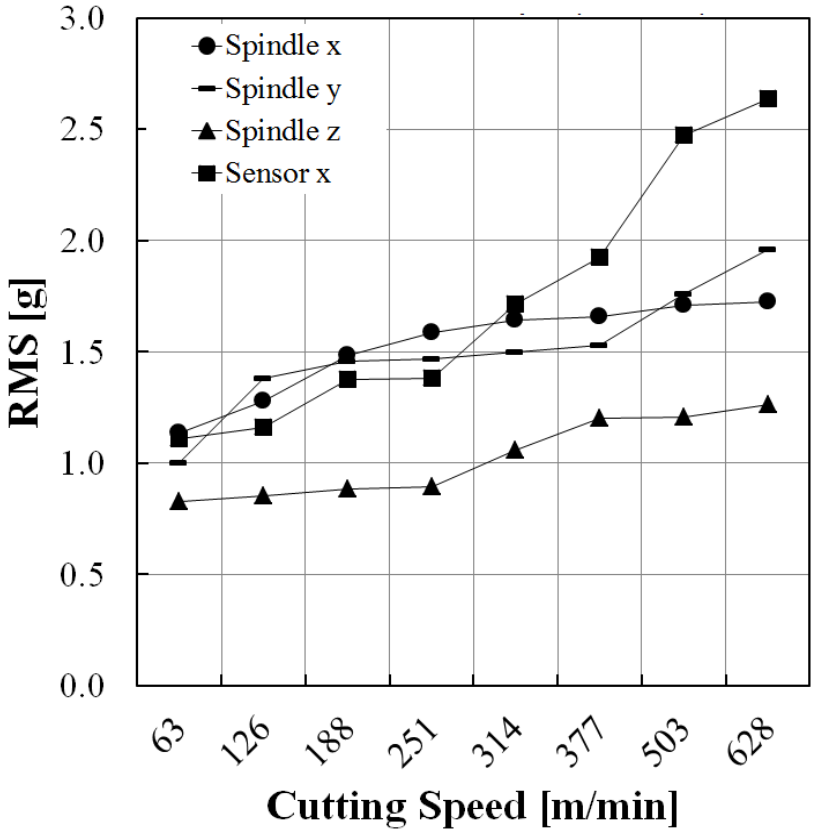

Figure 3.27 The change in RMS depending on cutting speed at 1000 mm/min feed rate and 0.2 mm depth of cut for material AA5083

The RMS value increases with the increase in the cutting speed in Figure 3.27.

Figure 3.28 shows the change in the RMS values depending on surface roughness under feed rates between 100 mm/min and 1000 mm/min at a constant cutting speed at 63 m/min and a 0.2 mm depth of cut.

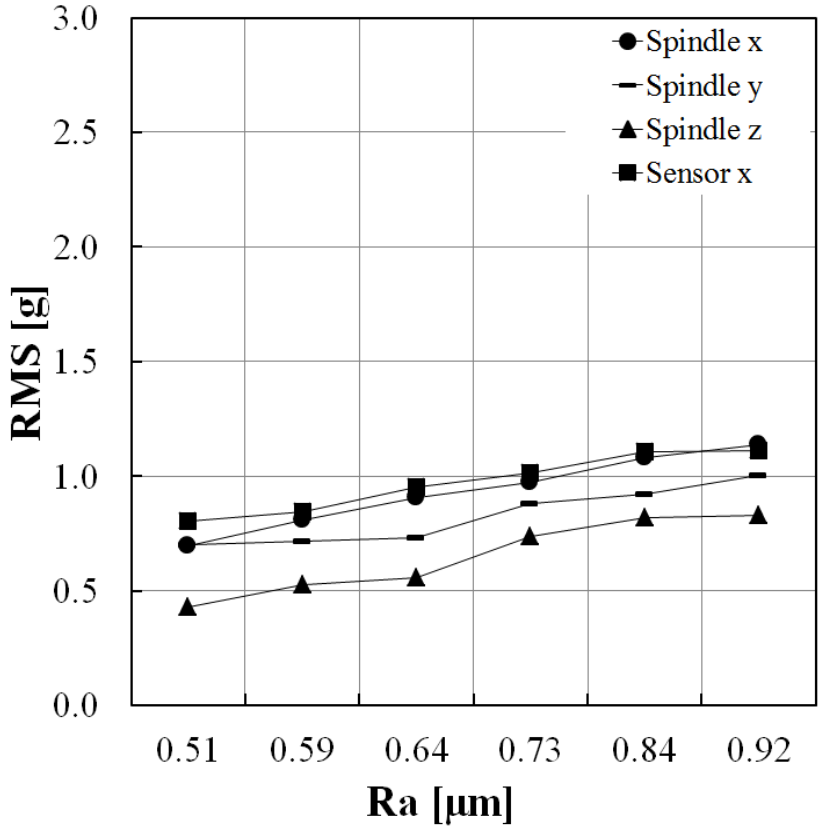

Figure 3.28 The change in RMS depending on surface roughness at 63 m/min cutting speed and 0.2 mm depth of cut for material AA5083

The RMS value increases with the increase in the surface roughness under the constant cutting speed in Figure 3.28.

Figure 3.29 shows the change in the RMS values depending on surface roughness under feed rates between 100 mm/min and 1000 mm/min at a constant cutting speed at 628 m/min and a 0.2 mm depth of cut.

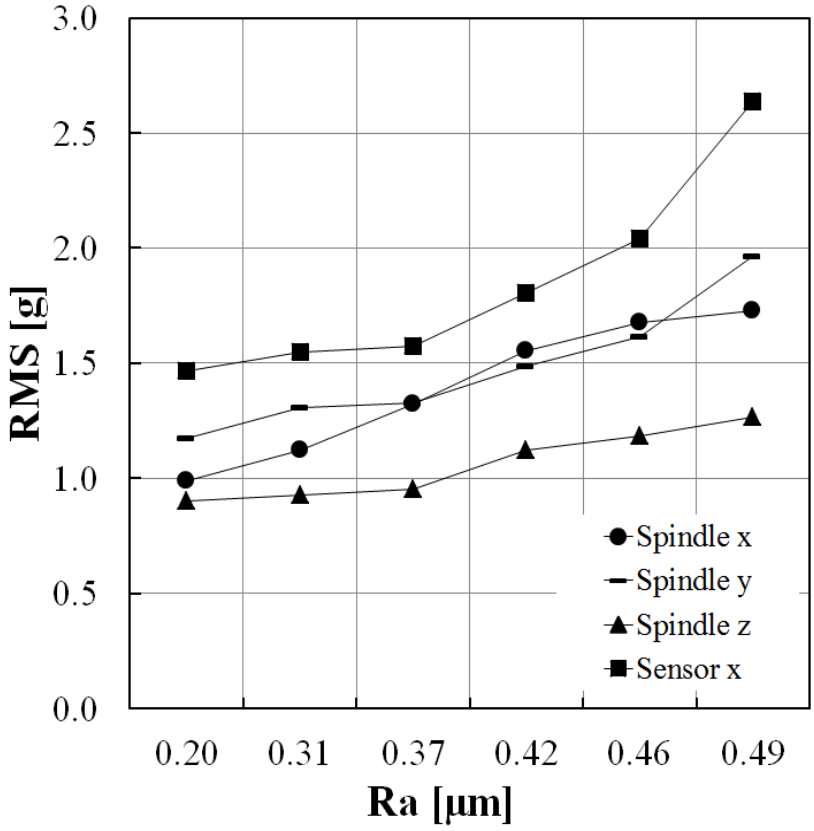

Figure 3.29 The change in RMS depending on surface roughness at 628 m/min cutting speed and 0.2 mm depth of cut for material AA5083

The RMS value increases with the increase in the surface roughness under the constant cutting speed related to the change at feed rate as shown in Figure 3.29.

Figure 3.30 shows the change in the RMS values depending on surface roughness under cutting speed between 63 m/min and 628 m/min at constant feed rate 100 mm/min and 0.2 mm depth of cut.

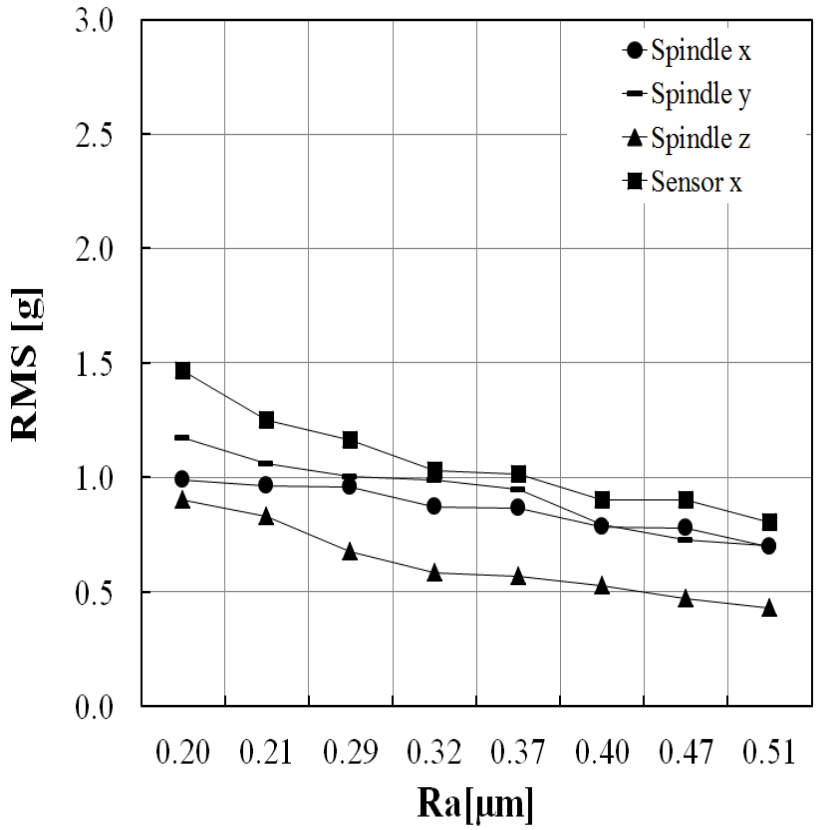

Figure 3.30 The change in RMS depending on surface roughness at 100 mm/min feed rate and 0.2 mm depth of cut for material AA5083

The RMS value decreases with the increase in the surface roughness under the constant feed rate in Figure 3.30.

In Figure 3.31, the change in RMS with respect to the surface roughness under cutting speeds between 63-628 m/min at a constant feed rate f=1000 mm/min a 0.2 mm depth of cut is given.

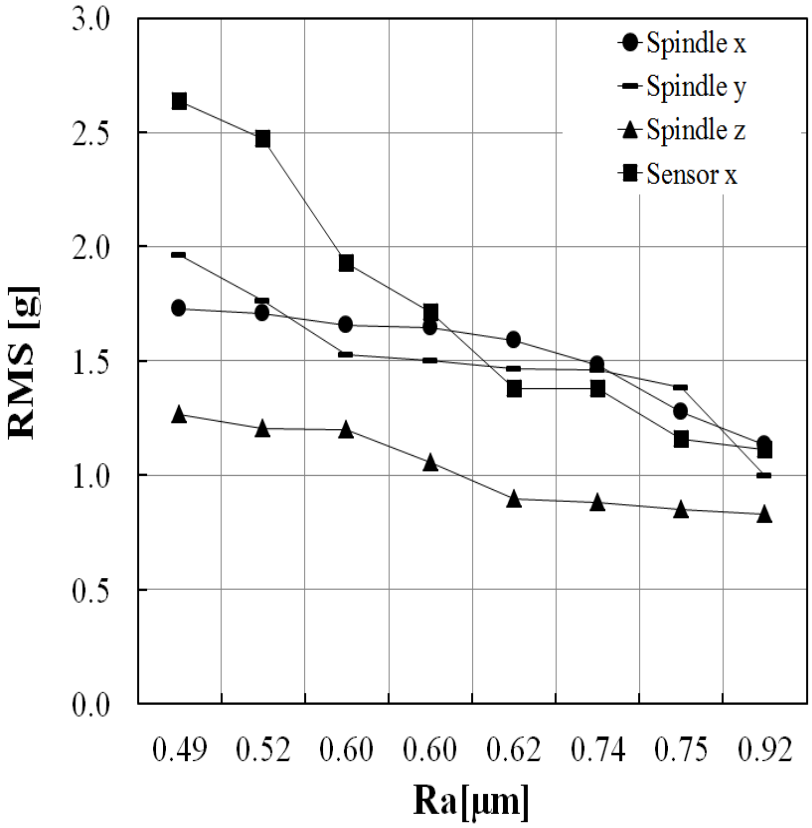

Figure 3.31 The change in RMS depending on surface roughness at 1000 mm/min feed rate and 0.2 mm depth of cut for material AA5083

The RMS decreases with the increase in the surface roughness approximately in direct proportion under the constant feed rate related to the change at cutting speed in Figure 3.31.

Figure 3.32 shows the change in the RMS depending on the feed rate under constant cutting speed at 63 m/min and a fixed depth of cut of 0.5 mm for AA5083 material.

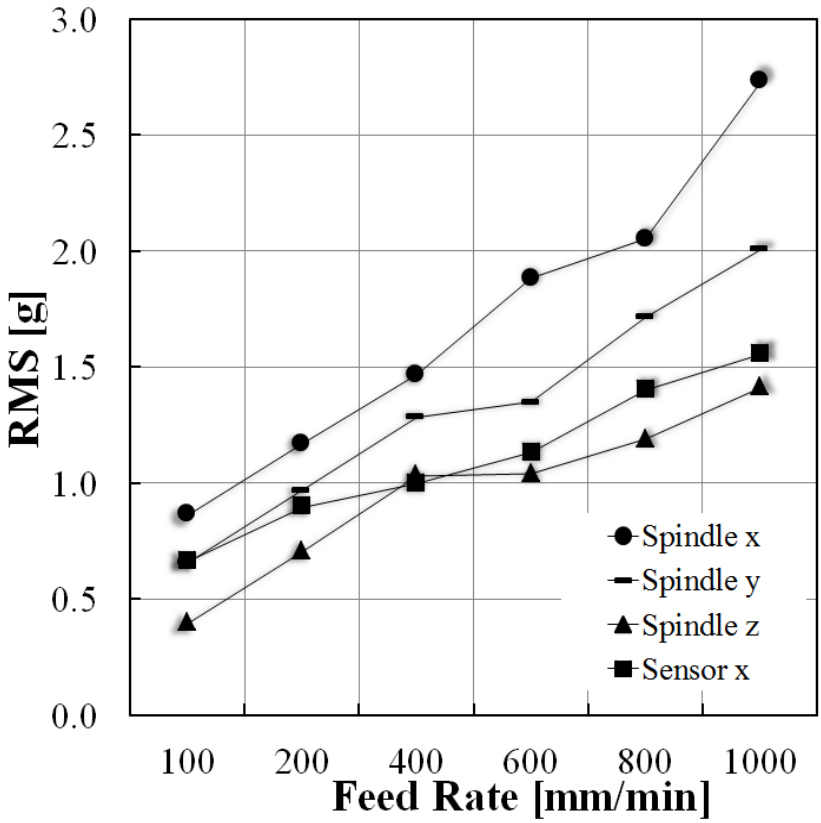

Figure 3.32 The change in RMS value depending on feed rate at 63 m/min cutting speed and 0.5 mm depth of cut for material AA5083

It is observed that the RMS value increases with the increase in the feed rate in Figure 3.32.

Figure 3.33 shows the change in the RMS values depending on the feed rate under constant cutting speed at 628 m/min and a 0.5 mm depth of cut.

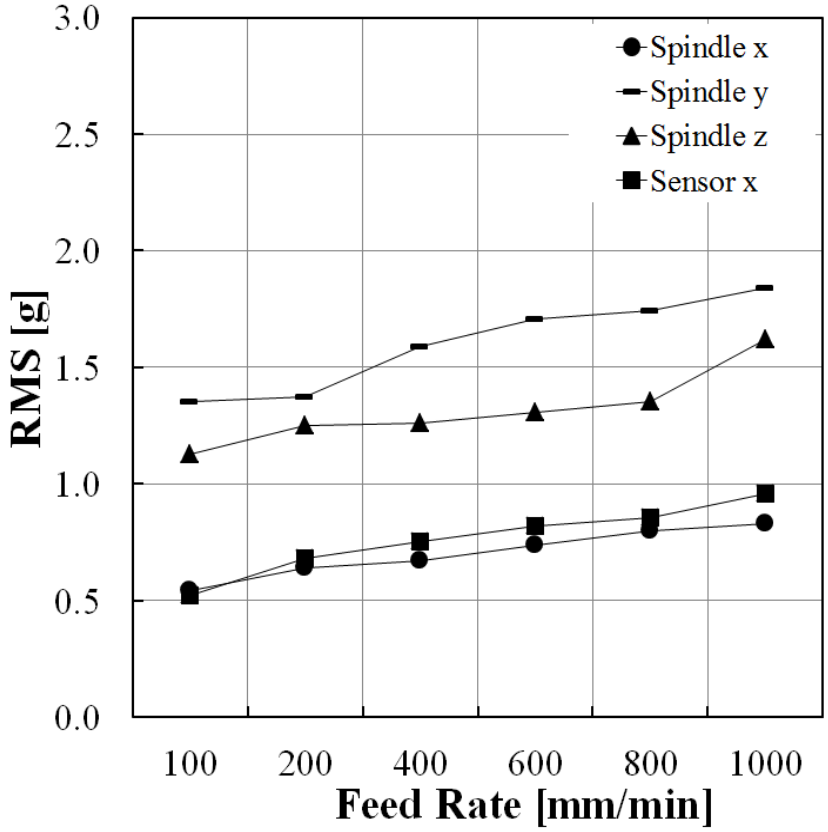

Figure 3.33 The change in RMS value depending on feed rate at 628 m/min cutting speed and 0.5 mm depth of cut for material AA5083

The RMS value increases with the increase in the feed rate in Figure 3.33.

Figure 3.34 shows the change in the RMS values depending on the cutting speed under constant feed rates at 100 mm/min and a 0.5 mm depth of cut.

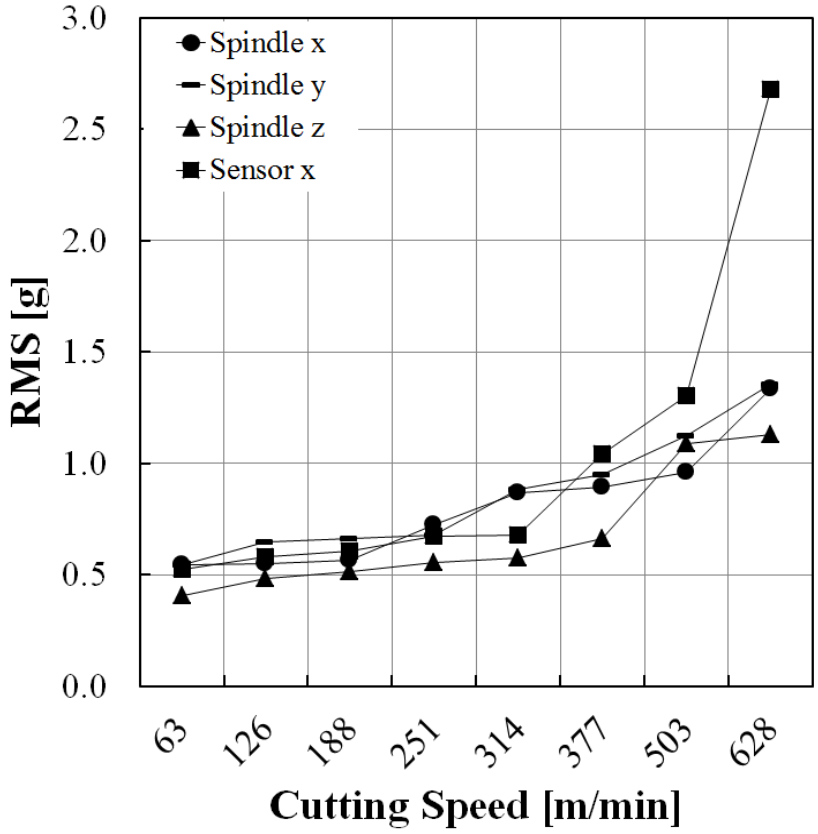

Figure 3.34 The change in RMS depending on cutting speed at 100 mm/min feed rate and 0.5 mm depth of cut for material AA5083

The RMS value increases with the increase in the cutting speed in Figure 3.34.

Figure 3.35 shows the change in the RMS values depending on the cutting speed under constant feed rates at 1000 mm/min and a 0.5 mm depth of cut.

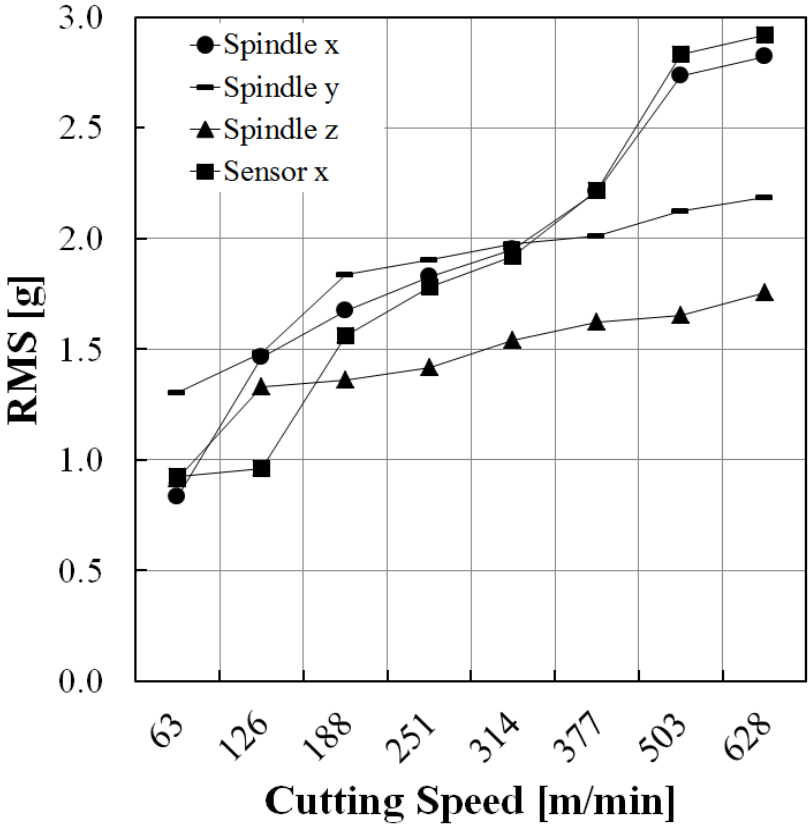

Figure 3.35 The change in RMS depending on cutting speed at 1000 mm/min feed rate and 0.5 mm depth of cut for material AA5083

The RMS value increases with the increase in the cutting speed in a similar way presented in Figure 3.35.

Figure 3.36 shows the change in the RMS values depending on surface roughness under feed rates between 100 mm/min and 1000 mm/min at a constant cutting speed at 63 m/min and a 0.5 mm depth of cut.

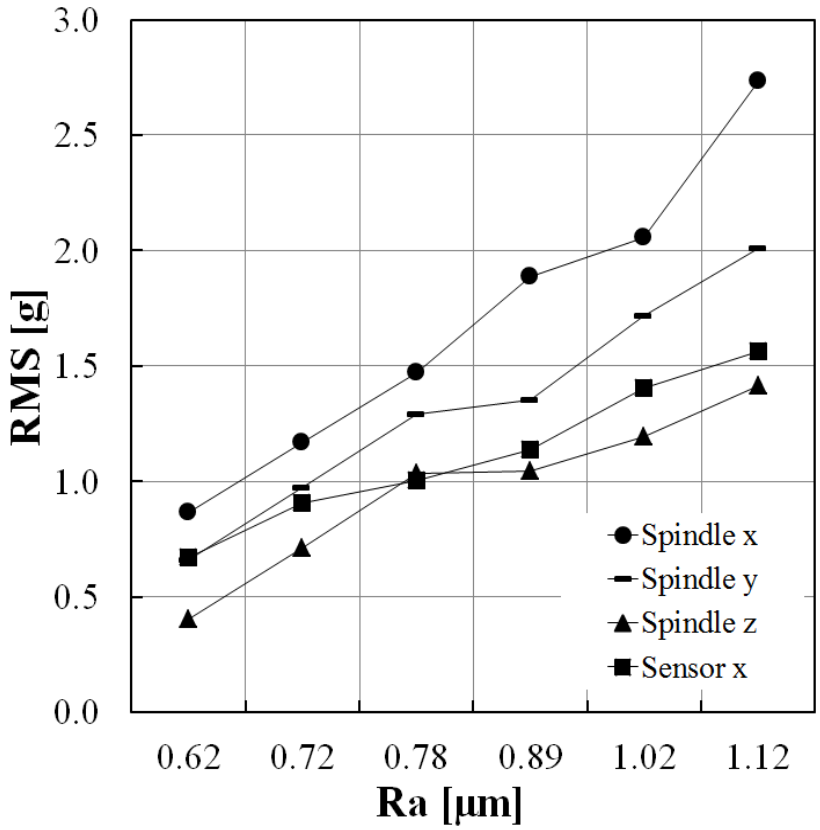

Figure 3.36 The change in RMS depending on surface roughness at 63 m/min cutting speed and 0.5 mm depth of cut for material AA5083

The RMS value increases with the increase in the surface roughness under the constant cutting speed in Figure 3.36.

Figure 3.37 shows the change in the RMS values depending on surface roughness under feed rates between 100 mm/min and 1000 mm/min at a constant cutting speed at 628 m/min and a 0.5 mm depth of cut.

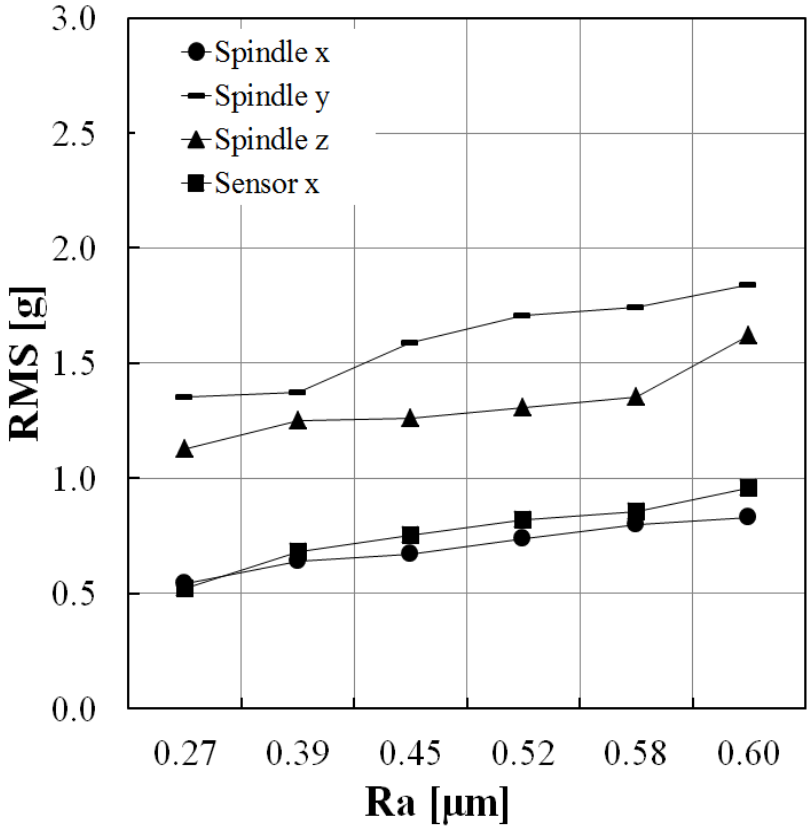

Figure 3.37 The change in RMS depending on surface roughness at 628 m/min cutting speed and 0.5 mm depth of cut for material AA5083

The RMS value increases with the increase in the surface roughness under the constant cutting speed related to the change at feed rate as shown in Figure 3.37.

Figure 3.38 shows the change in the RMS values depending on surface roughness under cutting speed between 63 m/min and 628 m/min at constant feed rate 100 mm/min and 0.5 mm depth of cut.

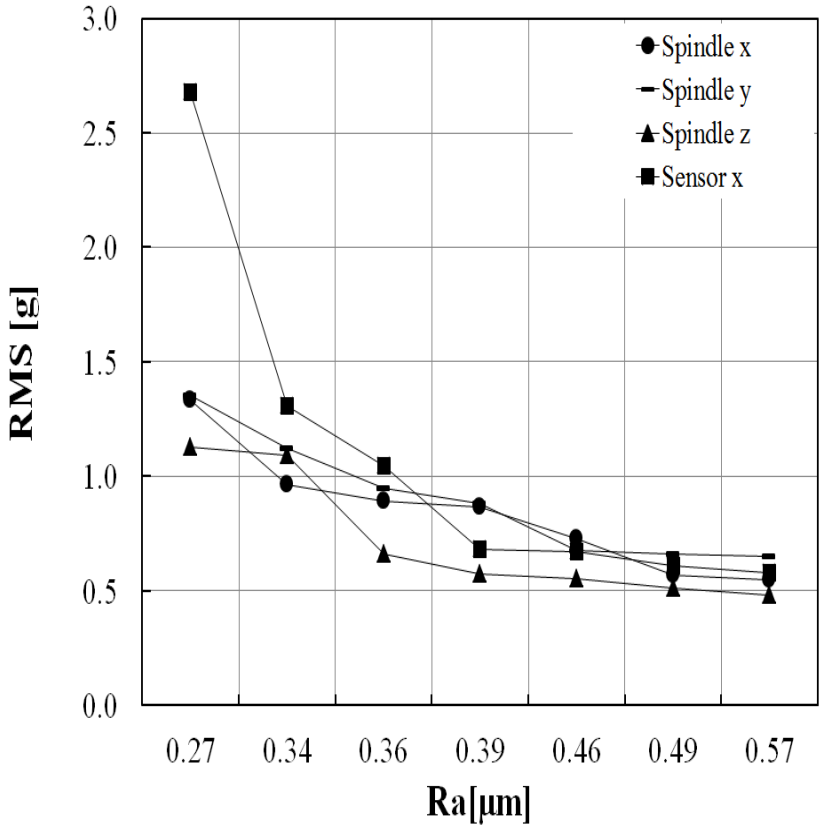

Figure 3.38 The change in RMS depending on surface roughness at 100 mm/min feed rate and 0.5 mm depth of cut for material AA5083

The RMS value decreases with the increase in the surface roughness under the constant feed rate in Figure 3.38.

In Figure 3.39, the change in RMS with respect to the surface roughness under cutting speeds between 63-628 m/min at a constant feed rate f=1000 mm/min and 0.5 mm depth of cut is given.

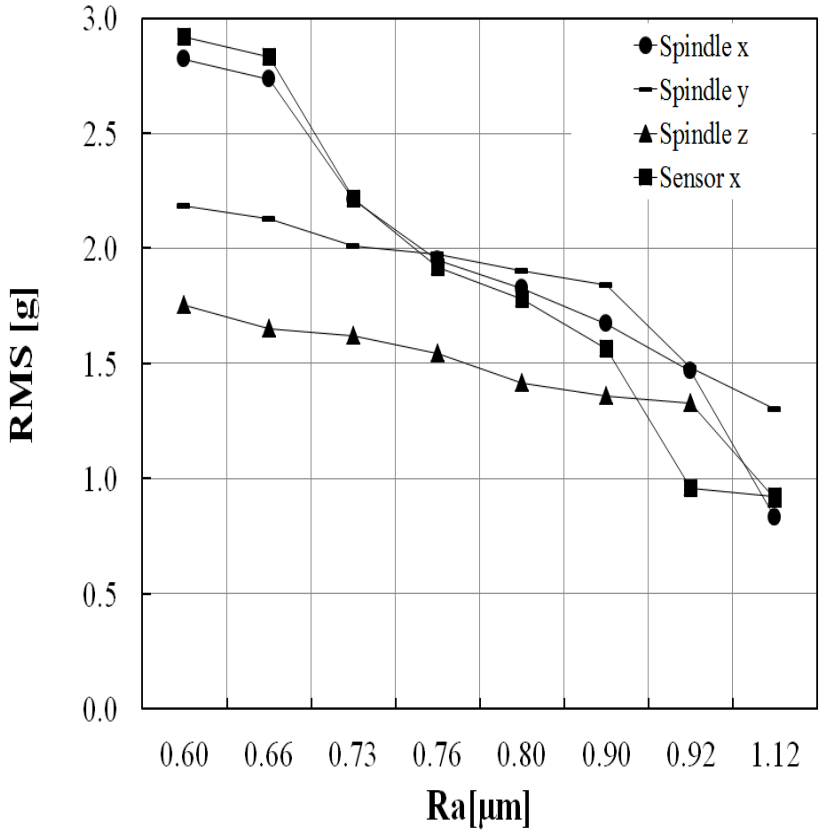

Figure 3.39 The change in RMS depending on surface roughness at 1000 mm/min feed rate and 0.5 mm depth of cut for material AA5083

The RMS decreases with the increase in the surface roughness approximately in direct proportion under the constant feed rate related to the change at cutting speed in Figure 3.39.

The increase in the depth of cut results in increasing acceleration RMS values. When these results are compared with the findings of similar studies in the literature, it is seen that the changes in RMS with the feed rate, cutting speed and depth of cut show similar behavior. In literature, Yılmaz, Dilipak, Sarıkaya, Yılmaz, and Meral (2014) observed that the vibration RMS value increases with the increase in cutting speed, feed rate and depth of cut.

In this chapter, dynamic characteristic of SRCS is given in detail. For this purpose, firstly, finite element analysis was performed to get mode shapes of the system. Then experimental setup was built for verifying analysis results and

collecting vibration data. In experimental studies, firstly hammer test was performed to find out natural frequencies of the system.

Experimental studies have been performed for idle state and during machining. Changes in the RMS value depending on feed rate, cutting speed, depth of cut and surface roughness are presented. The vibration of the system has increased with the increase of cutting speed, feed rate and depth of cut. Also the vibration of the system has been investigated with the surface roughness. According to measurement results, the vibration of the system increases with the increase in the surface roughness under the constant cutting speed. The vibration of the system decreases with the increase in the surface roughness under the constant feed rate.

Experimental results have been found consistent with the results presented in the literature.

CHAPTER FOUR
SURFACE ROUGHNESS CONTROL SYSTEM

4.1 Introduction

This chapter presents the hardware and software details of the proposed Surface Roughness Control System (SRCS). The hardware of the SRCS is mainly composed of a 3-axis CNC milling machine and an optical surface roughness sensor (OSRS). The components of this system are introduced in the following sections.

The economic facts could not be neglected during the development of the system. For this reason, the material of the main structure of the system was selected as Aluminum due to easiness in procurement and manufacturing, and two different aluminum materials (AA5083 and AA7075) are selected as workpiece material. Designed system is shown in Figure 4.1.

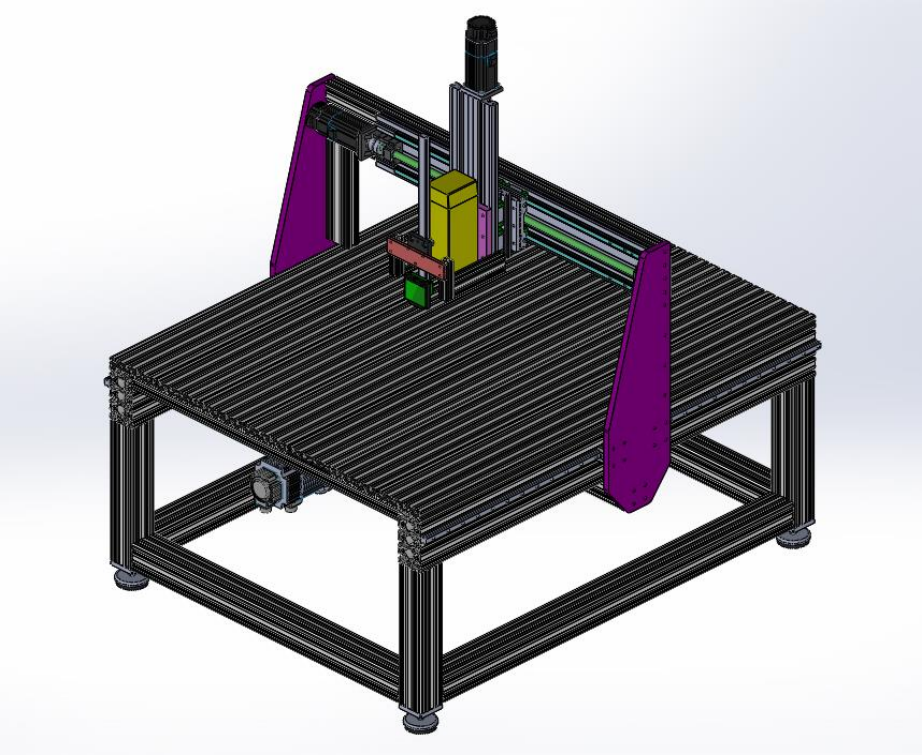

Figure 4.1 3D Solid model of the SRCS

4.2 The Hardware of SRCS

The SRCS is composed of a 3-axis CNC machine and an optical surface roughness sensor. The SRCS was designed and assembled in the scope of this study. 3-axis milling machine, optical surface roughness sensor and control software is shown in a line diagram in order to show the complete experimental setup (Figure 4.2). Here, OSRS is mounted on the spindle head of 3-axis milling machine. OSRS is connected to System Computer with RS-232 connection to transfer surface roughness data to the system software. According to measured roughness data, the system software transmits the calculated feed rate and cutting speed data to PLC control unit through RJ45 Ethernet connection in order to control the servo motors and spindle motor.

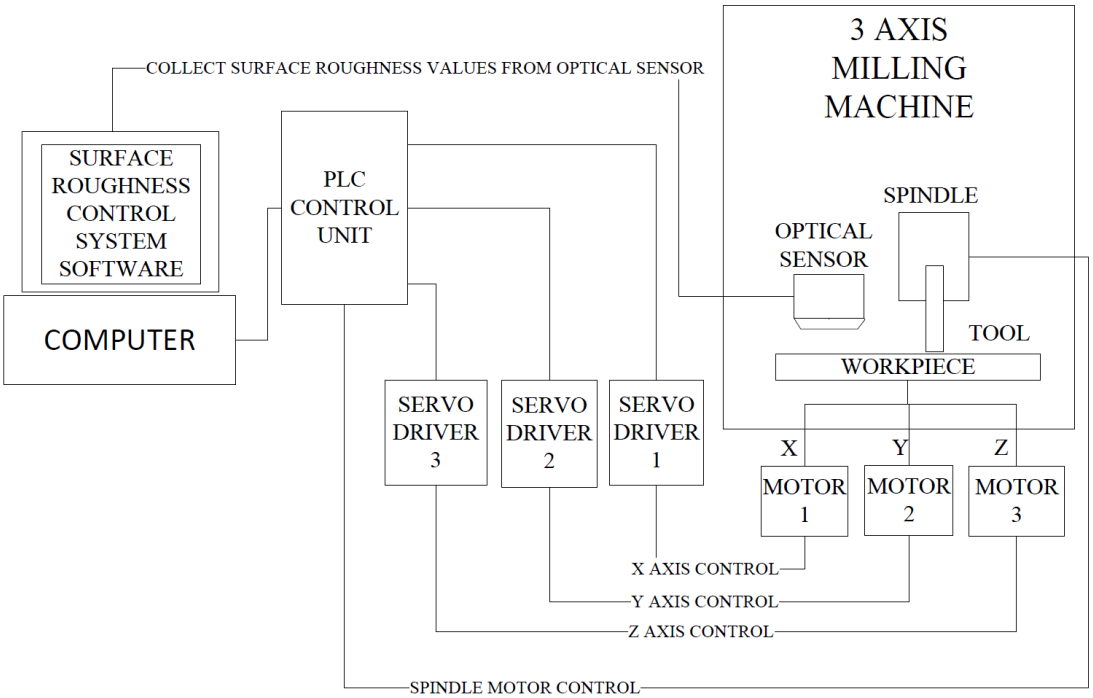

Figure 4.2 The line diagram of complete setup

The frame of the 3-axis CNC machine is constituted by 90x90 and 90x180 heavy-duty aluminum sigma profiles. In order to provide a 3-axis movement on the system, three servo motors with brakes are used. Movement on 3-axis are provided by delivering the motions coming from the servo motors by means of the anti-backlash couplings to ball screws. HSD brand MT 1090-Y6162Y0019 type of spindle has

been chosen for the machining part. The CNC milling machine used in the experiments has been produced and assembled in such a way that it has 4.5 kW head engine power and 18000 rpm maximum rotational speed (Figure 4.3).

Figure 4.3 HSD MT 1090-Y6162Y0019 spindle used in SRCS (HSD Mechatronics, n.d.)

ER32 Collet is used for tool holder in SRCS (Figure 4.4).

Figure 4.4 ER32 collet used in SRCS

ESTUN EMG series servo motor is used for x axis control; EMJ series are used for y and z axis control in the CNC Milling machine (Figure 4.5).

Figure 4.5 Servo motor (ESTUN EMJ Series) used in the system (Estun, n.d.)

Table 4.1 Technical specifications of Estun EMG/EMJ servo motor (Estun, n.d.)

Specification	**EMG**	**EMJ**
Rated output power	1 kW	1 kW
Rated torque	4.78 Nm	3.18 Nm
Instantaneous peak torque	14.3 Nm	9.55 Nm
Rated current	6.0 Arms	5.3 Arms
Instantaneous max current	18 Arms	15.9 Arms
Rated speed	2000 r/min	3000 r/min
Max speed	3000 r/min	4500 r/min
Brake rated power	19 W	11.5 W
Brake holding torque	10 Nm	3.2 Nm
Encoder	2500P/R incremental encoder	2500P/R incremental encoder
Working temperature	0 to +40° C	0 to +40° C

A list of all the mechanical parts used on the system is given in Table 4.2.

Table 4.2 Part list of SRCS

Part Name	**Brand**	**Model**
Linear rail	THK	HSR 25
Linear bearing	THK	HSR 25A 2SS
Ball screw	THK	25 mm 10 mm pitch
Flange nut	THK	25 mm 10 mm pitch
Shaft end,front bearing	SYK	MBC B15-E
Shaft end,back bearing	SYK	BF 15
Antibacklash coupling	SGS	GS 24
Braking servo motor 1kw	ESTUN	EMG 10AP A24 / EMJ 10AP B24
Movable cable conduit	CKS	CK25060 R75
Spindle	HSD	MT 1090-100 Y6162 Y0019
Optical sensor	HOHNER	D516
Sigma profile (heavy)	DOGUS KALIP	45X90, 90X90, 90X180
Tool holder		ER32 Collet

The developed experimental setup for surface roughness control measurements is shown in Figure 4.6.

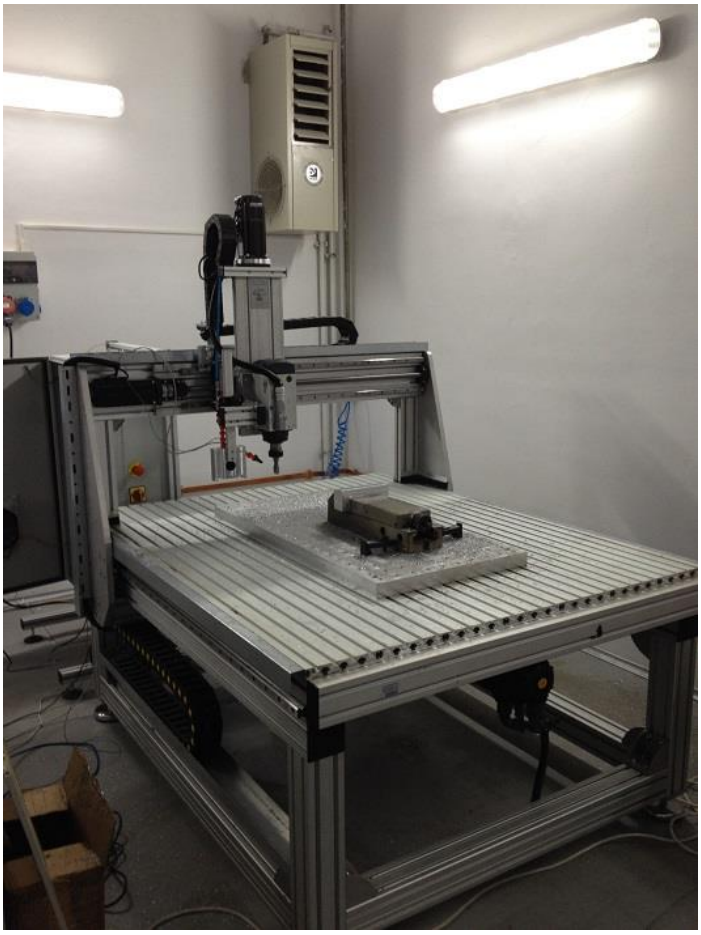

Figure 4.6 Developed experimental setup

4.2.1 Optical Surface Roughness Sensor (OSRS)

Surface roughness systems are able to make mechanical or optical measurements. However, mechanical measurement systems have not been approved for the system, because they have to contact the surface, work slow and they are expensive. Furthermore, they scratch the surface owing to the mechanical usage of stylus during the measurement. This constitutes a problem in situations requiring precise surface quality. Owing to the non-contact measurement capability, a Hohner Brand D516 type of optical surface roughness sensor is used to measure the surface roughness of the machined surface. Non-contact roughness measurements are performed continuously by OSRS. Choice of optical sensor has brought many advantages in the system. Rapid data transfer, adaptation to the developed program, easy integration to the CNC milling machine, low cost and suitability for measuring during the in-line

machining may be considered among the most significant advantages. Cross sectional area of optical surface roughness sensor is shown in Figure 4.7.

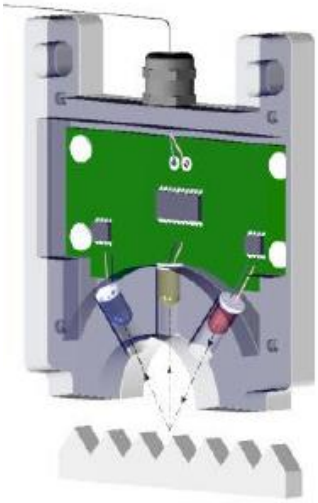

Figure 4.7 Cross sectional area of optical surface roughness sensor (Hohner, n.d.)

Working principle of the optical system is given in Figure 4.8. If R_a value is equal to zero as shown in Figure 4.8, ray of light will be reflected at the same angle ($\Theta_i=\Theta_r$).

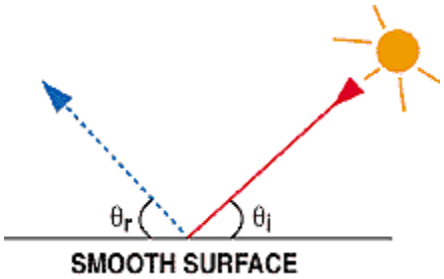

Figure 4.8 Working principle of optical sensor (Bloechle, n.d.)

4.2.1.1 Measurement Principle of OSRS

OSRS is able to measure the surface roughness of the machined metal surfaces between the 0.05µm and 20µm.

At the end of the machining operation, infrared light beams radiated by a light emitting diode (IR LED) are sent to the surface as shown in Figure 4.9. If the surface is perfectly smooth, the light will be reflected at an angle equal to the angle of incidence. In this case, reflection in any other direction will be zero and the ratio between the reflected and scattered beams is infinite. If the surface is absolutely rough, the incident light will scatter at any direction with equal amounts and the ratio between the reflected and scattered beams will be 1. The value of the surface roughness at a point on the surface is determined by comparing the amount of reflected and scattered lights measured by the OSRS. The ratio between the reflected and scattered beams is inversely proportional to the degree of surface roughness.

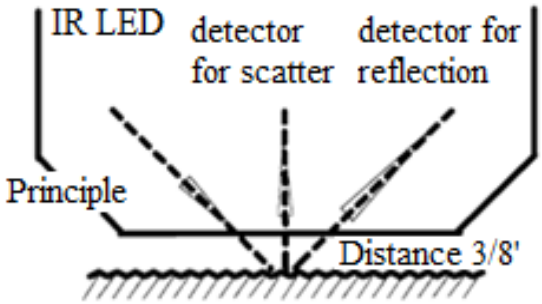

Figure 4.9 Measurement principles of OSRS (Hohner, n.d.)

In this measurement system, the surface roughness (R_a) is not measured directly. Firstly, according to surface profile, reflected and scattered infrared light values are collected by the optical sensor. These reflection and scatter data are related to surface roughness values with the sensor software. R_a is determined on the basis of the reflection/scatter ratio. Before measurement, the sensor is calibrated with the help of the workpieces having known surface roughness values. In the calibration process, the workpiece having lower surface roughness is scanned firstly. Then, the R_a corresponding to the reflection/scatter ratio acquired by the scanning is entered into the software. Then, the acquired R_a is also entered into the system by the repetition of the same processes for the surface quality of other workpiece having greater R_a. At the end of the calibration procedure, the sensor can measure the correct R_a value corresponding to the reflection/scatter ratio on every point using the calibration parameter *F*, which is defined as

$$F = (S_S - S_N) / (S_S + S_N) \quad (4.1)$$

Where S_S denotes the signal coming from the photo detector for reflection and S_N denotes the signal coming from the photo detector for scatter. Technical Specification of Hohner D516 is given in Table 4.3.

Table 4.3Technical Specifications of Hohner D516

Power:	Powered from PC or PDA (3.2...5V @ 30 mA)
Materials:	Housing = ABS natural Seal = Sealon PTFE Screws = stainless steel 301
Roughness formula:	see roughness patent
Connection:	9 pole D connector (Palm adaptor available)
Work distance:	3 / 8"
Resolution:	A number between 0 and 999 within 0.1% accuracy

4.3 ANN Model of SRCS

In this section, artificial neural networks, which constitute the fundamental structure of the milling system is discussed briefly. Erzurumlu and Öktem (2007) studied on the ANN model for the determination of surface roughness on the basis of cutting parameters. Also, the integration of neural network and genetic optimization technique were utilized in integrated purpose to determine the best cutting parameters (Öktem, Erzurumlu & Erzincanlı, 2006). Within the scope of this study, ANN is used in order to make an approximation of optimum machining parameters using the machining data acquired from experimental measurements. An ANN model is presented in Figure 4.10.

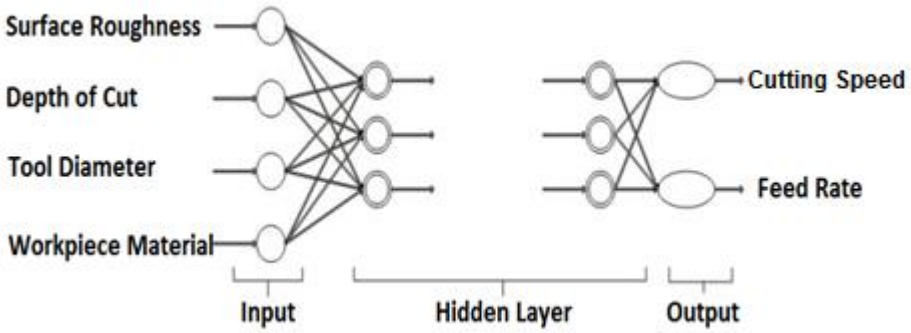

Figure 4.10 ANN model of the system

Multi layered feed-forward neural networks used in this study, are one of the popular structures among artificial neural networks. These efficient networks are widely used to solve complex problems by modeling complex input-output relationships. There are one input layer, two hidden layers and one output layer with each neuron fully connected with neurons of adjacent layer. 4 input neurons and 2 output neurons are for the input and output variables in Figure 4.10. However, FNNs often end up being over trained. They adopt trials-and-errors to seek possible values of parameters for convergence of the global optimum. The learning process of an FNN cannot guarantee the global optimum, sometimes trapping the network into the local optimum.

Backpropagation algorithm is selected as a training algorithm. The back-propagation algorithm is one of the most famous algorithms to train a feed forward network. It has great advantage of simple implementation (Che, Chiang &Che 2010). The back-propagation algorithm works correctly for networks with more than one input unit in which several independent variables are involved.

In this study, ANN model was developed with two hidden layer and 4 neurons in each layer for multilayer feed forward network. Weight values obtained from ANN model were used in the sigmoid function to get the result. Detailed ANN model of the system is given in Figure 4.11.

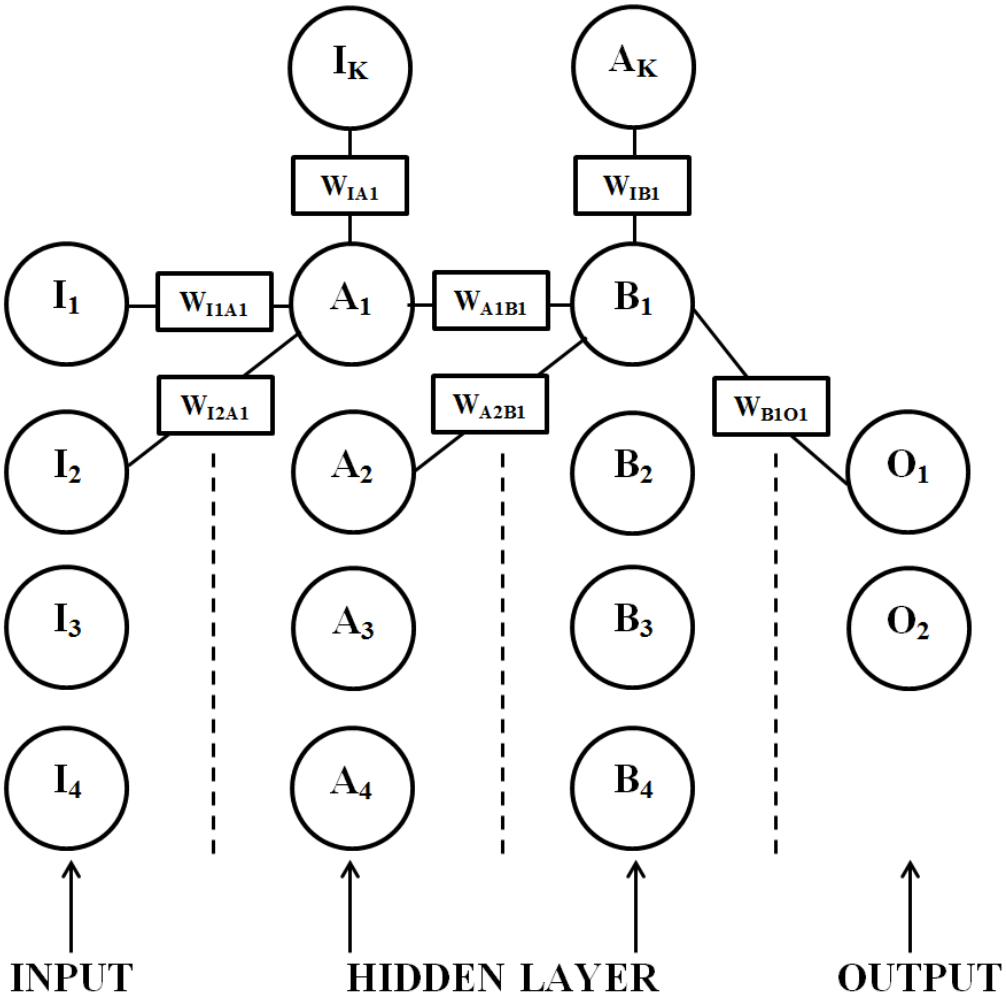

Figure 4.11 Detailed ANN model of the system

In modeling, the input elements are given as surface roughness, depth of cut, tool diameter and work-piece material. Output elements are cutting speed and feed rate. They are indicated in Table 4.4.

Table 4.4 Cutting parameters used in ANN model

Inputs of ANN				Outputs of ANN	
R_a (μm)	d (mm)	D (mm)	Material	Vc (m/min)	f (mm/min)

In the MATLAB environment, a custom code is developed to apply the formulations instead of neural network toolbox. The details about the developed MATLAB code are as follows: firstly a file with an extension of *.txt including experimental test results is read. Then, data at related columns are assigned to input

and output elements to calculate the weight functions and layer elements. Then, all of these data are written to an output file named as "V_f_result.mat". Later, the output file is used in the main Surface Roughness Control System (SRCS) as an input file. MATLAB program code logic for ANN is shown in Figure 4.12a.

(a)

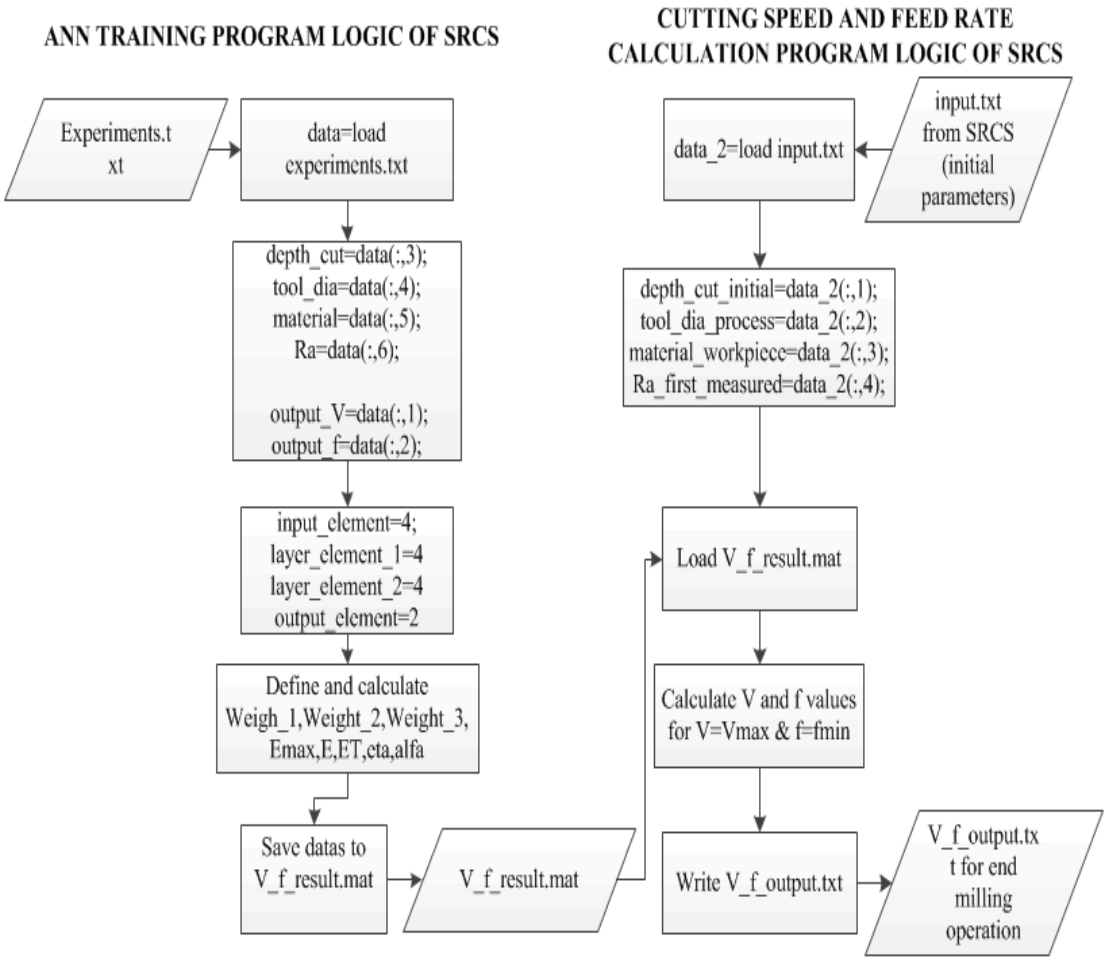

Figure 4.12 a) MATLAB program code logic for ANN b) Comparisons of experimental results for testing network and ANN prediction of developed code.

(b)

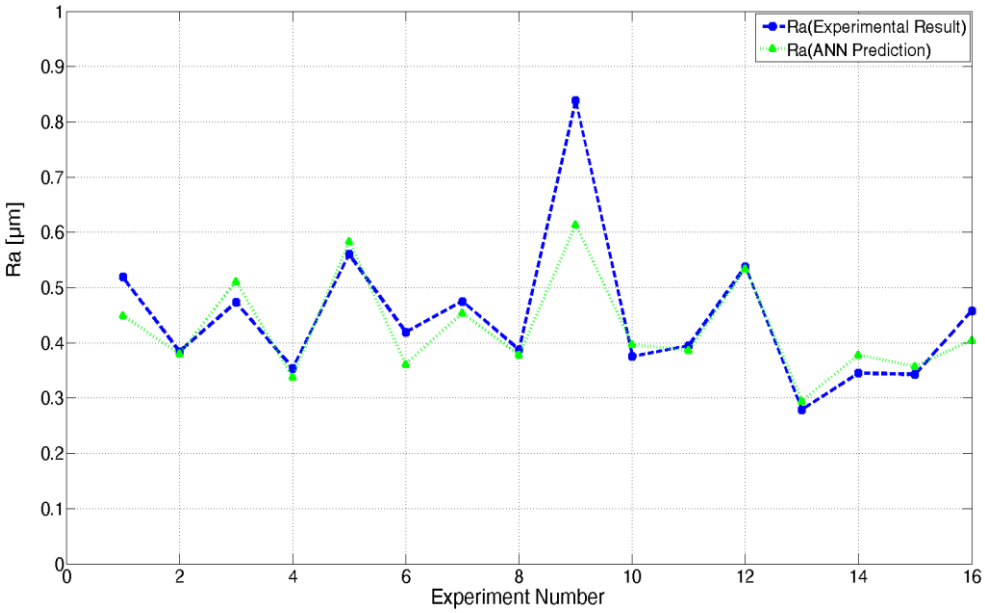

Figure 4.12 (a) MATLAB program code logic for ANN (b) Comparisons of experimental results for testing network and ANN prediction of developed code (Cont.)

The comparisons of experimental results for testing network and ANN prediction of developed system are given in Figure 4.12b. In the developed ANN code, the maximum error (E_{max}) is given as 0.09 for avoiding network overtraining. The loop is automatically closed when the difference between calculated and tested results are equal and smaller than the defined error.

4.4 The Software of SRCS

In order to practice the algorithm mentioned above, the system software has been developed. The interface of the system program and main control software are developed in the Visual Studio environment and cutting speed and feed rate calculation program developed by means of MATLAB, is integrated to the main control software.

Figure 4.13 shows the user interface of the system software. In the SRCS, servo motor motions in the x, y and z axes and all kind of communications with the machine are performed through the PLC.

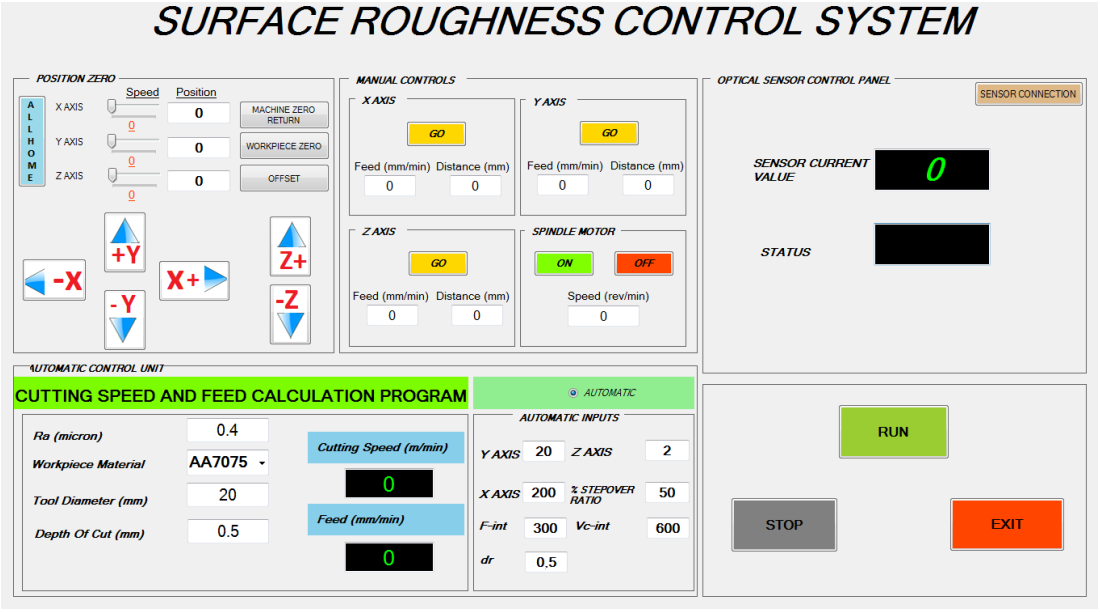

Figure 4.13 Main program user interface of the SCRS

The SRCS is composed of three sub-categories, which are the manual and automatic operator entry section, optical sensor measurement section and cutting parameters calculation section, as seen in the user interface (Figure 4.13). Initial-cut parameters of the system are defined in the section shown in Figure 4.14.

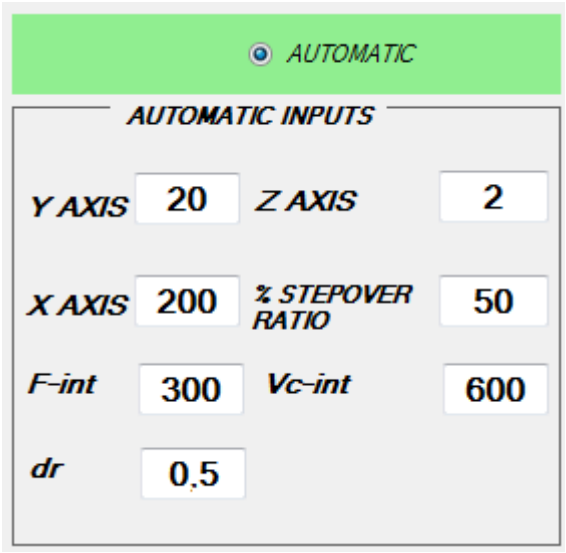

Figure 4.14 Initial parameters entry interface of the SCRS

At this point, the cutting limits in x, y, z axes, initial feed rate, cutting speed and the depth of cut for semi-finish cut can be entered. As seen in Figure 4.15, the desired value of the R_a, workpiece material, tool diameter and finishing depth of cut

determined as the input parameters in the experimental sets are entered into the system.

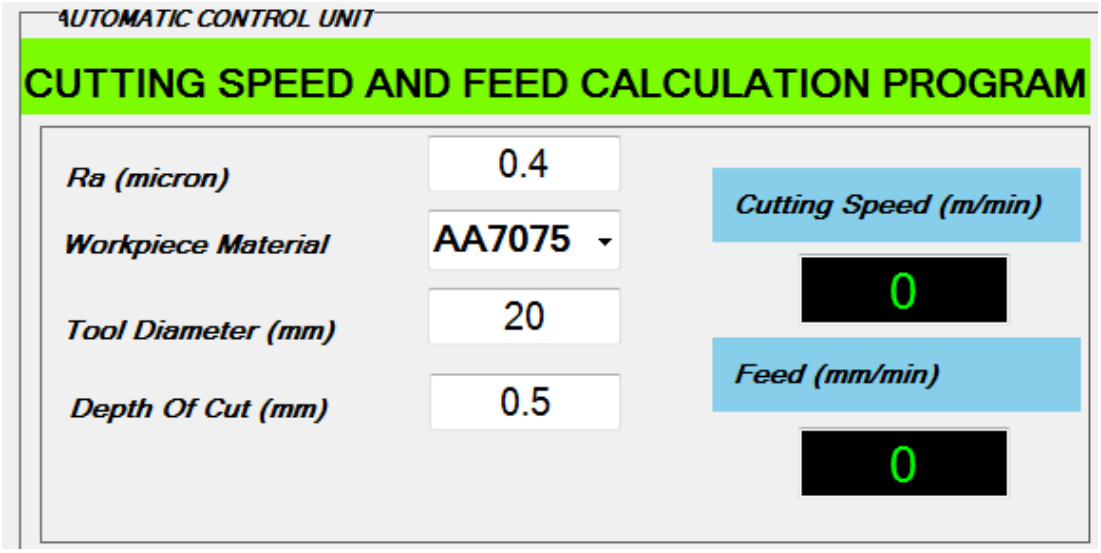

Figure 4.15 Cutting speed and the feed rate calculation program interface of the SCRS

The cutting speed and feed rate calculation program may give more than one cutting speed and feed rate couples. In this case, the process is completed by the selection of the cutting speed corresponding to the maximum feed rate value. The reason for selecting the maximum value of the feed rate is to reduce machining time. Ultimately, the same surface roughness results will be observed from the machined surface independent of the selection. The results of the optical sensor part are shown in Figure 4.16. The average roughness value measured with the optical sensor is seen at the top of the screen. The current condition of surface roughness is represented by "status" as shown at bottom of the screen. If the result is below or equal to the reference roughness value, the condition is indicated as "GOOD" and if above, the condition is indicated as "BAD".

(a)

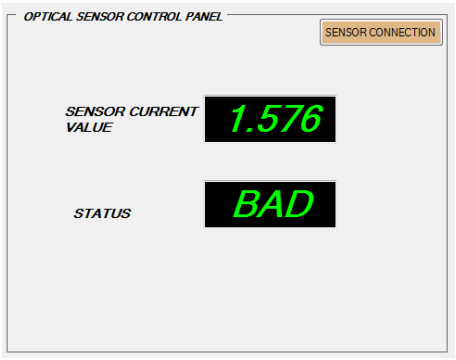

(b)

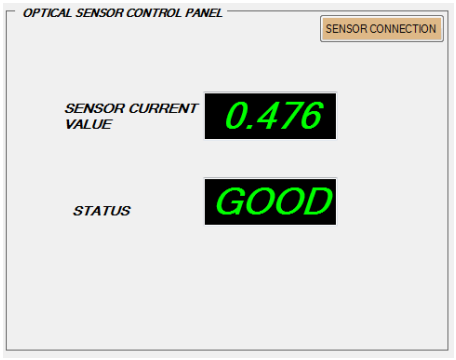

Figure 4.16 Status of the surface roughness measured by OSRS a) undesired result b) desired result

4.5 Control Structure of SRCS

The OSRS which constitutes the measurement part of the surface roughness control system (SRCS) and its working principle has been mentioned in the previous section. In this section, information about the system software and the working principle of the SRCS is presented.

The goal of the SRCS is basically to achieve the desired R_a for the system by determining optimum cutting parameters and conducting metal removal accordingly by measuring the R_a for the finish cut operation. Before the machining operation, values of the cutting speed and the feed rate for semi-finish cut and the constant depth of cut are entered into the system software. In addition, values of the desired R_a and also the depth of finishing cut are also specified. The system performs the semi-finish cut according to the parameters defined by the user. The sensor carries

out the surface roughness measuring process for the finishing operation. If the surface has the desired surface quality in accordance with the measured R_a, the system performs the cutting operation with the existing parameters and completes the process. If the measured R_a does not match the desired roughness value previous to finishing operation, the system predicts the parameters for the finishing cut according to the necessary R_a. The system carries out the end milling in compliance with the cutting speed and the feed rate determined by the system and completes the process by performing a confirmation measurement. Furthermore, data measured from the experimental set of actual machining parameters is used for the constant training of the system as a new reference set for ANN. Therefore, the SRCS developed in this study is evaluated as a system, which is applicable to other types of CNC milling machines and is able to train itself.

The algorithm shown in Figure 4.17 explains the working principle of the SRCS. The developed SRCS system determines the suitable cutting speed and feed rate values in order to obtain the desired surface roughness value at the end of the surface finishing operation with the aid of ANNs.

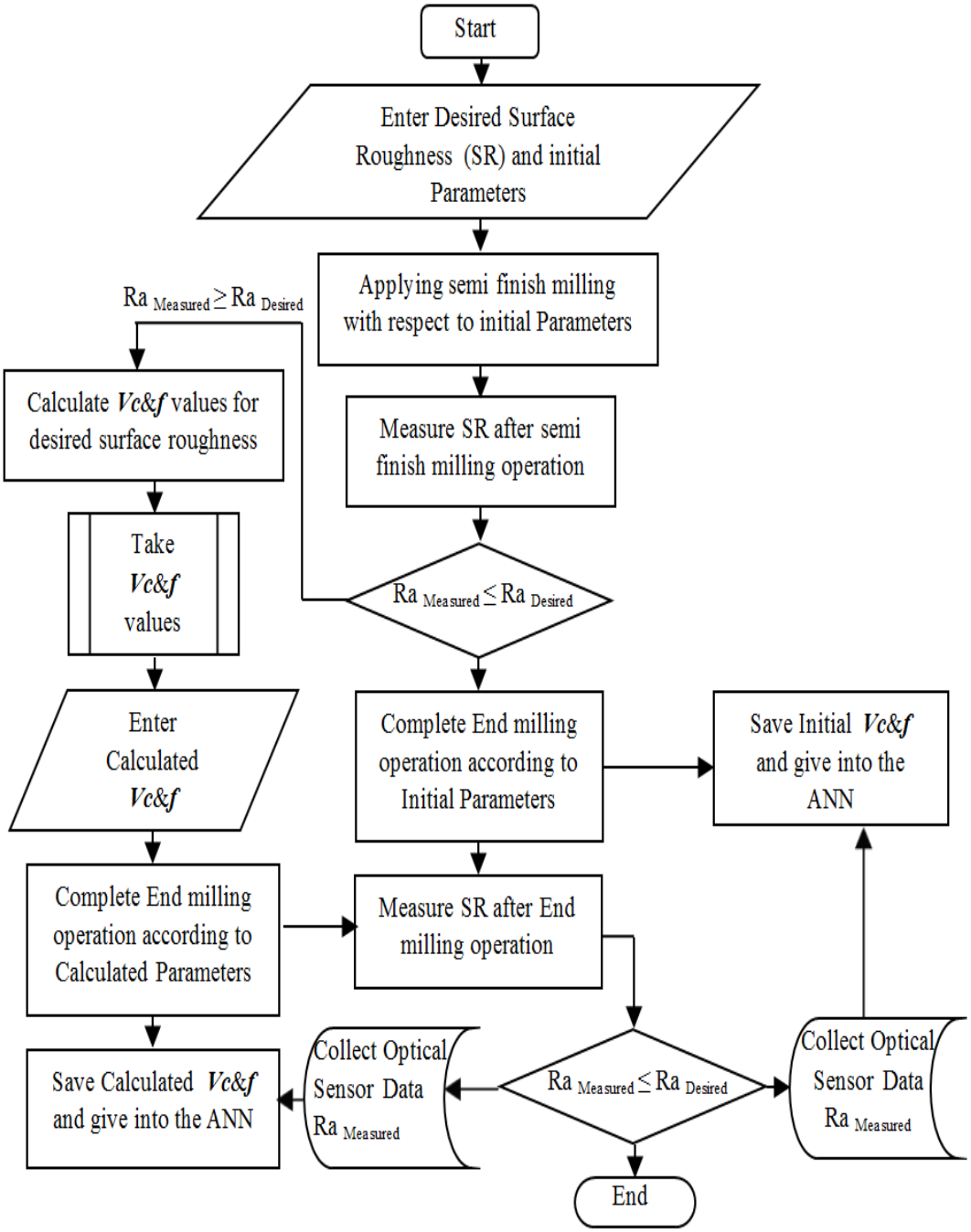

Figure 4.17 Proposed algorithm of the SRCS

In this chapter, the hardware and software of the SRCS are given in detail. Firstly, the mechanical components of the SRCS and optic measurement system are defined. Then, ANN structure of SRCS is determined. Finally, the software of SRCS is given with the control structure of the SRCS.

CHAPTER FIVE
EXPERIMENTAL RESULTS AND DISCUSSIONS

5.1 Introduction

In this chapter, experimental studies needed to establish the SRCS are given first. Experimental results for ANN training of SRCS will be presented in the second part. Then, experimental results of these results will be discussed for different parameters and also compared with previous studies.

5.2 Experimental Studies of SRCS

Experimental studies are carried out in order to test the performance of the developed Surface Roughness Control System. There are many parameters, which affect the roughness such as cutting speed, feed rate, and depth of cut, workpiece material and cutting tool. These fundamental parameters are taken into consideration in the experimental phase.

The cutting tool is chosen as Taegutec AES 2200 brand and 2-flute solid carbide end mill cutter for aluminum machining with Ø20 mm diameter. In the technical specifications of the Taegutec AES 2200, maximum cutting speed is defined as 300m/min for 8-10mm depth of cut but according to technical department of Taegutec Office, the maximum cutting speed may be taken as 650m/min for 1-2mm depth of cut. For this reason, the maximum cutting speed is determined as 628 m/min in this study.

The coolant is not used in the experimental studies so dry machining is performed. Commercially available AA5083 H111and AA7075 T6 Aluminum Alloys are used as the workpiece materials. Chemical compositions of these materials are given in Table 5.1.

Table 5.1 Chemical composition of the AA5083 and AA7075 materials used in the experiments

Material/ Composition	**Fe**	**Si**	**Mn**	**Cr**	**Cu**	**Mg**	**Zn**	**Hardness**
AA5083 H111	0.199	0.171	0.513	0.089	0.015	4.599	0.311	27 HRB
AA7075 T6	0.103	0.230	0.029	0.219	1.46	2.75	5.12	87 HRB

Cutting speed is changed from 63 m/min to628 m/min, and the feed rate is varied between 100 mm/min and 1000 mm/min as presented in Table 5.2. There are two experimental sets prepared for 0.2 mm and 0.5 mm depths of cut, since the depth of cut is an issue approached as a finishing operation.

Table 5.2 The experimental sets and cutting parameters used in the experiments

Cutting Speed (m/min)	**Feed Rate (mm/min)**	**Depth of Cut (mm)**	**Workpiece Material**	**Cutting Tool**	**Tool Holder**
63					
126	100				
188	200			2 flute end	
251	400	0.2	AA5083	mill cutter	ER32
314	600	0.5	AA7075	with 20 mm	Collet
377	800			diameter	
503	1000				
628					

Experiments are conducted for 192 different variations on the basis of the test conditions stated above in order to construct the ANN model. 30 of these sets were used for testing ANN model. At the end of the experiments, the R_a values have been measured with calibrated Mitutoyo SJ-310 contact-type surface roughness tester. These are used as the input data for the ANN model.

5.3 Experimental Results for ANN Training of SRCS

According to the results of the experiments conducted for both ANN training and analyzing the behavior of the system, changes in the R_a value depending on feed rate, cutting speed and depth of cut are presented in Figure 5.1. It shows the changes in the surface roughness depending on the cutting speed under constant feed rates between 100 mm/min and 1000 mm/min at a fixed depth of cut of 0.2 mm. It is observed that the surface roughness decreases under the constant feed rate, with an increase in the cutting speed.

(a)

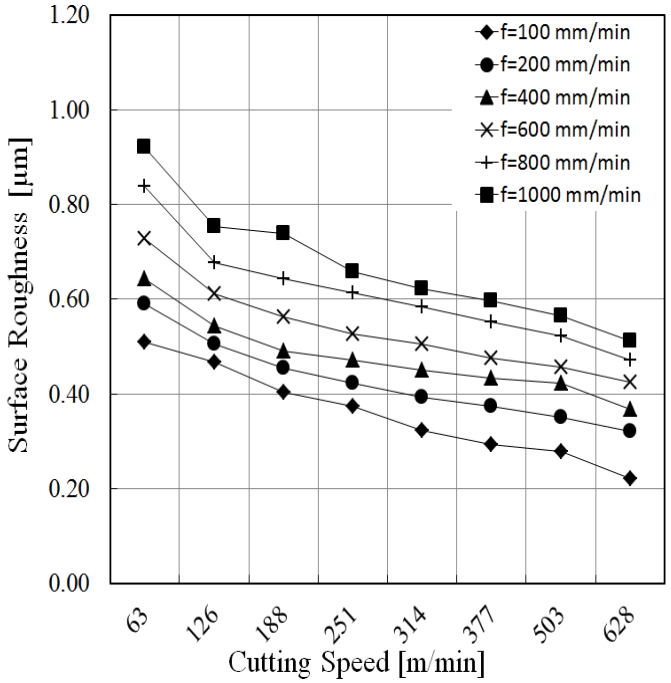

Figure 5.1 The change in R_a depending on cutting speed at 100-1000 mm/min feed rates interval for 0.2mm depth of cut (a) for material AA5083 (b) for material AA7075

(b)

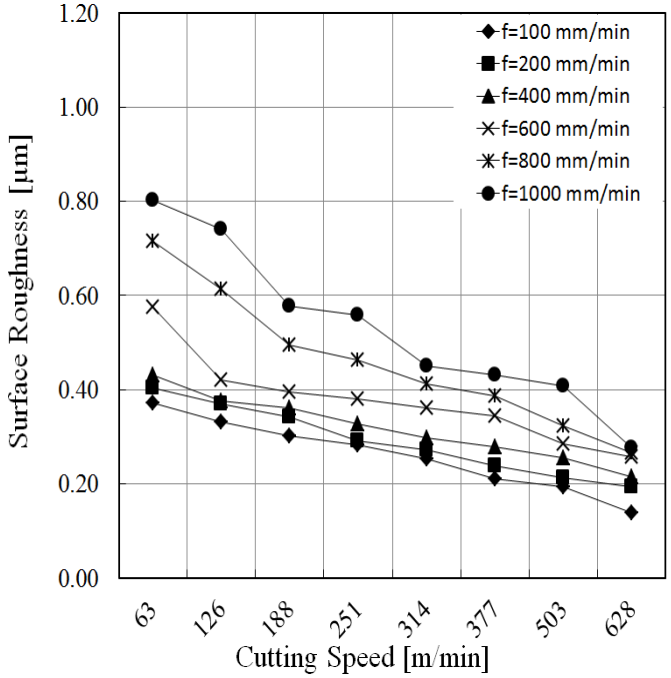

Figure 5.1 The change in R_a depending on cutting speed at 100-1000 mm/min feed rates interval for 0.2mm depth of cut (a) for material AA5083 (b) for material AA7075 (Cont.)

Figure 5.2 illustrates the relation between the cutting speed and roughness value for various feed rates. The roughness value increases as the feed rate increases for 0.2 mm depth of cut.

(a)

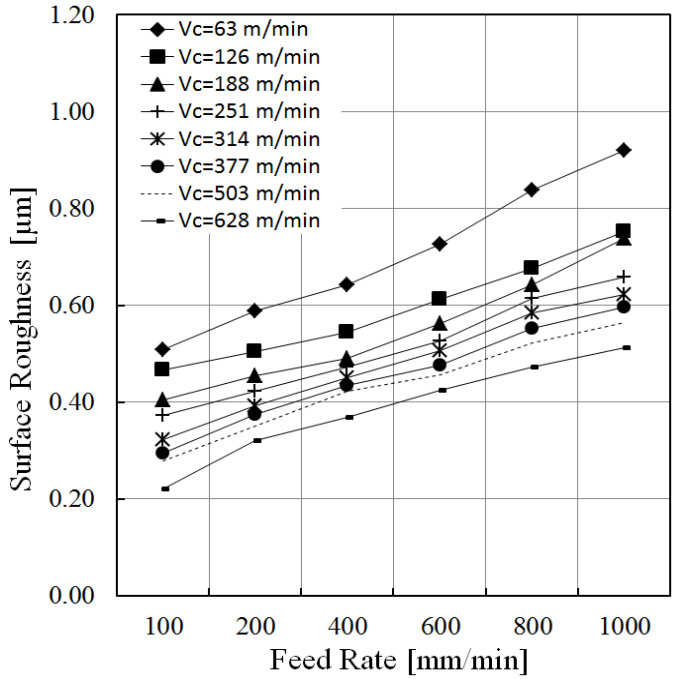

(b)

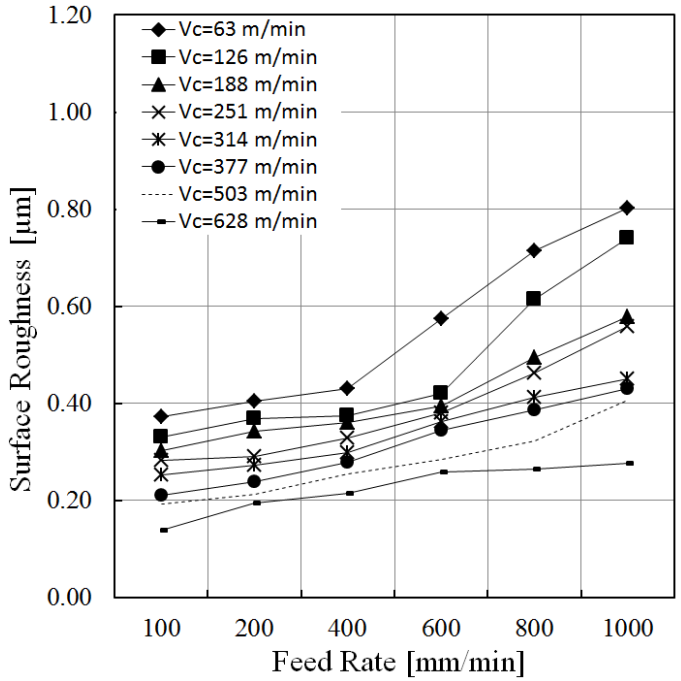

Figure 5.2 The change in R_a depending on feed rate at 63-628 m/min cutting speed interval for 0.2mm depth of cut (a) for material AA5083 (b) for material AA7075

Figure 5.3 shows the changes in the roughness values depending on the cutting speed under constant feed rates between 100 mm/min and 1000 mm/min at a 0.5 mm

depth of cut. The R_a value decreases with the increase in the cutting speed in a similar way presented in Figure 5.2.

(a)

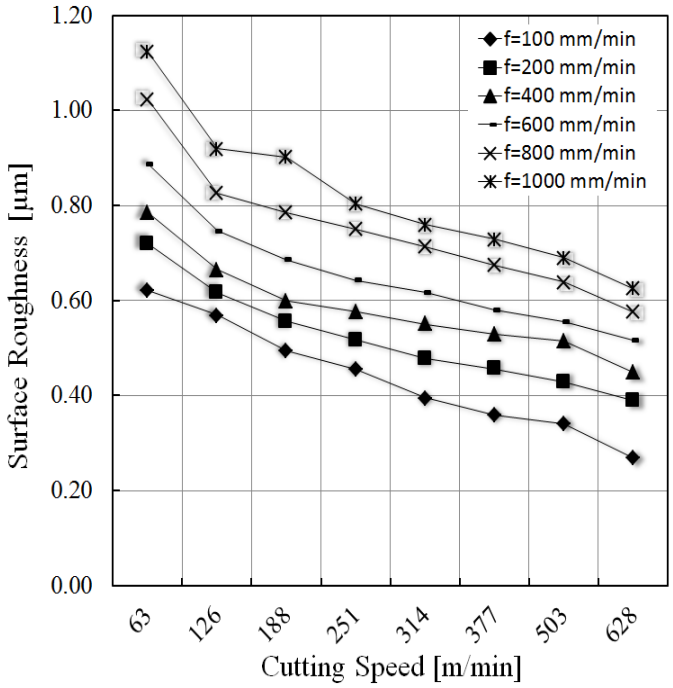

(b)

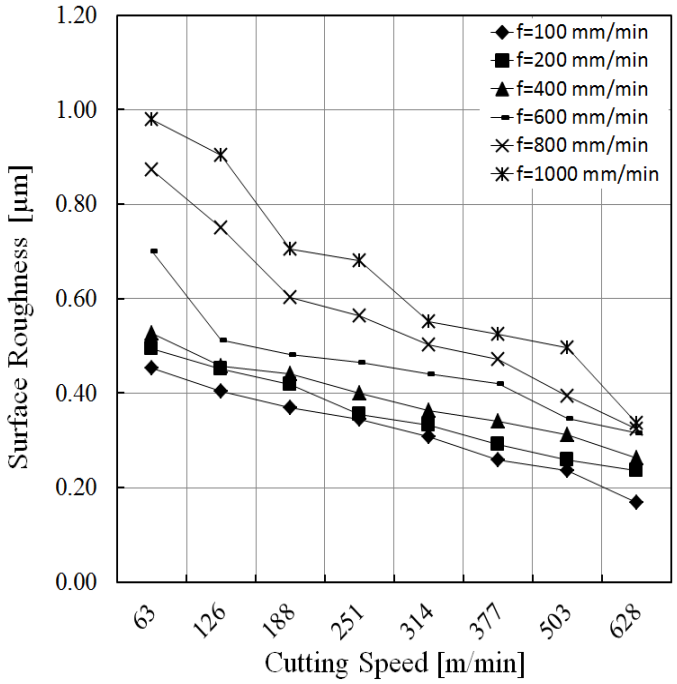

Figure 5.3 The change in R_a depending on cutting speed at 100-1000 mm/min feed rates interval for 0.5mm depth of cut (a) for material AA5083 (b) for material AA7075

In Figure 5.4, the change in R_a with respect to the feed rate under constant cutting speeds between 63-628 m/min at a 0.5 mm depth of cut is given. The R_a increases with the increase in the feed rate approximately in direct proportion in a similar way presented in Figure 5.2. The increase in the depth of cut results in increasing surface roughness values. When these results are compared with the findings of similar studies in the literature, it is seen that the changes in R_a with the feed rate, cutting speed and depth of cut show similar behavior. Especially, Palanikumar (2007) observed that the R_a value decreases with the increase in cutting speed, and it increases with the increase in feed rate and depth of cut.

(a)

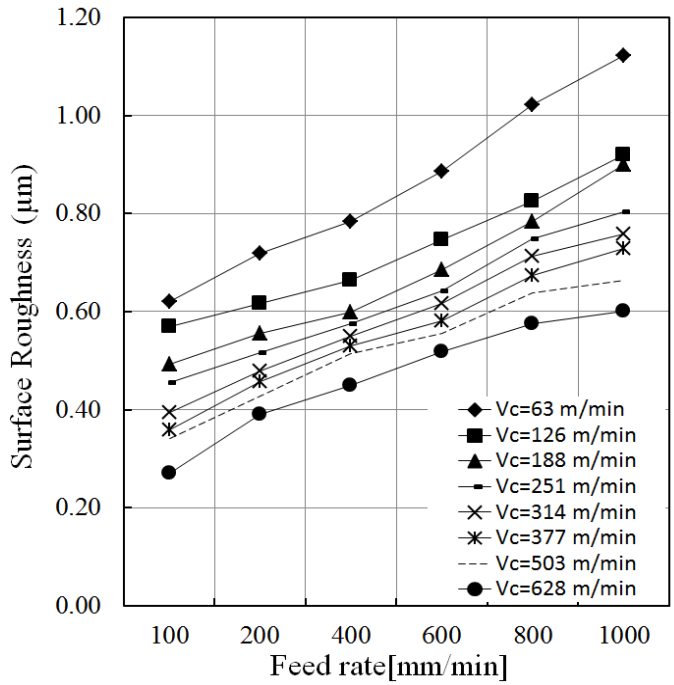

Figure 5.4 The change in R_a depending on feed rate at 63-628 rev/min cutting speed interval for 0.5mm depth of cut (a) for material AA5083 (b) for material AA7075

(b)

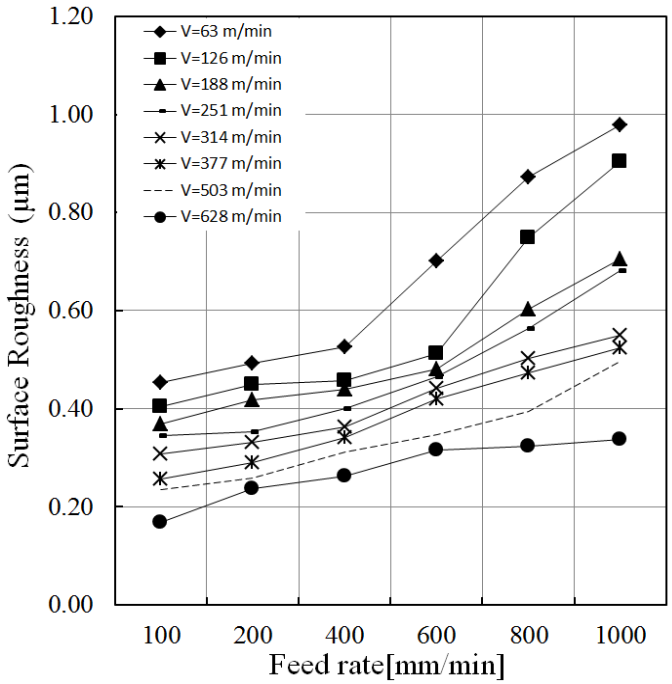

Figure 5.4 The change in R_a depending on feed rate at 63-628 m/min cutting speed interval for 0.5mm depth of cut (a) for material AA5083 (b) for material AA7075 (Cont.)

5.4 Experimental Results of SRCS

The results presented in Figures 5.1-5.4 are used to create the ANN model, which is the main part of the SRCS. Then, the performance of the surface roughness control system is examined experimentally for two different workpiece materials. The validation tests are carried out in down milling operations. In literature, the resultant cutting force in up milling is larger than that in down milling. Thus, surface roughness value in up milling is larger than in down milling. Dry cutting is used for the experiments. The surface roughness measurements by OSRS are performed during the cutting direction in this study.

In the first test, The initial values of the feed rate and cutting speed are chosen as 1200 mm/min and 251 m/min, respectively. The depth of cut is taken as 0.8 mm for semi-finish operation. The required value of R_a is assigned as 0.6 µm to the system. Moreover, the depth of finishing cut is determined as 0.2 mm. Using these parameters, the surface roughness measurement was performed during the cutting

direction by OSRS after the semi-finish cut operation as shown in Figure 5.5 and the R_a value is determined as 1.576 μm for AA5083 Aluminum alloy. The length of the OSRS measurement area is 50 mm. The measurement length can be adjusted in the SRCS.

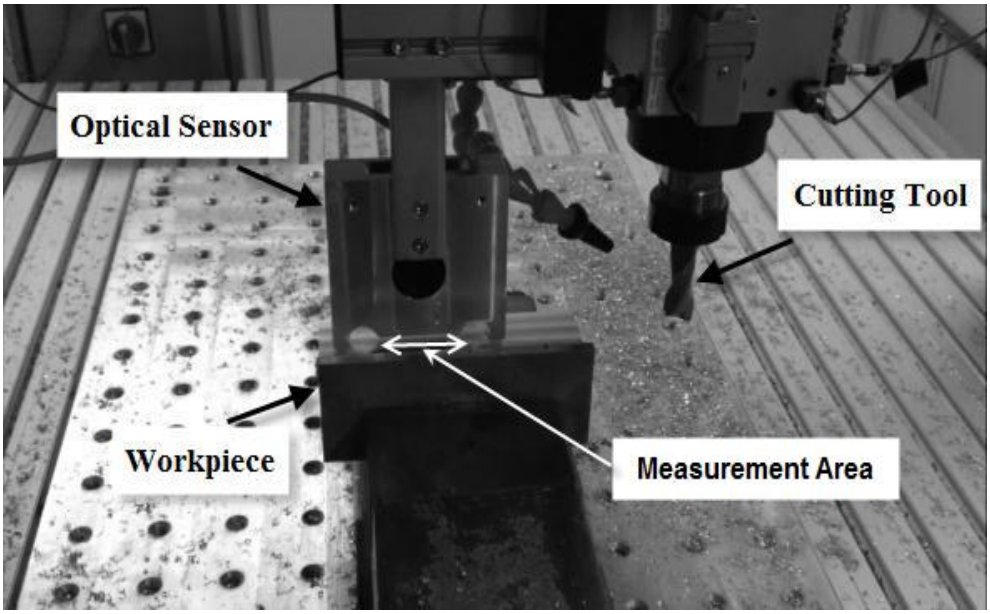

Figure 5.5 Spindle and the integrated optical measurement system

Since the resulting R_a value was greater than the desired value, the SRCS system calculated the cutting speed and feed rate to achieve the desired roughness level. The SRCS system determined the required optimum cutting parameters as Vc=477 m/min and f=303 mm/min for R_a=0.6 μm. Then the system machined the surface of the workpiece automatically with these new cutting parameters and then the roughness measurement was repeated. After the measurement, it was observed that the roughness value was obtained as 0.476 μm and the milling process was finished. Figure 5.6 illustrates the roughness values before and after the intervention of the SRCS for AA5083 alloy. The curve above 0.6 μm represents the surface roughness after the semi-finish cut, the curve on 0.6 μm represents the desired surface roughness limit and the curve below 0.6 μm represents the resulting roughness levels obtained by using the cutting parameters determined by the SRCS.

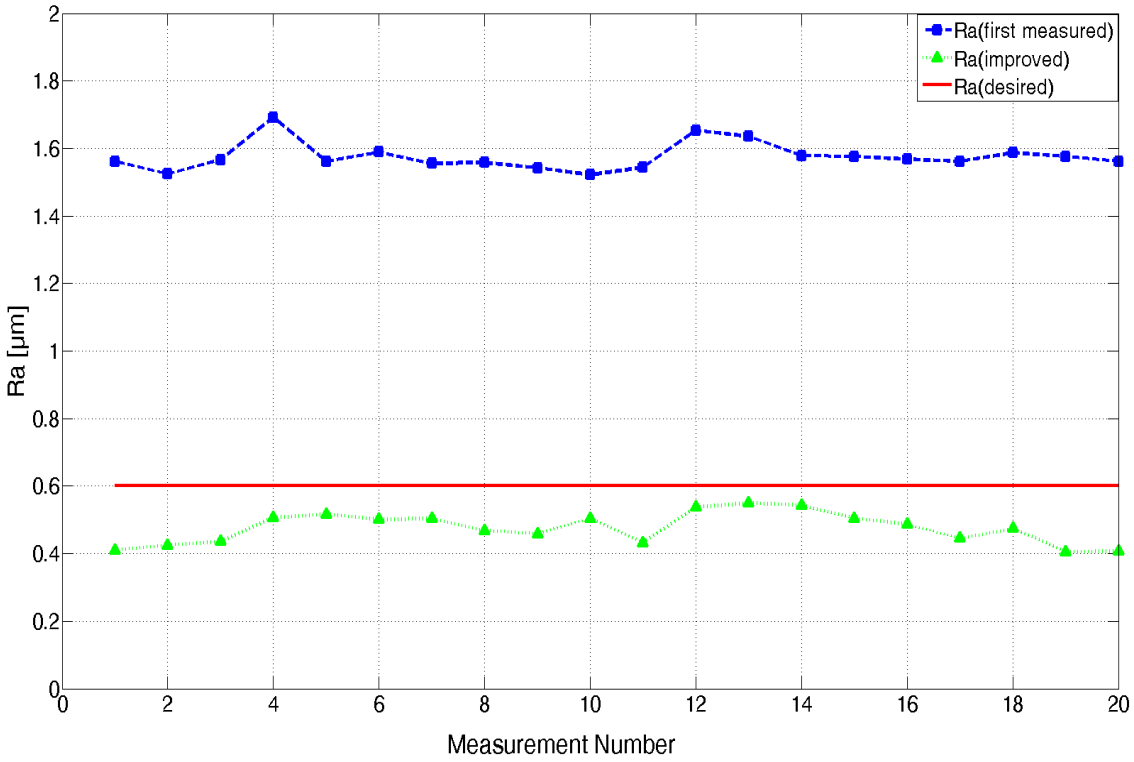

Figure 5.6 Surface roughness values before and after the developed system for AA5083

If a comparison is made between the results of the experimental studies carried out for the training stage of the ANN and the result of the SRCS, it can be seen from Figure 5.7 that the R_a value for the feed rate of 303 mm/min at Vc=503 m/min and d=0.2 mm is about 0.4 µm. This roughness value is very close to the roughness value obtained by SRCS and this indicates the efficiency of the developed system.

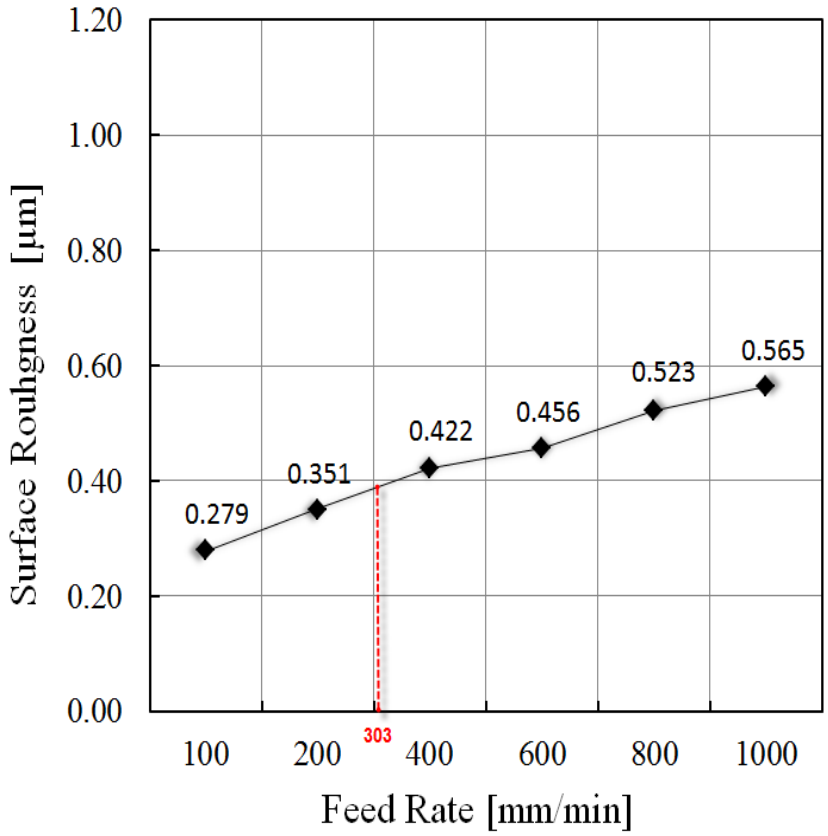

Figure 5.7 The change of surface roughness with respect to the feed rate at 503 m/min cutting speed and 0.2 mm depth of cut for AA5083

Figure 5.8 shows the microscope images of the machined surface magnified by 25 times before and after the intervention of the SRCS for the comparison purpose. Carl Zeiss Axioskop 2 Mat was used to get the surface image. As seen from the magnified surface image, which was machined according to the cutting parameters determined by SRCS for the finishing operation, there is a good improvement in the surface roughness.

(a)

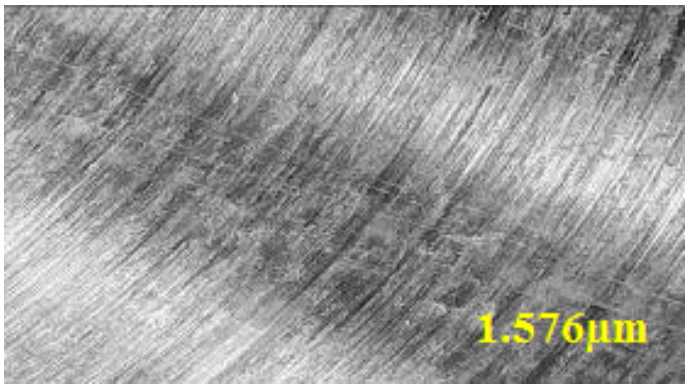

(b)

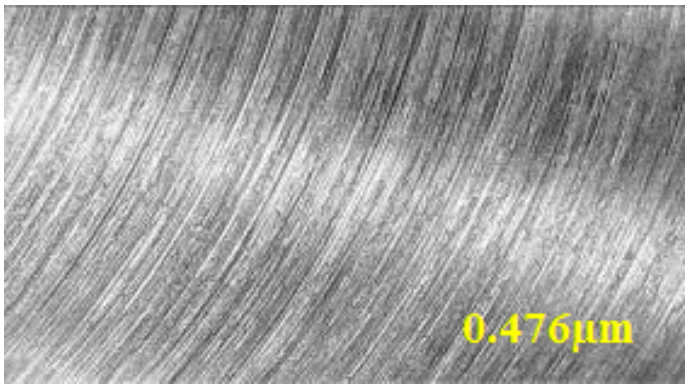

Figure 5.8 Machined surface images of AA5083 material(x25) (a) Vc=251 m/min, f=1200 mm/min, d=0.8mm (b) Vc=477 m/min, f=303 mm/min and d=0.2 mm

In a similar way, as a result of machining operation with initial parameters Vc=251 m/min, f=1200 mm/min and d=0.5 mm, for AA7075 alloy, R_a is measured as 0.914 µm. This value was also larger than the desired surface roughness of 0.4µm. The SRCS determined the cutting parameters as Vc=430 m/min and f=758 mm/min, for finishing operation to get desired R_a with constant depth of cut. Using the new cutting parameters determined by SRCS, end milling operation was completed with the resulting surface roughness R_a=0.348 µm. Figure 5.9 illustrates the roughness values for AA7075 alloy before and after the intervention of SRCS.

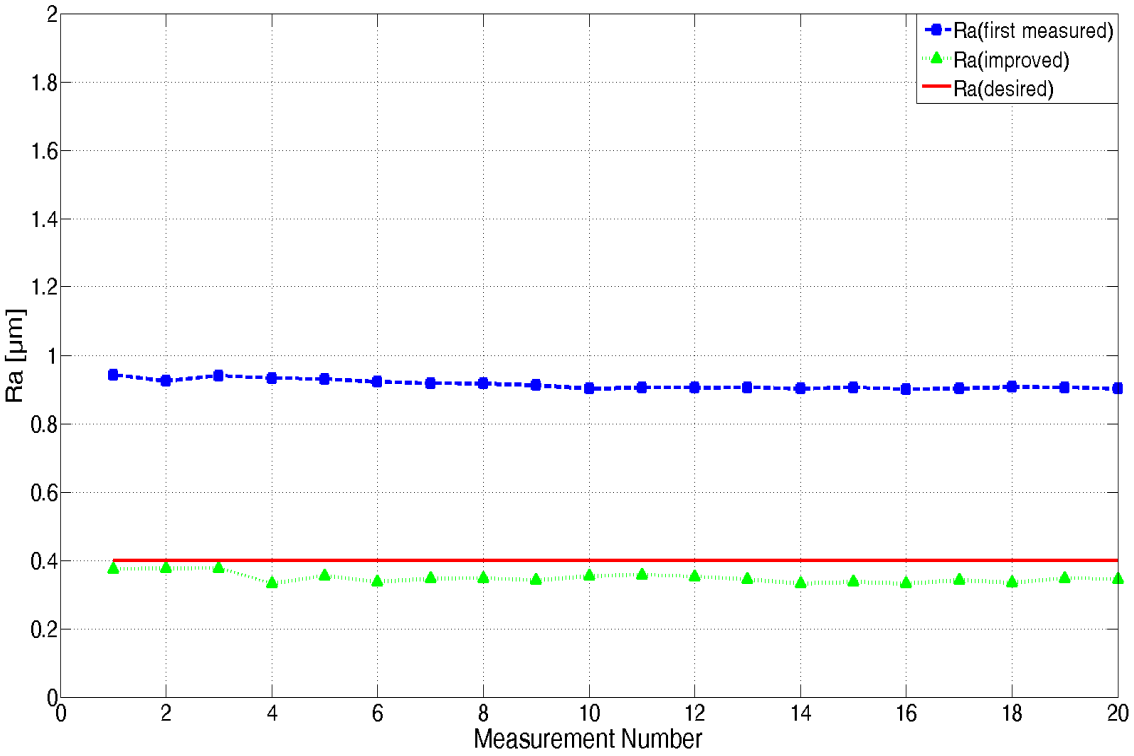

Figure 5.9 Surface roughness values before and after the developed system for AA7075

The roughness results for workpiece material AA7075 is better than those obtained for material AA5083 due to the reducing effects of built up edge (BUE).

The comparison between the cutting parameters determined by two different operators and the cutting parameters determined by SRCS for getting desired surface roughness were carried out in this part of the study. The aim is to find the approachability to the desired surface roughness with actual surface roughness generated by these operators.

In Figure 5.10, machined surfaces are shown for desired surface roughness of 0.5µm for depth of cut d=0.5 in accordance with optimum cutting parameters determined by two operators and SRCS. First operator defined Vc=440 rev/min and f=1500 mm/min as the cutting parameters to get desired surface roughness. According to defined parameters, actual surface roughness value was measured as 0.767µm.

Second operator defined Vc=314 m/min and f=1000 mm/min as the cutting parameters to get desired surface roughness. According to these parameters, actual surface roughness was measured as 0.621µm. Then, SRCS determined Vc=502 m/min and f=481mm/min as the optimum cutting parameters; and the result of the measured surface roughness was obtained as 0.407 µm.

(a)

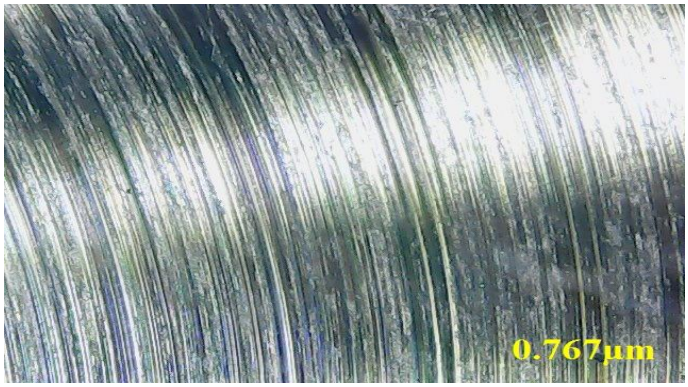

(b)

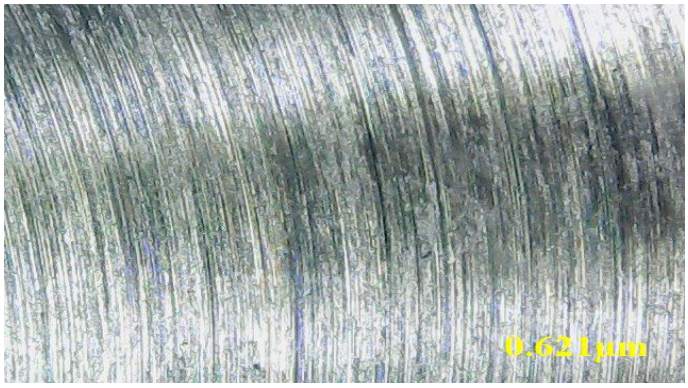

(c)

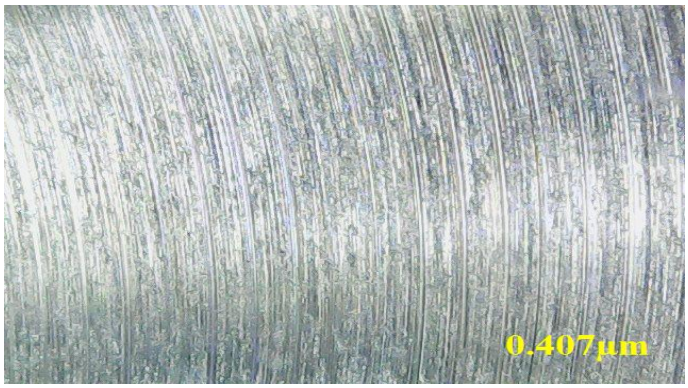

Figure 5.10 Machined surface images of AA5083 material (x25) d=0.5mm (a) Operator A (b) Operator B (c) SRCS

In Figure 5.11, the study on getting desired surface roughness as 0.6 µm is given. From these experiments, first operator defined Vc=251 m/min and f=1500 mm/min as the cutting parameters; second operator defined Vc=346 m/min and f=900 mm/min as the cutting parameters; and SRCS defined Vc=334 m/min and f=452 mm/min as the optimum cutting parameters. The result of measured surface roughness, for the first operator is 1.071µm; for the second operator is 0.654 µm; and for SRCS is 0.545 µm.

(a)

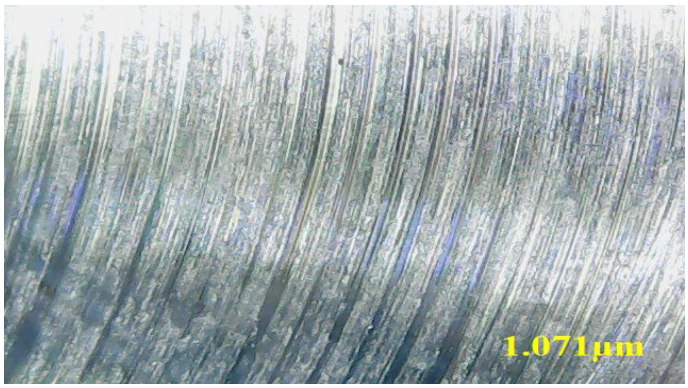

(b)

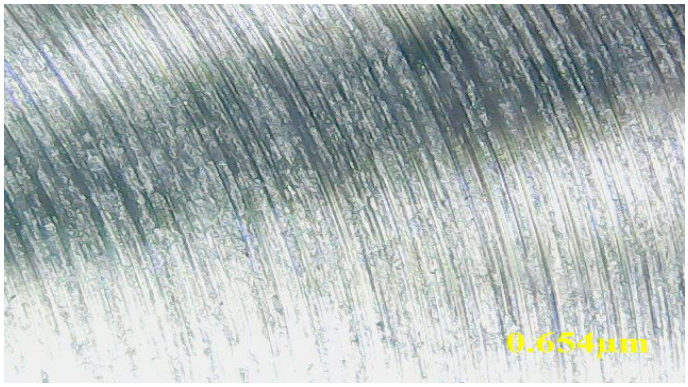

Figure 5.11 Machined surface images of AA5083 material (x25) d=0.5mm (a) Operator A (b) Operator B (c) SRCS

(c)

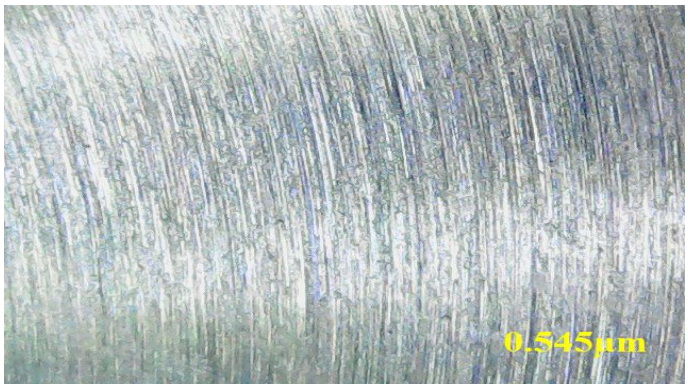

Figure 5.11 Machined surface images of AA5083 material (x25) d=0.5mm (a) Operator A (b) Operator B (c) SRCS (Cont.)

In Figure 5.12, the study on getting desired surface roughness as 0.4 µm is given. From these experiments, first operator defined Vc=377 m/min and f=800 mm/min as the cutting parameters; second operator defined Vc= 628 m/min and f=1000 mm/min as the cutting parameters; and SRCS defined Vc=353 m/min and f=131 mm/min as the optimum cutting parameters. The result of measured surface roughness, for the first operator is 0.565µm; for the second operator is 0.523 µm; and for SRCS is 0.386 µm.

(a)

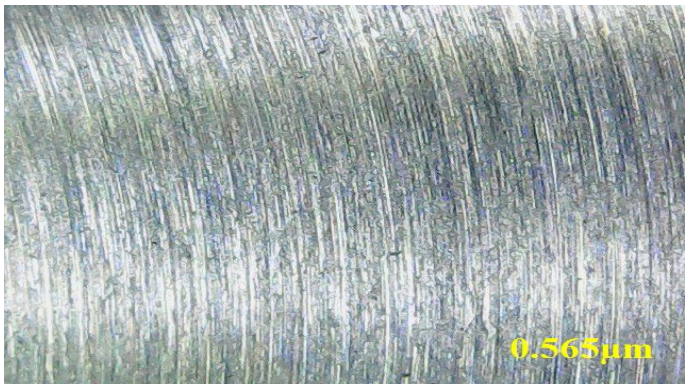

Figure 5.12 Machined surface images of AA5083 material (x25) d=0.5mm (a) Operator A (b) Operator B (c) SRCS

(b)

(c)

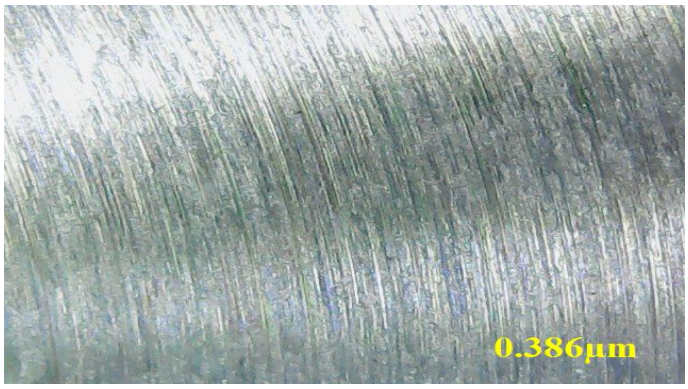

Figure 5.12 Machined surface images of AA5083 material (x25) d=0.5mm (a) Operator A (b) Operator B (c) SRCS (Cont.)

From all these experimental results presented above, SRCS achieved the roughness values equal or less than the desired surface roughness value.

The cutting parameters used in the milling operation of different samples for which the R_a values are measured, are given in Table 5.3.

Table 5.3 Cutting parameters used in the comparison of roughness measurement method

Sample Number	Vc (m/min)	f (mm/min)
1	251	1200
2	565	300
3	377	800
4	353	131
5	334	452
6	502	481
7	346	900
8	314	1000
9	440	1500

Figure 5.13 presents the correlation between the results of the roughness measurements performed by OSRS and calibrated contact type roughness measurement system Mitutoyo SJ-310 for two different materials.

(a)

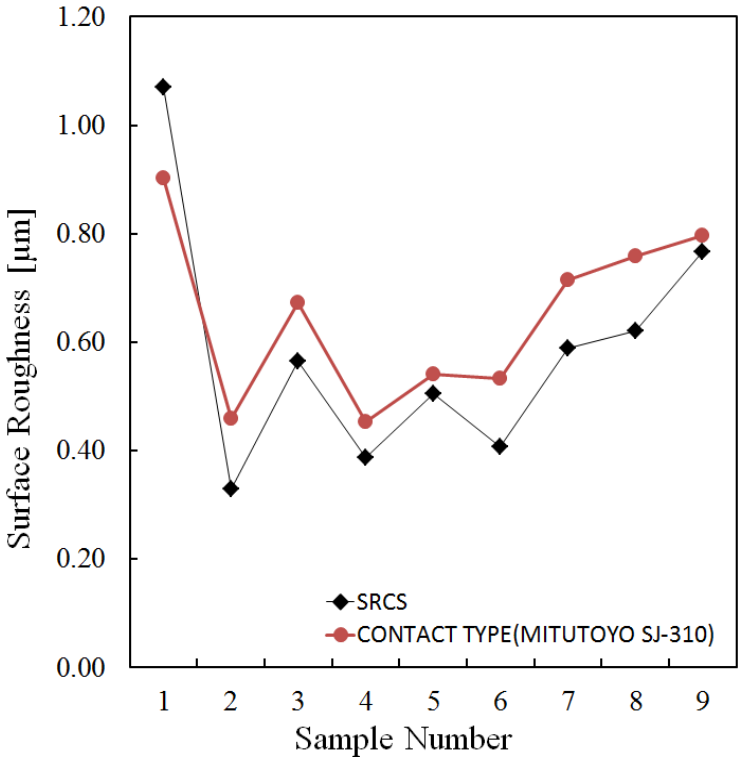

Figure 5.13 Comparisons of surface roughness levels of OSRS and contact type systems (Mitutoyo SJ-310) (a) for AA5083 (b) for AA7075

(b)

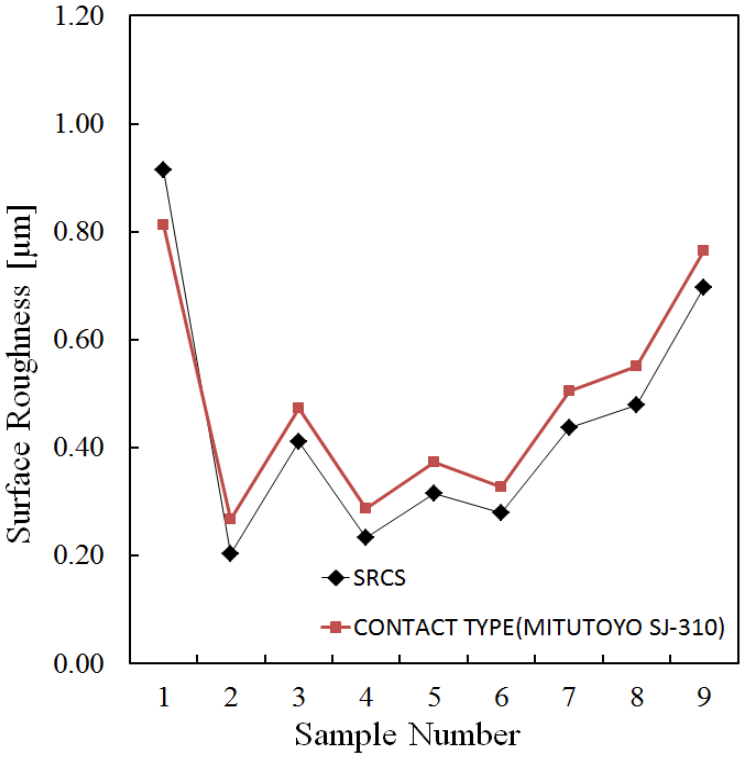

Figure 5.13 Comparisons of surface roughness levels of OSRS and contact type systems (Mitutoyo SJ-310) (a) for AA5083 (b) for AA7075 (Cont.)

The percentage deviations between the roughness values of optic and contact type measurement systems are 6% and 2% for materials AA5083 and AA7075, respectively. The reason for these small differences may be noise, ambient light and structural vibration. The results of the comparison presented in Figure 5.13 shows that, the OSRS developed in this study provides reliable R_a values in comparison with the contact type roughness measurement devices.

In this chapter, experimental studies and results for SRCS are given in detail. Firstly, experimental studies were performed collecting input data for training ANN model of the SRCS. These studies were consistent with literature. Then, experimental studies for verification of the SRCS were performed for different conditions. At the end, system verification was proved with the experimental results.

CHAPTER SIX
CONCLUSION

The surface roughness control is achieved on the basis of the optimum cutting speed and the feed rate determined during the finishing operation by means of the system developed in this study. ANN model was developed for predicting the proper cutting parameters of the system. For this purpose, experimental studies were performed in order to train the ANN model.

Natural frequency analysis of the system was performed both numerically and experimentally. Experimental studies were performed by measuring vibration of the system for idle state and during machining to extract the dynamic characteristic of the system.

The surface roughness control system hardware and software were given in detail. Optical surface roughness sensor was discussed in detail with its working principles. Software validation studies have been performed with experimental studies. Results were compared with the similar studies.

The experimental studies performed throughout this thesis and main findings are summarized below.

1. Experiments have been conducted to examine the dynamic characteristics of the system. The natural frequencies of the system were determined both numerically and experimentally for comparison purpose. There is a good harmony between the numerical and experimental results up to approximately 95%.
2. Vibration measurements for idle state have been performed. In this case, the optical sensor performed surface roughness measurement while machining operation is not active. Here, feed rate indicates just the axis movement. It was observed that the increase in feed rate resulted in increase in the vibration levels.

3. Vibration measurements have also been performed during the machining process. Here, acceleration and PSD responses of the system were investigated in relation to the variation of cutting speed, feed rate and depth of cut.

4. Acceleration values were found high when the first chip was removed. Here, accelerations of the system have increased with the increase of cutting speed, feed rate and depth of cut.

5. Results of the experiments have been used for training the artificial neural network model. The performance of ANN Model has been calculated 92%. Experiments were performed for investigating the effect of cutting speed, feed rate, depth of cut and workpiece material on the surface roughness levels.

6. Firstly, AA5083 and AA7075 were used as the workpiece material in the experimental studies. The surface roughness values of AA5083 are higher than AA7075 due to its lower hardness value. Wherein, tool wear is accepted negligible since both materials are aluminum.

7. The effect of cutting speed on the surface roughness has been examined. It was observed that the surface roughness decreases with the increase in the cutting speed.

8. According to the result of experiments, it was observed that the surface roughness increases with the increase in the feed rate.

9. According to the result of experiments, it was observed that the surface roughness increases as the depth of cut increases.

10. Experimental studies were conducted for different workpieces and depth of cut values for the validation of surface roughness control system.

11. The percentage deviations between the roughness values of optic and contact type measurement systems are 6% and 2% for materials AA5083 and AA7075, respectively.

12. The validation error is found to be 6.1% for AA5083 material and 4.5% for AA7075 material.

13. According to experimental results, surface roughness improvement procedure has been successfully achieved with the proposed surface roughness control system.

It was observed that the results obtained in this study agree well with the results presented in the literature.

The results of surface roughness measurements acquired for different cutting parameters show that it is possible to have better surface finish quality by using the proposed SRCS. By virtue of the developed system, the initiative of the operator on the proper selection of the cutting parameters is taken out and the time loss in the total machining process is economized by minimum operator intervention. With the proposed system, the surface roughness can be continually kept under control during the process and the quality of the surface roughness will be controlled within the production phase. The system with the learning property can be applicable for other types of CNC milling and turning machines.

In the future studies, instead of optical sensor, all the measurements may be performed on the related surface by using laser scan arm. Thus, quality control section may be completed in one setup.

Also in the future, the studies may be done with the cutting forces measurement by using ANN method. Better results may be achieved by making vibration isolation.

REFERENCES

Agarwal, N. (2012). Surface roughness modeling with machining parameters (speed, feed & depth of cut) in CNC milling. *MIT International Journal of Mechanical Engineering, 41*(2), 55-61.

Ali, S.M., & Dhar, N.R. (2010). Modeling of tool wear and surface roughness under MQL condition-a neural approach. *Canadian Journal on Artificial Intelligence, Machine Learning and Pattern Recognition*, *1*(2), 7-25.

Altıntaş, Y. (2012). *Metal cutting mechanics, machine tool vibrations, and CNC design* (2nd Ed.). New York: Cambridge University Press.

Avitable, P. (2003). *Mechanical vibrations, overview of experimental modal analysis*. Retrieved April 12, 2015, from http://faculty.uml.edu/pavitabile/22.457/VIBS_Modal_Overview_021703_MACL.pdf.

Baek, D.K., Ko, T.J., & Kim, H.S. (2001). Optimization of feed rate in a face milling operation using a surface roughness model. *International Journal of Machine Tools and Manufacture, 41*, 451–462.

Bajic, D., Lela, B., & Zivkovic, D. (2008). Modelling of machined surface roughness and optimization of cutting parameters in face milling. *Metalurgija, 47*(4), 331-334.

Bhushan, B. (2001). *Modern tribology handbook*. Florida: CRC Press.

Black, J.T. (1979). Flow stress model in metal cutting. *Journal of Engineering for Industry, 101*(4), 403-415.

Bloechle, W. (n.d.). Sensors Online Your Technical Resource for Sensing Communication and Control. *Measuring surface roughness with an optical sensor*. Retrieved December 18, 2015, from http://archives.sensorsmag.com/articles/0499/0499_58.

Bradley, C. (2000). Automated surface roughness measurement. *International Journal of Advanced Manufacturing Technology, 16*, 668-664.

Che, Z.G., Chiang, T.A., &Che, Z.H. (2010). Feed-forward neural networks training: A comparison between genetic algorithm and back-propagation learning algorithm. *International Journal of Innovative Computing, Information and Control, 7*(10), 5839-5850.

Chen, J.C., & Savage, M. (2001). A Fuzzy –Net Based multilevel in process surface roughness recognition system in milling operations. *International Journal of Manufacturing Technology, 17*, 670-676.

Chi, J., & Chen, L. (2010). The real-time prediction of surface roughness based on Genetic Wavelet Network. *Advanced Materials Research, 102-104*, 610-614.

Çolak, O., Kurbanoğlu, C., & Kayacan, M.C. (2007). Milling surface roughness prediction using evolutionary programming methods. *Materials and Design.28,* 657-666.

Ehmann, K.F., & Hong, M.S. (1994).A generalized model of the surface generation process in metal cutting.*CIRP Annals,43*, 483–486.

Erzurumlu, T., & Öktem, H. (2007). Comparison of response surface model with neural network in determining the surface quality of moulded parts. *Materials and Design, 28*, 459-465.

Estun (n.d.). Retrieved June 13, 2015, from http://estun-servo.en.made-in-china.com/product/CozEyqAUXiWl/China-EMJ-Series-AC-Servo-Motor-200w-400w-750w-1kw-High-Speed-Small-Capacity.html.

Fausett, L. (1993). *Fundamentals of neural network: architectures, algorithms and applications* (1st Ed.). UK: Prentice Hall.

Göloğlu, C., & Sakarya, N. (2008). The effects of cutter path strategies on surface roughness of pocket milling of 1.2738 steel based on Taguchi method. Journal of Materials Processing Technology, *206*, 7-15.

Hayajneh, M.T., Tahat, M.S., & Bluhm, J. (2007). A Study of the effects of machining parameters on the Surface Roughness in the End-Milling Process. *Jordan Journal of Mechanical and Industrial Engineering*, *1*, 1-5.

Hohner (n.d.). Retrieved May 10, 2015 from http://www.instant-analysis.com/Data-Sheets/D/516.htm.

HSD Mechatronics (n.d.). Retrieved June, 12, 2015, from http://www.hsdusa.com/viewdoc.asp?co_id=745.

Kuttolamadom, M.A., Hamzehlouia, S., & Mears, M.L. (2010).Effect of machining feed on surface roughness in cutting 6061 aluminum. *SAE International*, *3*(1), 108-119.

Lee, E.H., & Shaffer, B.W. (1951). Theory of plasticity applied to the problem of machining. *Journal of Applied Mechanics*, *18*, 405–413.

Lee, K.Y., Kang, M.C., Jeong, Y.H., Lee, D.W., & Kim, J.S. (2001). Simulation of the surface roughness and profile in high speed end milling. *Journal of Materials Processing Technology*, *113*, 410–415.

Lippmann, R.P. (1987). An introduction to computing with neural nets. *IEEE Magazine on Accoustics, Signal and Speech Processing*, *4*, 4-22.

Merchant, M.E. (1944). Basic mechanics of the metal cutting process. *ASME Journal of Applied Mechanics*, *11*, A168–A175.

Michalik, P., Zajac, J., Hatala, M., Mital, D., & Fecova, V. (2004). Monitoring surface roughness of thin-walled components from steel C45 machining down and up milling. *Measurement*, *58*, 416-428.

Moshat, S., Datta, S., Bandyopadhyay, A., & Pal, P.K. (2010). Optimization of CNC end milling process parameters using PCA-based Taguchi method. *International Journal of Engineering Science and Technology*, *2*(1), 92-102.

Nouri, M., Fussell, B.K., Ziniti, B.L., & Linder, E. (2014). Real-time tool wear monitoring in milling using a cutting condition independent method. *International Journal of Machine Tools and Manufacture*, *89*, 1-13.

Öktem, H., Erzurumlu, T., & Erzincanlı, F. (2006). Prediction of minimum surface roughness in end milling mold parts using neural network and genetic algorithm. *Materials and Design*, *27*, 735-744.

Oxley, P.L.B. (1989). *The mechanics of machining* (2nd Ed.). New York: Ellis Horwood Limited.

Palanikumar, K. (2007). Modelling and analysis for surface roughness in machining glass fibre reinforced plastics using response surface methodology. *Materials and Design*, *28*, 2611-2618.

Palmer, W.B., & Oxley, P.L.B. (1959). Mechanics of orthogonal machining. *Proceedings of the Institution of Mechanical Engineers*, *173*(24), 623–654.

Rosales, A., Vizan, A., Diez, E., & Alanis A. (2011). Prediction of Surface Roughness by Registering Cutting Forces in the Face Milling Process. *European Journal of Scientific Research*, *41*(2), 228-237.

Routara, B.C., Bandyopadhyay, A., & Sahoo, P. (2009). Roughness modeling and optimization in CNC end milling using response surface method: effect of workpiece material variation. *International Journal of Advanced Manufacturing Technology*, *40*, 1166-1180.

Taylan, F. (2006). Alın frezelemede deney şartları ve takım aşınması ölçüm metodları. *Süleyman Demirel Üniversitesi Fen Bilimleri Enstitüsü*, *2006*, Isparta.

Tomkiewicz, A.Z. (2010). Estimation of surface roughness parameter based on machined surface image. *Metrology and Measurement Systems*, *17*(3), 493-504.

Tsai, Y.H., Chen, J.C., & Lou, S.J. (1999). An in-process surface recognition system based on neural networks in end milling cutting operations. *International Journal of MachineTools and Manufacture*, *39*, 583-605.

Yılmaz, V., Dilipak, H., Sarıkaya, M., Yılmaz, C.Y., & Meral, G. (2014). Frezeleme işlemlerinde titreşimi ve yüzey pürüzlülüğünü etkileyen parametrelerin optimizasyonu. *SDU Journal of Technical Sciences*, *1*, 37-44.

Zhang, J.Z., Chen, J.C., & Kirby, E.D. (2007). Surface roughness optimization in an end-milling operation using the Taguchi design method. *Journal of Materials Processing Technology*, *184*, 233-239.

APPENDICES

A 1. NOMENCLATURE

Table A.1 Abbreviations used in thesis

Subscripts

ϕ	Shear angle
Vc	Cutting speed
τ_s	Shear stress
σ_s	Normal stress
F_R	Resultant force
F_C	Cutting force
F_P	Tool force
T_{int}	Tool-chip interface temperature
P_n	Normal plane
P_v	Velocity plane
ϕ_n	Normal shear angle
ϕi	Oblique shear angle
η	Chip flow angle
α	Normal rake angle
β	Friction angle
ω_{nx}	Natural frequency at x feed direction
ω_{ny}	Natural frequency at y normal direction
ξ_x	Structural damping ratio at x feed direction
ξ_y	Structural damping ratio at y normal direction
k_x	Spring constant at x feed direction
k_y	Spring constant at y normal direction
$F_x(t)$	Dynamic cutting forces at x feed direction
$F_y(t)$	Dynamic cutting forces at y normal direction
X	Input cluster at ANN model
w_{ki}	Weight ratio at ANN model
y_k	Activation function at ANN model

a	Slope of sigmoid function
σ	Standard deviation
η	Structural damping loss factor
S	Spindle Speed
f	Feed Rate
d	Depth of cut
S_S	Signal for reflection
S_N	Signal for scatter